

THE TRANSFORMATION FROM PLANETARY NEBULA NUCLEUS
TO WHITE DWARF: A SEISMOLOGICAL STUDY
OF STELLAR METAMORPHOSIS

APPROVED BY SUPERVISORY COMMITTEE:

THE TRANSFORMATION FROM PLANETARY NEBULA NUCLEUS
TO WHITE DWARF: A SEISMOLOGICAL STUDY
OF STELLAR METAMORPHOSIS

by

STEVEN DANIEL KAWALER, B.A., M.A.

DISSERTATION

Presented to the Faculty of the Graduate School of

The University of Texas at Austin

in Partial Fulfillment

for the Degree of

DOCTOR OF PHILOSOPHY

THE UNIVERSITY OF TEXAS AT AUSTIN

May 1986

PREFACE

Some of the results presented in Chapters 2-5 of this dissertation have appeared in publication form in the *Astrophysical Journal* (Kawaler et al. 1985a,b; Kawaler et al. 1986). To reduce unnecessary redundancy, no references have been made to these papers in the main text.

By nature, I usually end up working very late at night, alone. Most of the effort that went into producing this dissertation was put in at the computer, or with a pen and pad on my sofa, when most every one else with any sense was sound asleep. This is not to say that the work that I present here is that of a solitary individual working in an utter vacuum. Nothing could be further from the truth.

Until quite recently, my wife Leslie and I joked that I had never seen her asleep. That has changed. I have had it easy for the past year and a half compared to her. While I raked in the pennies of minimal graduate student support and played with my stellar models, she faced impossible filing deadlines, vague leadership from partners, and mountains of thrilling transcripts of utility rate hike hearings. Despite the monetary rewards for such self-destructive behavior, little satisfaction came to her in knowing that after coming home from work, we could only have a brief meal together, after which she had to go to sleep and I had to go to work. Despite this unnatural routine to which we had to adhere for the past year and a half, she is more than ever the perfect companion, colleague, friend, and lover. How she managed it, I don't know; what I would have done without her, I can't imagine.

While some doctoral students are fortunate enough to have a caring, stimulating, and patient supervising professor, I have had the extraordinary luck to have two of them: co-supervisors Don Winget and Carl Hansen. Don has been a continuous fountain of ingenious ideas and contagious enthusiasm from the time we first sat down to discuss the possibility of this thesis program to the presentation of the results at the recent AAS meeting in Houston. Carl has provided polished experience

and made available his breadth of knowledge despite the geographical distance between Boulder and Austin. His constant support and guidance inspired me to strive to meet his high standards. I am deeply grateful to Don and Carl for their personal friendship, and for treating me from the very start as a peer and colleague (and as a lowly student and imbecile when necessary). The completion of this dissertation is the beginning of a long collaboration with Don and Carl; I am very proud to be a part of the same profession as these two outstanding scientists.

It is a pleasure to acknowledge the help and encouragement of many members of the astronomical community. It is an honor to work with a scientist of such stature as Dr. Icko Iben, Jr.. Dr. Iben made it possible to explore many topics of importance by providing copies of his stellar evolution code, and by discussing at length the details of planetary nebula nucleus and hot white dwarf evolution. It has also been very valuable to have Ed Nather's sound astrophysical knowledge and keen intuition just two doors down the hall. I would also like to acknowledge the following people who have given helpful advice and shared their expertise: Hugh Van Horn, Gilles Fontaine, Ed Robinson, Art Cox, Sumner Starrfield, Matt Wood, Allen Hill, Jim Liebert, Craig Wheeler, Dean Pesnell, and Duane Dicus, as well as many others.

Dr. John Cox's influence on this work is evident on almost every page. This is not surprising, considering his personal and scientific influence on Don and Carl, and his many important contributions to the fields of stellar evolution and pulsation. In many ways, this dissertation is but a small tribute to his ingenuity, ability, and vision.

THE TRANSFORMATION FROM PLANETARY NEBULA NUCLEUS
TO WHITE DWARF: A SEISMOLOGICAL STUDY
OF STELLAR METAMORPHOSIS

Publication No. _____

Steven Daniel Kawaler, Ph. D.
The University of Texas at Austin, 1986

Supervising Professor: Donald E. Winget

The existence of several pulsating hot degenerates provides the exciting opportunity to study this transitory stage of stellar evolution with the techniques available from pulsation theory. We evolve $0.40\text{-}0.95M_{\odot}$ stellar models from the planetary nebula nucleus (PNN) phase to the cooling white dwarf phase using a variety of techniques, and solve the equations of linear adiabatic nonradial oscillations for these models. The g-mode periods are determined within the degenerate core at high luminosities. Below $100L_{\odot}$ (in models of $0.60M_{\odot}$), the region of period formation moves out into the nondegenerate envelope. The high radial overtone (20-40) and low order l (1-3) g-mode periods are comparable to those seen in the variable PG1159 stars. The period spacings agree as well, and appear to yield mode identifications.

Rates of period change can be used to probe the mass, structure, composition, and energy loss mechanisms of these degenerates. Periods generally increase with time for nonrotating models that are on the white dwarf cooling track below $1000L_{\odot}$. The rates of period change for PNNs are strongly dependent on the rate of energy loss via neutrinos. The timescale for period change is about 10^6 years. Evolutionary

changes in the rotation rate can be important also. The rate of change of the 516s period of PG1159-035 is consistent with the theoretical results incorporating this effect, and suggests that rotation strongly affects the observed rate of period change. At the relatively cooler temperatures of the DBV stars, the models suggest that the rates of period change should be observable, and may provide important independent constraints on the effective temperatures of these stars.

We also report preliminary results of fully nonadiabatic pulsation calculations for models of PNN. In all models, an active nuclear burning shell leads to the instability of some g-modes through the ϵ -mechanism. Only g-modes are unstable; in our models the unstable periods are confined to the range from 50s to 214s. We suggest that if hydrogen-deficient PNNs contain helium burning shells, then they should show pulsations with these periods.

TABLE OF CONTENTS

Preface	iii
Abstract	v
Table of Contents	vii
List of Tables	xi
List of Figures	xii
<u>Chapter 1.</u> An Overview of Stellar Pulsation in Post-Red Giant Phases	
1.1 Introduction	1
1.2 Observations of Pulsating Degenerates	8
1.2.1 Planetary Nebulae Nuclei	8
1.2.2 Pulsating PG1159-035 Stars	9
1.2.3 The DBV Stars	10
1.3 Summary of Previous Theoretical Work on Hot Degenerates	12
1.3.1 Evolutionary Models	12
1.3.2 Pulsation	13
1.4 The Scope and Plan of This Work	14
<u>Chapter 2.</u> Evolutionary Models of Post-Asymptotic Giant Branch Stars	
2.1 Background	16
2.2 Pure ^{12}C Models	17
2.3 Compositionally Stratified Models with Nuclear Burning	20
2.3.1 "Iben" Evolutionary Models	20
2.3.2 Other Models	21

2.4	Variation of Model Parameters	23
2.4.1	Luminosity and Effective Temperature	25
2.4.2	Stellar Mass	26
2.4.3	Equation of State	27
2.4.4	Composition	27
2.4.5	Neutrino Emission	28
2.5	Summary of Evolutionary Characteristics	29
2.5.1	Evolutionary Tracks	29
2.5.2	Luminosity Sources	32
2.5.3	Core Temperature Inversion	40
<u>Chapter 3.</u> Linear Adiabatic Nonradial Oscillations and Seismological Diagnostics		
3.1	Introduction	47
3.2	The Linearized Perturbation Equations	49
3.3	The Adiabatic Equations	51
3.3.1	The Adiabatic Approximation	51
3.3.2	The Dziembowski Formulation	52
3.3.3	Adiabatic Boundary Conditions	53
3.4	A Local Analysis: Propagation Diagrams	55
3.4.1	Dispersion Relation	55
3.4.2	The Propagation Diagram	56
3.5	Numerical Solution of the Adiabatic Equations	57
3.6	Variational Principle and Weight Functions	60
3.7	Rotational Splitting of the Eigenfrequency	63
<u>Chapter 4.</u> Adiabatic Oscillations of Hot Degenerates		
4.1	Introduction	65
4.2	Period Spectra and Eigenfunctions for DOV Models	66
4.3	Characteristic Mode Spacings	71
4.3.1	Period Spacing of g-Modes	74
4.3.2	Frequency Spacing of p-Modes	75

4.4 Weight Functions in the DOV Models	77
4.5 Adiabatic Periods in DBV Models	80
 <u>Chapter 5. Evolution of the Adiabatic Pulsation Properties</u>	
5.1 Introduction	86
5.2 Calculation of Rates of Period Change	87
5.3 Rates of Period Change for DOV Models	89
5.3.1 Pure ^{12}C Models	89
5.3.2 The Stratified DOV Sequences	97
5.4 Neutrino Emission and $d(\ln\Pi)/dt$	103
5.5 Effects of Spin-up and Rotational Splitting	107
5.6 Rates of Period Change for DBV Models	116
5.6.1 Numerical Results	116
5.6.2 Comparison With a Simple Cooling Model	117
5.7 Other Effects	123
 <u>Chapter 6. G-Mode Instabilities in PNN Models Driven By Nuclear Burning</u>	
6.1 Introduction	126
6.2 Linear Nonadiabatic Oscillations	127
6.3 An Integral Expression for the Stability Coefficient	128
6.3.1 The Work Integral	128
6.3.2 The ϵ -Mechanism	130
6.4 Numerical Results	131
 <u>Chapter 7. Pulsations in Hot Degenerates: Summary and Applications</u>	
7.1 Summary	139
7.2 Period Spectra as Seismological Indicators	140
7.2.1 The DOV Stars	141
7.2.2 DBV Stars	145
7.3 Rates of Period Change	146
7.3.1 DOV Stars	146

7.3.2 DBV Stars	147
7.4 Pulsations in PNN	149
7.5 Now What?	150
Appendix	154
A.1 The Cooling Rate of a White Dwarf Photosphere	154
A.2 Upper Limit to Rotation Effects on $d(\ln \Pi_{\text{obs}})/dt$	155
References	157
Vita	163

LIST OF TABLES

2.1	Summary of Evolutionary Sequences	24
4.1	Pulsation Periods for Sequence W60GC1C	67
4.2	Pulsation Periods for Sequence W78GC1C	68
4.3	Pulsation Periods for Sequence W95GC1C	69
4.4	Pulsation Periods for Sequence I60BC1Y	70
4.5	Characteristic Mode Spacings for DOV Models	76
4.6	Periods for the $k=25$, $l=2$ Mode in DBV Models	83
4.7	Characteristic Mode Spacings for DBV Models	85
5.1	Rates of Period Change for Sequence W60GC1C	90
5.2	Rates of Period Change for Sequence W78GC1C	91
5.3	Rates of Period Change for Sequence W95GC1C	92
5.4	Rates of Period Change for Sequence I60BC1Y	100
5.5	$d(\ln\Pi)/dt$ for Different Neutrino Emission Rates ($0.60M_{\odot}$, $l=1$, $k=25$)	106
5.6	Rotational Splitting Parameters for Pure ^{12}C $0.60M_{\odot}$ PWD Models (Sequence W60GC1C)	110
6.1	Periods and Damping Times for $l=1$ g-Mods in PNN Models	137
7.1	The Period Spectrum of PG1159-035	142

LIST OF FIGURES

1.1 Pulsating Degenerates in the H-R Diagram	5
2.1 Evolutionary Tracks for 0.60M _O PWD Models	31
2.2 Evolutionary Tracks for Pure ¹² C PWD Models	34
2.3a Luminosity as a Function of Time in 0.60M _O PWD Models	37
2.3b Contributing Luminosity Sources in a Stratified 0.60M _O PWD Model . . .	39
2.4 Luminosity vs. Age for Pure ¹² C PWD Models	42
2.5 Structural Properties of PWD Models	44
2.6 Central Temperature vs. Age for 0.60M _O PWD Models	46
3.1 A PWD Propagation Diagram	59
4.1 Eigenfunctions for $k=25$, $l=1$ Mode in 0.60M _O PWD Models	73
4.2 Weight Functions for $k=25$, $l=1$ Mode in 0.60M _O PWD Models	79
4.3 Running Integral of the Weight Functions	82
5.1 $d(\ln\Pi)/dt$ for Pure ¹² C PWD Models	94
5.2 Expanded Propagation Diagrams	99
5.3 $d(\ln\Pi)/dt$ for 0.60M _O PWD Models of Different Breeding	102
5.4 Effect of Neutrinos on $d(\ln\Pi)/dt$ in PWD Models	105
5.5 $d(\ln\Pi_{\text{Obs}})/dt$ vs. Luminosity in Rotating PWD Models	113
5.6 $d(\ln\Pi_{\text{Obs}})/dt$ vs. Rotation Rate for a PWD Model	115
5.7 Rate of Period Change vs. Effective Temperature in DBV Models	119
5.8 Same as Figure 5.7, but Plotted on Logarithmic Scales	122
6.1 The ϵ -Mechanism in Action in a PNN Model	132
6.2 Mode Selection in a PNN Model	136
7.1 Characteristic Period Spacing as a Function of Luminosity	144

CHAPTER 1

AN OVERVIEW OF STELLAR PULSATION IN POST-RED GIANT PHASES

1.1 Introduction

Most temporal astrophysical phenomena occur over timescales that are much longer than anything occurring within the usual circle of human experience. This is, by and large, a fortunate circumstance. For example, the fact that the sun's luminosity and temperature have remained essentially constant over the past five billion years has allowed life to develop and flourish on Earth. Yet, in everyday life, it is temporal change that relieves an otherwise tedious routine. Likewise, if *all* astrophysical phenomena remained constant over several human lifetimes, astronomy would be far less exciting than it has turned out to be.

Striking examples of temporal changes in astrophysics are the pulsating variable stars. These stars have captured the attention of amateurs and professionals alike for centuries. The first pulsating star to be identified was Mira (Omicron Ceti). Mira has been observed regularly since Fabricius discovered its variability in 1596 (Ledoux and Walraven 1958). This star varies in brightness by a factor of 250, falling from moderate naked-eye brightness to invisibility and brightening again, over a period of about 310 days. Mira is an intrinsically bright red giant star, with a radius of about $300 R_{\odot}$, but with a mass only about twice that of the sun, which pulsates in the radial fundamental (or first overtone) mode (Tuchman, Sack, and Barkat 1979, Willson 1979).

In modern times, pulsations with amplitudes of thousandths of a magnitude and periods of minutes have been accurately monitored with the sophisticated techniques of high-speed photometry, developed largely by R.E. Nather at the University of Texas (Nather 1972). In 1968, the first member of a second important

class of pulsating variable star was discovered using this technique when A. Landolt observed the first pulsating white dwarf, HL Tau 76 (Landolt 1968). A second similar variable, ZZ Ceti (R548), was discovered by Lasker and Hesser (1971), and lent it name to the new class of variable stars. Subsequent discoveries of additional ZZ Ceti stars indicate that they are the most numerous type of pulsating star in the Universe (McGraw 1977). In contrast to red giant stars such as Mira, white dwarfs are one of the most compact types of stars ($R \sim 10^{-2} R_{\odot}$, mean density $\sim 2 \times 10^5 \text{ g/cm}^3$). Also unlike the Mira variables, the ZZ Ceti stars are undergoing nonradial gravity-mode pulsation. As the name implies, this form of pulsation involves radial and horizontal mass motions with gravity as the restoring force. The periods associated with these pulsation modes are longer than the periods characteristic of radial pulsation; in the ZZ Ceti stars, the observed periods are between 100 and 1000 seconds, whereas the radial pulsation periods for cool white dwarfs are less than 10 seconds.

The observed variations of pulsating stars reflect periodic changes in the instantaneous structure of the star. Since most stars evolve on timescales of millions of years the pulsation properties, like other time-averaged properties of a star, are essentially constant over millions of pulsation cycles. Hence, though the study of pulsating variables involves temporal changes, variable stars do not usually show the effects of secular evolutionary changes in the structure of the star. Within this context, one could say that the periodic pulsation of the star is part of the "tedious routine."

Recently, however, a new class of pulsating variable stars has been identified that promises to provide direct observational evidence for stellar evolution. Several extremely hot DO degenerate dwarf stars have been reported to be multiperiodic pulsating variable stars. The first of these was PG1159-035, initially reported by McGraw *et al.* (1979). Other stars with similar spectra have been found to pulsate with similar periods: PG1707+427 and PG2131+066 have periods around 500 seconds (Bond *et al.* 1984). A related discovery by Grauer and Bond (1984) is that the central star of the planetary nebula K1-16 is a single variable star with periods of the order of 1700s. Spectroscopic evidence indicates that the central star of K1-16 (hereafter K1-16) has an effective temperature well in excess of 100,000K, making it one of the hottest stars known (Kaler and Feibelman 1985).

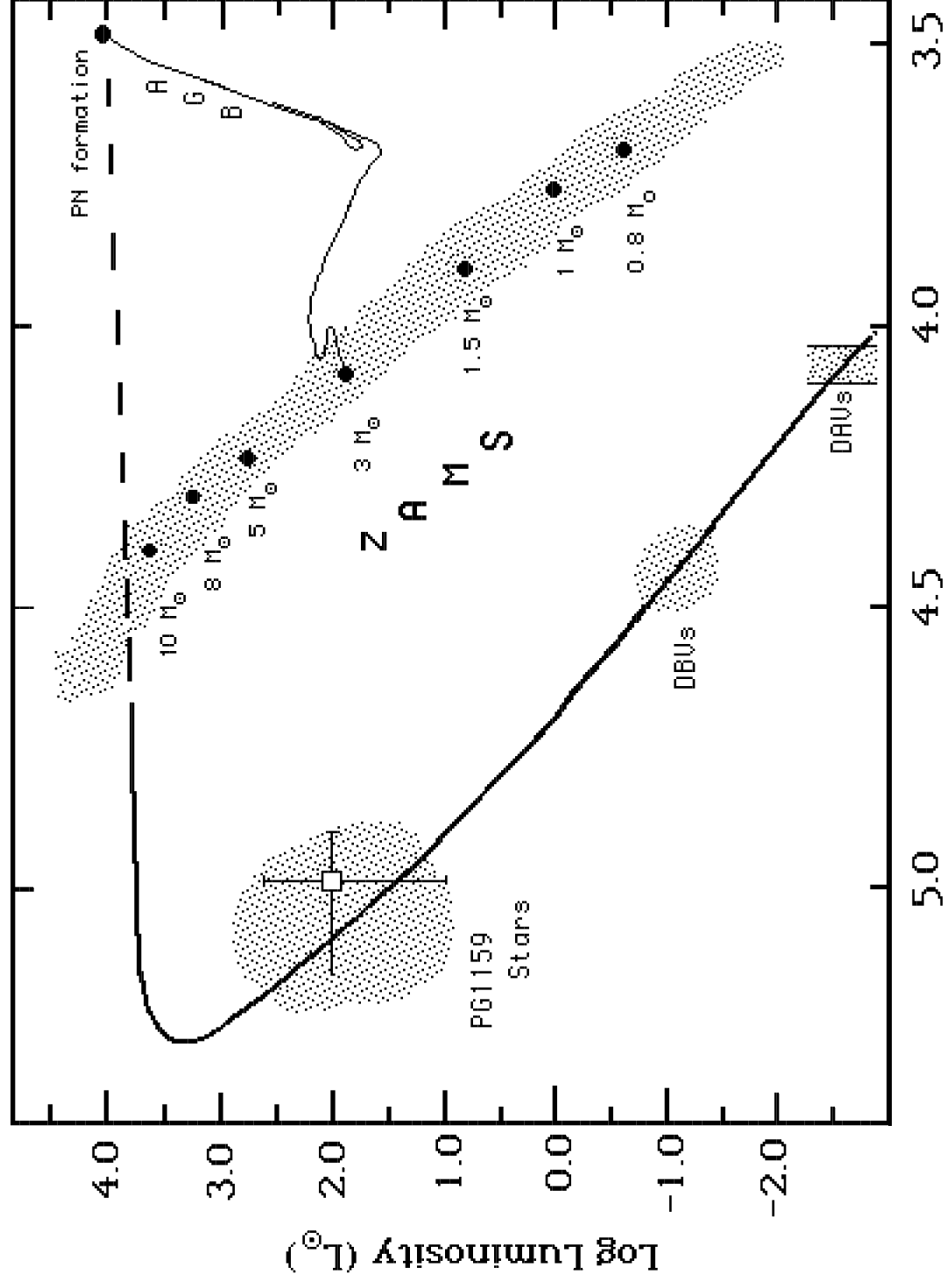
Since the pulsating PG1159 stars and K1-16 are hot degenerates, the observed pulsation periods are much longer than the expected radial pulsation periods (on the order of the dynamical timescale in hot white dwarfs, ~ 20 -50 seconds). This, along with the multiperiodic nature of their light curves, strongly suggests that, like the ZZ Ceti stars, they are undergoing nonradial g-mode pulsation. The initial theoretical investigations of stellar pulsation in this area, conducted by Starrfield and collaborators (Starrfield *et al.* 1983, 1984), support this interpretation of the luminosity variations. We will discuss the properties of nonradial oscillations in detail in Chapter 3.

The conclusion that hot degenerates are undergoing nonradial g-mode pulsations provides a direct connection with the two other classes of variable degenerates. We refer to these three classes of variable star using the classification scheme of Sion *et al.* (1983): the DAVs, or ZZ Ceti stars; the DBVs, or pulsating DB white dwarfs; and the DOVs, or pulsating PG1159-035 stars. The coolest of the variable white dwarfs, the hydrogen-rich DAVs, are found in a narrow, well defined instability strip at an effective temperature near 12,000K. The hydrogen deficient DBVs lie in a region near $\log(L/L_{\odot})=-1.3$ and $T_{\text{e}}=25,000\text{K}$. The relative location of the DOVs and DBVs in the H-R diagram, as well as their helium rich surface composition, are increasingly suggestive of a direct evolutionary connection between the two classes of objects (Sion *et al.* 1985). However, the current limits on the He/H ratio in the DOVs cannot rule out the possibility that the DOVs could be DA progenitors as well.

To discuss the evolutionary status of the hot degenerates, we begin with the "birth pang" of the luminous hot degenerate: the transition from an asymptotic giant branch (AGB) star to a PNN. In Figure 1.1, we indicate the general regions of the theoretical Hertzsprung-Russel diagram in which the pulsating degenerates are located. Also shown in Figure 1.1 is a representative evolutionary track for a $3.0M_{\odot}$ model from the zero-age main sequence to the AGB, and the evolutionary track for a $0.60M_{\odot}$ model from the PNN stage to the final white dwarf cooling phase. Following the exhaustion of helium in the core, intermediate mass stars (~ 2 - $8M_{\odot}$) move onto the AGB as they burn hydrogen and helium in thin shells surrounding a degenerate carbon/oxygen core. A very extended envelope containing roughly 80% of the mass of

Figure 1.1:

The regions of the H-R diagram occupied by the pulsating degenerates. Also shown is the zero age main sequence (ZAMS), with the representative positions of different mass main sequence stars indicated with solid dots. The thin line shows the evolutionary track for a $3.0M_{\odot}$ model from the main sequence to the asymptotic giant branch (AGB). The rapid phase of evolution of the $0.60M_{\odot}$ core that remains of the $3.0M_{\odot}$ AGB model following ejection of a planetary nebula is indicated by the dashed horizontal line; the model then rounds the knee and evolves as a white dwarf along the thick solid track. The error box indicates the probable position of PG1159-035 in the H-R diagram.



Log Effective Temperature (K)

the star surrounds the core (the proto-white dwarf) out to a radius of several astronomical units.

As hydrogen and helium are processed through the respective burning shells, the mass of the core increases and the star becomes more luminous. Two significant processes occur as the star evolves up the AGB. First, the mass loss rate increases as the star becomes more luminous, approaching rates of $10^{-5}M_{\odot}/\text{yr}$ (Knapp *et al.* 1982). Second, the rate of processing of material through the hydrogen-burning shell occurs at a much faster rate than through the helium burning shell, rendering the double-shell burning configuration thermally unstable. This instability, well studied theoretically (Iben and Renzini 1983 and references therein), leads to helium shell flashes on the AGB when the mass of helium deposited on the shell exceeds some critical value.

By some as yet unidentified mechanism, the steady mass loss plus possible dynamic effects during shell flashes combine to remove much of the extended envelope of the star over 10^4 to 10^5 years. When the mass above the hydrogen shell drops below about $0.01M_{\odot}$, the effective temperature of the star increases rapidly with further mass loss, and the star, reduced to only about 20% of its initial mass, departs from the AGB and evolves quickly across the H-R diagram. The star moves to the blue side at almost constant luminosity (at roughly the luminosity as at the time of departure from the AGB) because the time for evolution across the H-R diagram is very short. The material in the recently ejected envelope, along with additional material from the stellar wind, becomes ionized by the increasingly hot star, and the planetary nebula becomes visible. In many cases, the mass loss continues until helium-rich material below the extinguished hydrogen shell is uncovered, as evidenced by the existence of helium-rich planetary nebulae such as Abell 78 and Abell 30 (Jacoby and Ford 1983).

The lifetime of the PNN phase may be inferred from theoretical evolutionary calculations described below. Typically a $0.60M_{\odot}$ model will cover the horizontal portion of the evolutionary track in only about 10,000 years. The star rounds the "knee" and settles down on the PWD cooling track in Figure 1.1 as the luminosity from the shell burning source goes away. An independent estimate of the PNN

evolution rate can be obtained from the expansion rate of the nebula itself. Typically, the nebular expansion velocity implies that the surface brightness of the nebula will drop below detectability over roughly 25,000 years. Visibility of the central stars throughout the observed range in size of the nebulae suggests that the stars must remain bright over at least a similar length of time.

McGraw *et al.* (1979) pointed out that if PG1159-035 is a pre-white dwarf star that was once a PNN, then its rapid evolutionary changes in structure might be indirectly observable through observations of secular period changes. This suggestion was elaborated upon by Winget, Hansen, and Van Horn (1983, hereafter WHVH), who estimated that pulsating PG1159 stars should exhibit period changes with e-folding times (τ) of $\sim 10^6$ yr. With such relatively short timescales (by stellar standards) they proposed that τ could be measured over just a few observing seasons. In addition, their preliminary calculations, using crude subdwarf models, indicated that the rate of change of period ($d\Pi/dt$) for PG1159-035 should be negative; that is, its period should be decreasing with time. The recent determination of $d\Pi/dt = -1.2 \times 10^{-11}$ s/s for the 516s period of PG1159 (Winget *et al.* 1985) confirms those preliminary expectations.

The pulsating hot degenerates have already given us the first clear opportunity to study stellar evolution as a spectator sport. These stars, in effect, are changing before our eyes. Since they populate a region of the H-R diagram that at present has only been explored in a cursory manner, they present the unique opportunity to greatly refine the preliminary theoretical models of this rapid phase of stellar evolution. For example, the locations of the DBV and DOV stars in the H-R diagram are not precisely known, and thus do not place very tight constraints on the theoretical models (Winget *et al.* 1983). The introduction of an additional observational constraint, through the determination of rates of period change, will help relieve this situation. One of the goals of this work is to investigate this constraint in the context of the DOV and DBV stars, and their possible evolutionary connection.

We begin by reviewing the current state of the observational study of the pulsating degenerates in the next section. In Section 1.3, we review the relevant

previous theoretical explorations of stellar evolution and stellar pulsation. We conclude this chapter with an outline the particular issues to be addressed in this dissertation in Section 1.4.

1.2 Observations of Pulsating Degenerates

1.2.1 *Planetary Nebula Nuclei*

Central stars of planetary nebulae (PNNs) are currently the hottest "normal" stars known. In general, they lie in a region of the H-R diagram at temperatures from 60,000K to well above 100,000K, with luminosities ranging from $10L_{\odot}$ to $3000L_{\odot}$. Temperature determinations for these stars depend on the proper removal of nebular continuum and line emission from the stellar spectra. Often the central star temperature is estimated by use of the Zanstra method, which equates the amount of energy necessary to excite the observed nebular emission with the total energy output of the central star. Such temperature estimates are often considered only as lower limits to the stellar temperature (Kaler 1985), especially for high excitation nebulae.

The effective temperature and luminosity of K1-16 are very uncertain. The HeII Zanstra temperature for K1-16 as reported by Kaler (1983) is $>90,000\text{K}$ with a luminosity $\geq 2500L_{\odot}$. Further work by Kaler and Feibelman (1985) indicates a UV color temperature $>100,000\text{K}$, and perhaps as high as $400,000\text{K}$. The optical CIV absorption lines are perhaps somewhat narrower than those of the PG1159 stars (see below), suggesting a lower surface gravity for K1-16 (Sion *et al.* 1985).

Grauer and Bond (1984) reported that K1-16 is a photometric variable. The dominant peak in the power spectrum of the light curve is at a period of 1698s. The maximum amplitude of the light curve is about 0.01 magnitudes in white light. As Grauer and Bond indicate, if the 1698s peak is stable in amplitude and phase, it should be possible to measure its rate of period change in a relatively short time. Unfortunately, the 1698s period is apparently not very stable over the current observational time base (Grauer 1985, private communication). With a longer time baseline, a determination of $d\Pi/dt$ may be possible if the 1698s peak can be resolved.

1.2.2 Pulsating PG1159-035 Stars

The term "PG1159" stars as used in the literature actually describe a *spectroscopic* class of hot DO white dwarfs. Presently there are seven members of this class: PG0122+200, PG1151-029, PG1159-035, PG1424+535, PG1520+525, PG1707+427, and PG2131+066 (Wesemael *et al.* 1985). Spectroscopically, these stars show HeII lines in absorption (with possible narrow emission cores), and absorption lines of CIV and OVI (Wesemael *et al.* 1985, Sion *et al.* 1985). The uncertain width of the absorption lines, coupled with the probable existence of central emission components to the lines, makes identifications of the lines, and any analysis of the line profiles somewhat uncertain, rendering determination of the surface gravity of these objects very difficult. The best available model atmosphere analysis suggests a surface gravity of $\log(g) \geq 7$ (Wesemael *et al.* 1982, 1985). It is the apparent lack of surface hydrogen, coupled with high surface gravities, that implies an advanced evolutionary state for these stars.

The surface temperatures of the PG1159 stars are even more difficult to pin down than the surface gravities. Considerable evidence that they are extremely high, however, does exist. Temperature estimates for the prototype, PG1159-035, range from 80,000K to ~150,000K (Wegner *et al.* 1982). The energy distribution of PG1159-035 as measured with I.U.E. indicates an effective temperature of ~100,000K (Wesemael *et al.* 1985). Observations of the continuum in the 912—1150Å band with the ultraviolet spectrometer aboard Voyager 2 lead Barry *et al.* (1985) to estimate a temperature of $150(+40,-20) \times 10^3$ K for this star. A detection of PG1159-035 with the Einstein observatory also implies a very high surface temperature (McGraw *et al.* 1979). Barstow and Holberg (1985, private communication) observed PG1159—035 with EXOSAT, deriving a lower limit of $T_e=100,000$ K from the observed soft X-ray flux, and an upper limit of 125,000K from the amount of interstellar absorption. With these limits on the effective temperature and surface gravity of PG1159—035, and assuming these results are representative of the other stars in the class, the approximate location of the PG1159 stars in the H—R diagram is between the planetary nebula regime and the white dwarfs.

They are most likely rapidly evolving and cooling down into the white dwarf region of the H-R diagram.

Of the seven PG1159 stars, three have been found to be variables: PG1159-035, PG1707+427, and PG2131+066 (McGraw *et al.* 1979, Bond *et al.* 1984). The periods of pulsation in PG1707 are about 450s and 333s, while PG2131 shows a few peaks at around 400s in its power spectrum. The semi-amplitude of variation for these stars in the B band is about 0.017 magnitudes (Bond *et al.* 1984). This amplitude is typical for all pulsating degenerates.

The most comprehensively observed of these DOV stars is PG1159-035. The light-curve of PG1159-035 shows the well-known effects of beating between modes of similar period. Winget *et al.* (1985) performed a very detailed analysis of the power spectrum of PG1159, and showed that at least 8 periods are simultaneously present in the light curve. Of these, periods of 516.0s, 538.9s, 451.5s, and 495.0s are the strongest; other lower amplitude peaks are at 831.7s, 645.2s, 424.4s, and 390.0s. Only the 516.0s period was found to be stable both in phase and amplitude over the entire baseline of observations. The maximum amplitude of the variation is about 0.01 magnitudes, in white light. Using EXOSAT, Barstow and Holberg (1985, private communication) found periodic modulations of the flux in the soft X-ray band (44-150Å). The most significant period (at the 3σ level) in their data was around 516s, with a semi-amplitude of 0.15 magnitudes.

A very important result of the work by Winget *et al.* (1985) is their determination of the rate of period change for the 516s period of PG1159-035. They found the period to be decreasing at the rate of $dP/dt = -(1.21 \pm 0.12) \times 10^{-11}$ s/s. As discussed in WHVH, a decreasing period implies that the effects of residual contraction are important to the observed oscillation spectrum (see Chapter 5).

1.2.3 *The DBV Stars*

Winget and collaborators began the search for the DBV stars to follow up on the suggestion, based on theoretical arguments (Winget 1981, Winget *et al.* 1983), that

certain DB white dwarfs should be nonradial g-mode pulsators. This search resulted in the discovery of the first DBV, GD358, in 1982 (Winget, Robinson, Nather and Fontaine 1982). The power spectrum of GD358 is very complex, with about 28 periods simultaneously present in the light curve. The grouping of periods in the power spectrum suggests possible rotational splitting (see Chapter 3) of several $l=2$ modes into their five m components.

Three other DBV stars have been found so far: PG1654+160 (Winget, Robinson, Nather, and Balachandran 1984), PG1351+489 and PG1115+158 (Winget, Nather and Hill 1986). The light curve of PG1351+489 is consistent with only two periods, dominated by a single, large amplitude (0.07 mag) peak at 489s. The non-sinusoidal pulse shape results in several harmonics of the 489s period in the power spectrum (Hill 1985, private communication). The amplitude of white-light variations for PG1351 is about 0.02 magnitudes. PG1115+158 has periods of about 1100s, with an amplitude of about 0.01 magnitudes, but the pulsations may be unstable (Winget, Nather and Hill 1986).

An initial estimate of the effective temperature of GD358 was made by Koester, Weidemann and Vauclair (1983) using the low resolution spectrophotometer of the IUE satellite; they obtained $T_e=26\pm 2\times 10^3\text{K}$. Another estimate for the effective temperature was made by Oke, Weidemann, and Koester (1984) on the basis of optical multi-channel spectrophotometry using the 5-meter Hale telescope. Most recently, the effective temperature has been re-determined by Koester *et al.* (1985). They used all the data from the two previous investigations and incorporated additional optical data, combined with new model atmosphere calculations, to arrive at $T_e=24\pm 1\times 10^3\text{K}$, and $\log(g)=8.0\pm 0.3$. The temperature scale for the DB stars, has also been discussed by Liebert *et al.* (1986) based on I.U.E. observations alone. Their temperature determinations for the DB stars are somewhat higher. A comparison of I.U.E. and optical data is discussed by Koester *et al.* (1985). The actual position of the instability strip for the DBV stars remains somewhat uncertain, although it is clear that it is contained within the range from 20,000K to 30,000K.

1.3 Summary of Previous Theoretical Work on Hot Degenerates

1.3.1 *Evolutionary Models*

The interior structure of pre-white dwarf stars ("PWDs") may be inferred from what is known of their possible progenitors and their descendants, the white dwarfs ("WDs"). One attractive possibility is that the progenitors of the PG1159 stars are the nuclei of planetary nebulae. The evolution of PNN has been studied from a theoretical standpoint by several investigators (Paczynski 1971; Iben 1982, 1984; Iben and Tutukov 1984; Kovetz and Harpaz 1981; Schönberner 1979, 1981, 1983) but several basic questions remain.

PNN are assumed to be the hot cores of low mass asymptotic giant branch stars which have ejected most of their hydrogen rich envelopes during the planetary nebula formation phase. Early evolutionary calculations by Paczynski (1971) showed the evolution of the remnant cores of red giants to high effective temperatures, at constant luminosity. Such evolutionary tracks pass through the region of the H-R diagram populated by the PNNs. By altering the amount of hydrogen and helium-rich material remaining in the envelope following nebula ejection, Iben (1984) demonstrated a variety of evolutionary possibilities for PNN models. His models go through various phases of shell helium and hydrogen burning before reaching the PWD phase. Schönberner (1979, 1981, 1983) has also followed the evolution of AGB stars by including a Reimers-like stellar wind. His models also experience episodes of shell burning following nebular ejection while evolving through the PNN phase to a PWD configuration.

The results of these various investigations of PNN evolution bear a qualitative resemblance as a result of the similarities in the structure of the degenerate cores of the models. The basic model of a $0.60M_{\odot}$ PNN consists of a hot, mostly degenerate core of about $0.58M_{\odot}$. The combined effects of energy loss by neutrino emission and nuclear shell burning of helium and, perhaps, hydrogen produce one or more temperature inversions in the core. The maximum temperature of the core is not at the center, but at about half way out in mass because the deep interior of the model is

cooled by neutrino emission. There can also be a second temperature inversion between that point and the nuclear burning shell. Since the time scale for temperature change in the degenerate core is 10 to 100 times longer than the e -folding time for changes in luminosity (the evolutionary timescale), this residual thermal structure is retained through the PWD phase.

On the other hand, the thermal timescale for the outer layers is of the same order as the e -folding time for luminosity. Therefore, the details of shell flashes and mass loss in the AGB phase, and of nuclear burning on the remnant core, are important for determining the compositional and thermal structure of the outer layers of the PNN model at the approach to the PWD phase. While the properties which affect pulsations in the high luminosity phases may be sensitive to the uncertainties of PNN evolution, these uncertainties should diminish in importance (through thermal relaxation) as the model cools.

1.3.2 *Pulsation*

Some preliminary work on the pulsation properties of hot white dwarf models appropriate to PG1159 has been reported by Starrfield *et al.* (1983, 1984). Their studies, employing static stellar envelopes based on published evolutionary tracks of PWD models, show that partial ionization of oxygen and/or carbon at $\sim 10^{-10} M_{\odot}$ below the surface can drive high overtone nonradial g -modes. This work indicates that the blue edge of the corresponding instability strips are very sensitive to the thermal structure and composition. Pure carbon envelopes show a blue edge at $T_e < 100,000$ K, while static envelopes with a composition of half carbon and half oxygen show a blue edge at $T_e > 150,000$ K. Many periods in the range from ~ 400 -800 seconds were found to be unstable, in good agreement with the observed periods. One difficulty, however, with carbon or oxygen partial ionization driving is the presence of significant amounts of helium in the observed spectrum. Theoretical models with such compositions show the effects of helium "poisoning," and are found to be more stable (Pesnell 1984, private communication).

The same authors conducted an investigation of more luminous models

appropriate to K1-16 (Starrfield *et al.* 1985). In that study, they searched for instabilities in periods that were of order 1000-4000 seconds. They found such instabilities in models with homogeneous compositions of half carbon and half oxygen, with the longest unstable periods in models at around 155,000K and 2000 L_{\odot} . The region of peak driving in these models was found to be at a mass of $\sim 10^{-8}M_{\odot}$ below the surface, and is attributed to the cyclical ionization of oxygen.

1.4 The Scope and Plan of this Work

The recently demonstrated measurability of the rate of period change, and therefore the rate of evolution, in objects representing the transitory phase of stellar evolution between PNNs and WDs places new demands on stellar models and the physics that goes into them.

Throughout the DOV phase, and in the hotter parts of the DB instability strip, the plasmon neutrino energy losses are a significant fraction of the photon luminosity of the star. The rate of evolution of a cooling PNN is, therefore, controlled to a large extent by neutrino energy loss. As shown by WHVH, a measurement of the rate of change of the pulsation period of a variable degenerate is a direct measurement of the cooling and contraction rates in the region of the star where the period is determined. Thus observations of $d\Pi/dt$ may put interesting limits on the theoretically determined plasmon neutrino emission rates.

Observational measurement of $d\Pi/dt$ will provide a sensitive probe of the structure and evolution of DB white dwarfs. The cooling rate is a monotonic function of the effective temperature. By comparing the observed value of $d\Pi/dt$ for a DBV star with the results of pulsation calculations using evolutionary models of $0.60M_{\odot}$, we can place independent constraints on the effective temperature of the star.

This dissertation is an attempt to create a self-consistent theoretical framework of evolutionary models within which we can interpret observations of the hot pulsating white dwarfs. We examine the effect of the physics peculiar to the PNN and PWD models; the temperature inversion caused by neutrinos and the effects of nuclear

burning in particular are especially important. Chapters 3-5 explore the dependence of the adiabatic pulsation properties (such as the period spectrum and $d\Pi/dt$) on quantities such as stellar mass, composition, evolutionary phase, rotation, and neutrino emission. In Chapter 6, we examine the nonadiabatic properties of the evolutionary models. We identify the nuclear burning shell as a region of the model that contributes to vibrational instability. Finally, we will be able to comment on the evolutionary status of the DOV and DBV stars based on the results of this investigation.

"Any fool can make a white dwarf."

-Icko Iben, Jr.

CHAPTER 2

EVOLUTIONARY MODELS OF POST-ASYMPTOTIC GIANT BRANCH STARS

2.1 Background

To study the pulsation properties of PNN and PWD models, we require self-consistent evolutionary models which represent their important physical properties. In particular, models of early PWD stars should reflect the thermal structure of their PNN progenitors. That structure determines, to a great extent, the period spectrum. Because of the difficulties and uncertainties in modelling evolutionary histories of stars in their later stages, certain assumptions and approximations must be made. These are discussed below.

To establish the sensitivity of the pulsation results to the details of the input physics, we have constructed several PNN and PWD evolutionary sequences with different physical properties. For the study of the effects of stellar mass and neutrino emission, we constructed PWD sequences of pure ^{12}C composition for masses of $0.40M_{\odot}$, $0.60M_{\odot}$, $0.78M_{\odot}$, and $0.95M_{\odot}$. For the study of the effects of surface layer composition and nuclear burning, we used the evolutionary codes of Iben (1984); we also used a modified version of the code by Paczynski (1970,1974) to construct models of PNN with active nuclear shell burning regions, and PWD in which shell burning is negligible. We computed models of pure ^{12}C composition using an evolutionary code designed for the detailed study of white dwarf evolution employing the best current equation of state (Winget, Lamb and Van Horn 1993). The Iben models include a sophisticated treatment of the effects of nuclear shell burning through prior evolutionary phases. The easily modified Paczynski code allows us to explore

the effects of varying fundamental parameters such as core composition, neutrino emission, and total stellar mass, in an economical way. Taken together, these models form a framework of equilibrium models for pulsation analysis that will allow us to interpret observations of the pulsating degenerates.

In the following sections of this chapter we present the details of the models used for the pulsation analysis. We present the details of the the input physics and computational techniques in Sections 2.2 and 2.3. We exploit the systematic variations in the physical properties of the resulting evolutionary sequences in the manner outlined in Section 2.4. Finally, we review the evolutionary properties of the PNN and PWD models in Section 2.5.

2.2 Pure ^{12}C Models

We used an updated version of the Lamb and Van Horn (1975) white dwarf evolution code (WDEC) to produce evolutionary models of pure ^{12}C PWDs for the pulsation study. This code solves the equations of stellar evolution using the usual Henyey-type relaxation algorithm. The interior model contains shells up to a mass where gravitational contributions to the luminosity are negligible and the static envelope approximation is valid. Typically, the last mass shell was at $q_S(\equiv[1-M_r/M_*]) = 2 \times 10^{-5}$. The outer boundary conditions were obtained by interpolation, within a grid in the $\log(R), \log(L/L_0)$ plane, of static envelopes integrated from the surface down to q_S . These envelopes were calculated with a modified version of the white dwarf envelope code described by Fontaine and Van Horn (1976). To minimize the number of envelopes retained in computer memory, the evolution code employs the method of moving triangles described by Kippenhahn, Hoffmeister and Weigert (1967). (In the preparation of equilibrium models for the pulsation analysis, static envelopes with the appropriate luminosity and radius for the core were integrated using a version of the white dwarf envelope code and fit to the interior models.)

In the degenerate core this code uses the equation of state described in detail in Lamb (1974). This equation of state accurately includes the effects of Coulomb

interactions between the ions and electrons and other non-ideal effects important to white dwarf evolution at PWD and later stages. The negative correction to the internal energy due to Coulomb effects increases in magnitude with decreasing temperature and results in a gradual increase in the specific heat of PWD interiors (Lamb 1974, Lamb and Van Horn 1975). Therefore, with these effects taken into consideration in a self-consistent way, models of PWD stars can be expected to cool slightly more slowly than standard PNN studies (Iben 1984) have indicated when nuclear burning is not important.

Although we did not include nuclear burning in these models, we do include energy losses by neutrino emission. We calculate rates of neutrino emission via the plasmon, pair, photo- and recombination neutrino processes using the analytic formulae of Beaudet, Petrosian and Salpeter (1967). We follow the method of Festa and Ruderman (1969) to calculate the rate of bremsstrahlung neutrino emission. We compare the validity of these neutrino emission rates with more modern rates (Munkata *et al.* 1985) in Section 2.4.5.

For the envelope calculations, we base our equation of state on that tabulated by Fontaine *et al.* 1977 (FGVH) for a Weigert V (0.999 ^{12}C by mass) composition. Early in this investigation we found an inconsistency in this equation of state. Apparently an ionization stage was left out of the original FGVH equation of state for carbon partial ionization. This error, although incorporated in FGVH, is an artifact of the original Livermore equation of state which formed a basis for the equation of state compiled by FGVH. In the region of carbon partial ionization under non-degenerate conditions the FGVH equation of state does not give self-consistent values for interpolated quantities. In the un-ionized and fully ionized states, as well as when degenerate and partially ionized, the FGVH equation of state appears self-consistent. We have recalculated the equation of state in the region of difficulty and incorporated the corrections into the remainder of the FGVH tables.

The hot envelopes of the PWD models made it necessary to extend the bounds of the equation of state tables at the low density, high temperature edge. To make these corrections and extensions, we used a perfect gas–radiation equation of state,

adding analytic electrostatic corrections as described by Cox (1968, Chapter 15). We note that the results of the investigation of the adiabatic pulsation properties are not at all sensitive to any resulting inconsistencies in the envelope equation of state in this regime; the mass of envelope material involved is always less than $10^{-8}M_{\odot}$. The mass in the surface convection zone was always less than $10^{-10}M_{\odot}$. These layers are well outside the region of period formation for the modes of interest (see Chapter 4).

One of the goals of this work is to explore the importance of the peculiar thermal structure of PWD stars on the pulsation properties. To isolate this effect from uncertainties in nuclear burning and surface composition, we did not include any nuclear burning in the pure ^{12}C models. However, we required starting models for the ^{12}C PWD calculations that accurately represent the prior history of AGB evolution, including the thermal structure appropriate to helium shell burning. For this purpose, we selected initial models for ^{12}C PWD evolution from the early parts of a PNN sequence calculated using the modified Paczynski code (see Section 2.3.2). The core of the starting models is about 90% carbon and 10% oxygen, and is surrounded by a thin ($0.02M_{\odot}$) shell of helium. Because of the high energy loss rates from neutrino emission in these hot evolutionary stages, the inner core shows a pronounced temperature inversion. In addition, the $0.60M_{\odot}$ model has a secondary temperature maximum at the position of the helium burning shell source.

The switch from the chemically inhomogeneous PNN models to the pure carbon PWD models necessitates some thermal relaxation to compensate for the slight change in the equation of state and opacities. At the epoch of the change in equation of state, the thermal timescale of the envelope (or, rather, the surface helium layer of mass ΔM),

$$\tau_{\text{th}} = \int_0^{M^*} (c_{\text{v}}T/L) dm = \langle c_{\text{v}}T \rangle \Delta M/L \quad (2.1)$$

(where L is the photon luminosity), is on the order of the evolution timescale (~ 1500 years) through the rapid contraction phase. Therefore, relaxation to the new equation of state is accomplished by the time the sequence reached the PWD cooling track.

To demonstrate the importance of energy loss by neutrino emission, we constructed two additional pure ^{12}C sequences with suppressed neutrino emission. One of the sequences was evolved with neutrino emission rates reduced by a factor of two, while the other included no neutrino emission. To retain consistency with the WDEC calculation that included neutrinos, the starting models for these sequences are from PNN sequences constructed with the Paczynski code that descended from AGB models with the corresponding reduction in neutrino emission. The construction of the starting models is described in more detail in Section 2.3.2.

2.3 Compositionally Stratified Models with Nuclear Burning

Although the pure ^{12}C models are not completely realistic, they allow us to explore the dependencies of pulsation properties on physical properties such as total stellar mass in a systematic way. As far as we know, a PNN is chemically inhomogeneous, with a core composed of the ashes of helium burning surrounded by an active helium shell source, and, in some, "topped" with a hydrogen shell source and a thin envelope of primordial composition. In the detailed study of PNNs the effects of nuclear burning and compositional structure are very important to the nonadiabatic analysis. For these reasons, we have constructed PNN - PWD models with which to explore these physical properties. The stars under consideration exhibit spectra with lines of helium, carbon, and oxygen. There is no evidence for hydrogen at the surface of the DOV and DBV stars; hence we will restrict our examination to models without surface hydrogen layers (but see Chapter 7).

2.3.1 *"Iben" Evolutionary Models*

Two sequences of helium-rich PNN models have been produced using the stellar evolution code of Icko Iben, Jr. (1975, 1976, 1983). The current version of this code was generously provided by Dr. Iben during his visit to the University of Texas in February 1985. For one of the two sequences, the equation of state includes Coulomb interactions, using the analytic treatment described in detail in Iben and Tutukov (1984). To judge the importance of these non-ideal effects, we calculated a parallel sequence without including the Coulomb interactions. Energy generation by

nuclear burning of helium (Fowler, Caughlan and Zimmerman 1975), and energy loss by neutrino emission (Beaudet, Petrosian and Salpeter 1967, and Festa and Ruderman 1969) are included in these sequences. The mass included in the surface layer integrations was reduced to $10^{-12} M_{\odot}$ for this study. This permits us to use just the interior of the evolutionary models in the pulsation analysis without loss of accuracy, since the region of period formation is well below $10^{-12} M_{\odot}$ for all modes of interest (see Section 4.4).

The starting model for these stratified sequences is a hydrogen deficient $0.60 M_{\odot}$ PNN model at $\log(L/L_{\odot})=3.5$, (Iben 1984, Figure 8). This model has a $0.02 M_{\odot}$ helium envelope, and a core composition of 55% carbon and 45% oxygen, by mass. Details of the prior evolutionary history of this model can be found in Iben (1983,1984). While this model does not include the effects of Coulomb interactions in the equation of state, the Coulomb effects were added at the beginning of the sequence. Since such effects are quite small at this high luminosity the model relaxed to the new equation of state almost immediately.

2.3.2 *Other Models*

To produce starting models for the WDEC sequences, we used a modified version of the evolution code of Paczynski (Paczynski 1970,1974, Kawaler 1982). The PNN models produced with this code also provide us with an independent set of compositionally stratified PNN models with an active helium burning shell source. We will compare these models with the Iben sequences to test the sensitivity of the pulsation results to the details of the evolutionary model construction and input physics.

This code uses the equation of state for an ideal, ionized, arbitrarily degenerate plasma for both the interior and envelope (Paczynski 1969,1970). The equation of state does not include any non-ideal effects such as Coulomb interactions. Neutrino emission, when included, is calculated using the prescriptions of Beaudet, Petrosian and Salpeter (1967) and Festa and Ruderman (1969). Nuclear reaction rates for burning of hydrogen and helium are from Harris *et al.* (1983), with screening effects

included (Salpeter and Van Horn 1969). As in WDEC, the method of triangles was used for obtaining outer boundary conditions for the stellar interior calculations. In the PNN phase, $0.0001M_{\odot}$ was left in the static envelope calculations. These envelopes were integrated using our version of the stellar envelope code described in detail in Paczynski (1969). To prepare these models for the pulsation calculations, we re-fit a static envelope of $0.0001M_{\odot}$ to the core using the same envelope code.

This code uses tabular interpolation for all constitutive relations and nuclear burning rates, allowing very inexpensive calculation of extensive evolutionary sequences. This allowed us to evolve a model from the zero-age main sequence to the thin double shell burning phase very economically. To produce the eventual PNN model, we have evolved spherical, nonrotating main sequence Population I composition models of $3.00M_{\odot}$, $4.25M_{\odot}$ and $5.00M_{\odot}$ up into the AGB phase. Once the mass in the shell burning region became sufficiently small ($\sim 0.02M_{\odot}$) we removed most of the convective envelope of the model, comprising roughly 80 percent of the original stellar mass. Removal of mass from the AGB model was done in stages, with sufficient time allowed for the models to relax thermally following each reduction in mass. The final masses for the 3.0, 4.5, and $5.0M_{\odot}$ models were 0.60, 0.78, and $0.95M_{\odot}$ respectively. Typically, less than $0.01M_{\odot}$ of hydrogen remained above the hydrogen shell source.

For the hydrogen deficient models, the final episode of mass stripping was the removal of mass down to the helium rich region below the hydrogen shell. This resulted in an initial drop in luminosity, which was followed by a return to the previous luminosity after a few time steps, as the helium shell source adjusted to the new configuration.

In the models to be used as starting models for the pure ^{12}C sequences of Section 2.2, nuclear burning in the resulting PNN models was artificially turned off as the models evolved across the PNN regime towards the constant-radius WD cooling track. Note, however, that the thermal timescale of the degenerate core is sufficiently long that the thermal structure resulting from the prior evolution is "remembered" for long periods of time, and is therefore incorporated in the pure carbon models.

To illustrate the importance of neutrinos to the pulsation and evolutionary properties, we produced a $0.60M_{\odot}$ PNN sequence with neutrino emission rates reduced by a factor of two, and one with no neutrino emission. Simply turning off neutrinos in a PNN whose parent included neutrinos does not change the thermal structure in a consistent way. In standard stellar models, the central temperature inversion resulting from neutrino energy losses is established on the AGB over several million years. Since the PNN evolves so rapidly, compared to the thermal timescale of the core, the temperature profile of the core is almost unchanged through the PNN phase. Therefore, the parent model of the PNN must be evolved with the desired neutrino rates. To ensure this self-consistency in the treatment of the temperature profile of the core, the parent model for these sequences were $3.00M_{\odot}$ asymptotic giant branch models evolved with reduced neutrino emission from the time of core helium exhaustion. The outer $2.40M_{\odot}$ of the AGB models were then removed following the procedure outlined above, leaving $0.60M_{\odot}$ PNNs to evolve towards the PWD phase with interior thermal structures consistent with reduced neutrino energy losses.

2.4 Variation of Model Parameters

The philosophy of this investigation is to exploit the observed pulsation characteristics of PWDs and PNNs in order to explore the current areas of uncertainty in hot white dwarf structure and evolution. We accomplish this by systematically varying one parameter of a model at a time to see the effects on the pulsation properties of the star. We adjust the parameters within the limits of our knowledge (or ignorance) based on observation of PNNs and PWDs and, in some cases, on very clear theoretical arguments. In this section we summarize the models used in the pulsation study.

We have produced models with the three evolution codes described earlier in this section that vary in total stellar mass, composition, treatment of nuclear burning, equation of state, and assumed rate of energy loss by neutrino emission, as shown in Table 2.1. Of course, the evolution of the model within the sequence provides models

Table 2.1
Summary of Evolutionary Sequences

<u>Name</u>	<u>M/M₀</u>	<u>Code</u>	<u>Surface</u>	<u>Burning</u>	<u>E.O.S.</u>	<u>Neutrinos⁸</u>
W40GC1C	0.40	WDEC ¹	Pure ¹² C	No	Coulomb ⁴	BPS+FR
W60GC1C	0.60	WDEC	Pure ¹² C	No	Coulomb ⁴	BPS+FR
W60GC2C	0.60	WDEC	Pure ¹² C	No	Coulomb ⁴	1/2(BPS+FR)
W60GC0C	0.60	WDEC	Pure ¹² C	No	Coulomb ⁴	not included
I60BC1Y	0.60	Iben ²	0.02M ₀ He	Yes	Coulomb ⁵	BPS+FR
I60BI1Y	0.60	Iben	0.02M ₀ He	Yes	Ideal ⁶	BPS+FR
P60BI1Y	0.60	Pacz ³	0.02M ₀ He	Yes	Ideal ⁷	BPS+FR
P60BI2Y	0.60	Pacz	0.02M ₀ He	Yes	Ideal ⁷	1/2(BPS+FR)
P60BI0Y	0.60	Pacz	0.02M ₀ He	Yes	Ideal ⁷	not included
W78GC1C	0.78	WDEC	Pure ¹² C	No	Coulomb ⁴	BPS+FR
W95GC1C	0.95	WDEC	Pure ¹² C	No	Coulomb ⁴	BPS+FR

-
1. Lamb (1974), Lamb and Van Horn (1975)
 2. Iben (1984), Iben and Tutukov (1984)
 3. Paczynski (1970,1974), Kawaler (1982)
 4. Lamb (1974), augmented Fontaine, Graboske and Van Horn (1977)
 5. Iben and Tutukov (1984)
 6. Iben (1975,1976)
 7. Paczynski (1969,1970)
 8. Beaudet, Petrosian and Salpeter (1967); Festa and Ruderman (1969)

of different luminosity and effective temperature. The nomenclature used to describe the various evolutionary sequences is as follows. Sequence names are of the form P60BI1Y: the first letter gives the code used for calculating the sequence (P=modified Paczynski, I=Iben, W=WDEC), the next two digits are the total stellar mass, in solar units $\times 100$. The two letters following the mass indicate the treatment of nuclear burning (G=contraction and cooling only, B=burning included) and the equation of state (I=ideal, arbitrarily degenerate gas, C= Coulomb and/or other nonideal effects included). The next entry is a digit that tells the factor by which the neutrino emission rates are multiplied (1=standard value, 0=neutrinos not included, 2=neutrinos cut by a factor of 2). The final letter describes the composition of the stellar envelope (X=hydrogen and helium around a C/O core, Y=helium around a C/O core, C=pure ^{12}C). Hence the P60BI1Y sequence is a modified Paczynski model of $0.60M_{\odot}$ that includes nuclear burning, uses an ideal gas equation of state, employs standard neutrino energy loss rates, and has a helium-rich envelope.

Each of the evolution codes has its own advantages and disadvantages. The WDEC employs the best available equation of state, but only in calculating a pure ^{12}C model with no nuclear burning. The Iben models treat nuclear burning and composition transition zones carefully, but are very expensive to compute. Also, the Iben equation of state does not allow for partial ionization of elements heavier than helium. The modified Paczynski models have the virtue that the mass and composition in the outer layers are easily varied, as are the nuclear burning and neutrino rates; however, these models employ a greatly simplified interior equation of state. We can take advantage of the individual strengths of these codes to explore a wide range of parameters of the real stars, and to pinpoint the reasons for different pulsation results from different models.

2.4.1 *Luminosity and Effective Temperature*

As outlined in Chapter 1, the effective temperatures and luminosities of the DOV and DBV stars are uncertain, demanding that we consider models spanning large ranges in these quantities. We have computed many PNN-PWD sequences, each of

which spans large regions in the H-R diagram around the "knee" and down into the cooler WD regime. The effective temperatures of these models range from approximately 100,000K to the maximum temperature of 200,000K, and then down to 20,000K in the DBV region. Luminosities range from $\log(L/L_{\odot})=3.5$ down to about $\log(L/L_{\odot})=-2.0$.

We concentrate on three regions of the H-R diagram that are known to contain variables. For the variable PNNs, we used models surrounding the point of maximum effective temperature. For the pulsating PG1159 stars, models in the luminosity range of about $\log(L/L_{\odot})=2.8$ to 1.0 are most appropriate. Models with effective temperatures between 20,000K and 30,000K are used to represent the DBV stars.

2.4.2 *Stellar Mass*

For PNN, the mass limits are constrained by the extreme mass dependence of the timescale for crossing the H-R diagram from AGB-like temperatures to 10^5 K (Paczynski 1971, Schönberner 1979,1981). Iben (1984) has pointed out that this timescale is inversely proportional to the mass of the star to the tenth power. The vast majority of hot degenerates with detectable nebulae must have masses of around 0.56 - $0.64M_{\odot}$ based on the lifetimes of the associated nebulae. Based on his models, Schönberner indicates a lower limit of $0.55M_{\odot}$ (1983, also Drilling and Schönberner 1985). Since K1-16 has an associated nebula, the most appropriate mass to consider for that star is $0.60M_{\odot}$. However, the same constraint is not necessarily applicable to the DOV stars with no associated nebulae, such as PG1159, and for those variables the effects of stellar mass on the pulsation properties must be explored (although see below).

We have constructed parallel pure ^{12}C sequences of $0.40M_{\odot}$, $0.60M_{\odot}$, $0.78M_{\odot}$, and $0.95M_{\odot}$ (W40GC1C, W60GC1C, W78GC1C, W95GC1C). The starting model for the W40GC1C sequence was the same as for the $0.60M_{\odot}$ sequence, but was homologously transformed down to $0.40M_{\odot}$. This model does not reach thermal equilibrium until a luminosity of $200L_{\odot}$, and therefore is probably only useful for PG1159 and DBV studies. Observationally, the mass distribution of single white

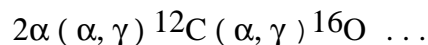
dwarfs is quite narrow, and centered on $0.6M_{\odot}$ (Weidemann and Koester 1983, 1984). For this reason our emphasis will be on models of $0.60M_{\odot}$.

2.4.3 Equation of State

Each of the evolution codes that we have used employs a different treatment of the equation of state. As a result we can expect that differences in the pulsation properties between sequences will be partly caused by equation of state differences. To help understand the influence of the non-ideal effects, we have calculated two parallel PNN-WD sequences of Iben models. In one, we use the perfect degenerate ionized gas equation of state (I60BI1Y), while in the second sequence (I60BC1Y) we include the modifications due to Coulomb interactions (Iben and Tutukov 1984).

2.4.4 Composition

The core composition of a PWD is determined by the reactions of helium burning:



The relative abundances of ${}^{16}\text{O}$ and ${}^{12}\text{C}$ depend sensitively on the core helium burning conditions, and on the history of helium shell flashing. The Iben models have cores of about 55% carbon and 45% oxygen, while the modified Paczynski models are close to 90% carbon and 10% oxygen reflecting differences in the treatment of nuclear burning in the two codes.

The envelope composition of PNN and PWD depends on the stage at which the star leaves the AGB, as well as the details of mass loss in the constant luminosity phase of PNN evolution. As illustrated by the calculations of Iben (1983,1984), the amount of helium between quiescent nuclear shell sources on the AGB is sensitive only to the stellar luminosity. This relationship has also been noted for the modified

Paczynski AGB sequences of this work. At the time the AGB core reaches $0.60M_{\odot}$, the helium layer mass is about $0.02M_{\odot}$. For a core in the PNN region of high effective temperatures, the mass of hydrogen above the helium shell is less than $\sim 0.005M_{\odot}$. Since the observed DOV and DBV stars are strongly hydrogen deficient, we consider models which have lost all of their surface hydrogen during the transition from AGB star to PNN. The initial mass of the surface layer of helium for the stratified sequences is taken as the amount of helium left following the departure from the AGB. The composition transition zone structure is assumed to be unaffected by diffusion, as the evolutionary timescale for these stars is much shorter than the relevant diffusion timescales (Fontaine and Michaud, 1979, Iben and McDonald 1985) in the DOV range; in the DBV range, this treatment is unrealistic. We will show that the pulsation properties of DBV models are sensitive to the envelope composition. Diffusion would increase the width of the carbon-helium transition layer slightly, emphasizing somewhat the differences that we find between the pure carbon and stratified sequences.

2.4.5 Neutrino Emission

As discussed in Sections 2.2 and 2.3, the neutrino energy loss rates used in the construction of the evolutionary models are those derived by Beaudet *et al.* (1967, BPS) and Festa and Ruderman (1969). These rates are based on calculations within the Feynman and Gell-Mann (1958) formulation of the theory of weak interactions. The unification of the weak and electromagnetic forces within the framework of the Weinberg-Salam theory (Weinberg 1967, Salam 1968) led Dicus (1972) to investigate the implications of this theory on the pair, plasmon, and photo-neutrino energy loss rates for astrophysical plasmas. With the mass of the W-meson of 81GeV the results of Dicus's calculations indicate that the plasmon neutrino rate, which is the most important for the models considered here (see Section 2.5.3), is within a few percent of the rates in BPS.

The neutrino energy loss rates for a wide range of densities and temperatures have been recalculated by Munkata *et al.* (1985) using the Weinberg—Salam theory. They state that for the plasmon neutrino process, the ratio of the BPS plasmon

neutrino rate to the rate of their work is:

$$(1/2 + 2 \sin^2\theta_w)^2 + (n/2 + 2 n \sin^2\theta_w)^2$$

where $\sin^2\theta_w$, the square of the sine of the Weinberg angle, is quoted as 0.217, and n is the number of massless neutrino species. Hence, the energy loss rate from plasmon neutrino emission has been overestimated by BPS by only about 10-15%. In principle, since neutrino emission from the interior of hot white dwarfs provides a significant fraction of the cooling, any measurement of the cooling rate of these stars could provide a stringent test of these theoretically determined neutrino rates.

The modified Paczynski models are the most appropriate for systematically changing the roles of nuclear burning and neutrinos. We have constructed three parallel sequences of $0.60M_{\odot}$ models with this code, as described in Section 2.3.2, to investigate the effect of varying the neutrino energy loss rates in a simple way. One sequence (P60BI1Y) uses the standard rates for nuclear burning and neutrinos. Another sequence (P60BI2Y) is evolved with neutrino emission rates cut by a factor of 2, while the third has no neutrino emission (P60BI0Y). Models from these three sequences were used to initiate three corresponding ^{12}C WDEC sequences: W60GC1C, W60GC2C, and W60GC0C.

2.5 Summary of Evolutionary Characteristics

2.5.1 *Evolutionary Tracks*

Because of the nature of the degenerate stellar configuration of the white dwarf model in the constant radius phase, the specific input physics used for a model of a given mass does not radically affect its evolutionary track in the H-R diagram. In Figure 2.1, the tracks for some of the $0.60M_{\odot}$ models are plotted together to show the effects of different input physics. Figure 2.1 shows how little the input physics affects the position of the evolutionary track below about $10L_{\odot}$. The divergence of the I60BC1Y and W60GC1C tracks at higher luminosities is primarily the result of the

Figure 2.1:

Evolutionary tracks in the H-R diagram for $0.60M_{\odot}$ PWD models. The solid tracks are for the Iben model that has a helium envelope and includes Coulomb effect in the equation of state (labeled I60BC1Y), and the pure ^{12}C sequence with neutrino emission (labeled W60GC1C). For comparison, we also show the ^{12}C sequence with no neutrinos (W60GC0C, short-dashed line) and the Iben sequence without Coulomb effects (I60BI1Y, dashed line).

different initial conditions, such as the temperature profile that results from nuclear burning. The timescale for evolution down to $100L_{\odot}$ is sufficiently short (on the order of 5×10^4 years) that differences in surface composition and thermal structure have not damped out. The dashed track that lies somewhat above the rest in parts of this diagram is the Iben sequence with no Coulomb interactions (I60B11Y). This sequence has a slightly greater radius at a given effective temperature because of the slightly higher pressure in the core compared with the Iben sequence that includes Coulomb effects. Above $10L_{\odot}$, the WDEC sequence with no neutrinos (W60GC0Y) lies above the other tracks. Compared to the pure ^{12}C sequence that includes neutrinos, this sequence has a hotter core for a given effective temperature because of the lack of the cooling effect of neutrino losses.

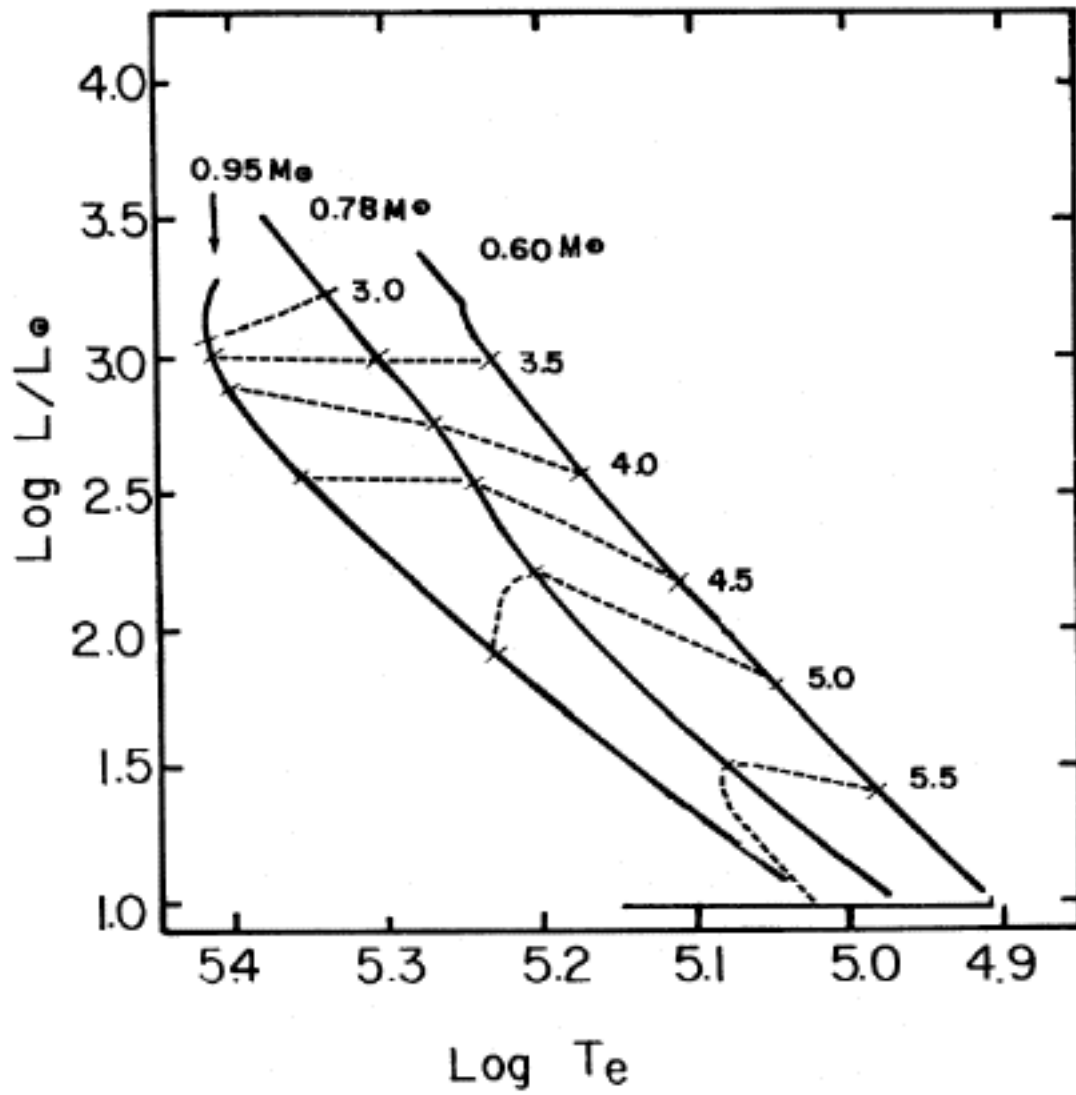
In Figure 2.2, evolutionary tracks for the 0.60 , 0.78 , and $0.95M_{\odot}$ pure ^{12}C sequences are plotted together. The dominant effect here is the well known mass-radius relation for degenerate configurations. The radius of a white dwarf well below the Chandrasekhar limit is inversely proportional to the $1/3$ power of mass; hence at a given effective temperature, lower mass white dwarfs have larger radii and therefore higher luminosities.

2.5.2 *Luminosity Sources*

The PNNs are an important transition phase in stellar evolution. In this phase, the primary luminosity source switches from nuclear burning to gravitational contraction. From the initial ignition of hydrogen in the core of its zero-age main sequence ancestor through the PNN phase, active nuclear burning provides the bulk of an intermediate-mass star's radiant energy. In the constant luminosity phase of PNN evolution, the dominant energy source is the nuclear shell burning. In the case of PNNs that have lost mass down to the helium-rich layers, the dominant energy source is the helium-burning shell. In the PWD phase, the helium shell source "runs out of steam" and the star shines by release of gravitational energy for the first time since the pre-main sequence contraction phase. "Gravitational" luminosity is supplied by the release of heat from the core that has been stored throughout the prior evolution of the

Figure 2.2:

Evolutionary tracks of pure ^{12}C PWD models of 0.60 , 0.78 , and $0.95M_{\odot}$. Lines of constant ages are indicated by dashed lines; these are labeled by the logarithm of the age in years. The ages are normalized to $t=3000\text{yr}$ at $\log(L/L_{\odot})=3.0$. The solid bar indicates the probable T_{e} limits for PG1159-035.



star, and from the release of gravitational energy by overall stellar contraction. For hydrogen-deficient stars, this is the final phase of evolution as they slowly become true blue white dwarfs.

As we will see in Chapter 5, the details of nuclear shutdown in PWD models can affect the behavior of the rate of period change as a function of stellar luminosity. In addition, in models for which nuclear burning can contribute to the instability of a nonradial mode, the shutdown of the nuclear source eventually turns off the instability. We discuss this effect in Chapter 6.

Figure 2.3a shows the total photon luminosity as a function of time for various $0.60M_{\odot}$ models. The ages for all sequences are normalized to $t=3000\text{yr}$ at $\log(L/L_{\odot})=3.0$. We separate out the contributions of nuclear burning, neutrinos, and gravitational luminosity in I60BC1Y in Figure 2.3b, following Figure 3 of Iben and Tutukov (1984). It is immediately apparent that at luminosities above $100L_{\odot}$, the luminosity drops faster in models that do not include nuclear burning. The core composition of P60BI1Y is essentially pure ^{12}C , allowing us to compare the curves for the Paczynski sequence (P60BI1Y) with the pure ^{12}C sequence (W60GC1C). We see that below $50L_{\odot}$ the curves nearly overlay. This is a clear indication that nuclear burning is unimportant as an energy source by the time the star reaches this luminosity. The difference between the Iben curve and the pure ^{12}C curves below $100L_{\odot}$ may be accounted for, in part, by the difference in core composition. The Iben models, with 45% oxygen by mass in the core, evolve slightly faster. This is because the cooling rate of the core depends inversely on the mean atomic weight. Hence, with heavier nuclei in the core, the Iben models evolve more quickly than the pure ^{12}C models. The nonideal contributions to the equation of state do not affect the cooling rate. Only below $0.1L_{\odot}$ does the model with Coulomb interactions fade more slowly than the model without them.

The effects of neutrino emission are clear in Figure 2.3 and Figure 2.4(a-c). Below $100L_{\odot}$ the WDEC sequence with neutrino emission (W60GC1C) evolves on a much shorter timescale than the sequence with no neutrinos (W60GC0C). From

Figure 2.3 (a):

Luminosity as a function of time for $0.60M_{\odot}$ PWD sequences. The solid lines are for the stratified model with Coulomb effects (labeled I60BC1Y) and the pure ^{12}C sequence (W60GC1C). The short-dashed curve is the pure ^{12}C sequence with no neutrino emission, and the dashed line is the modified Paczynski sequence that includes nuclear burning (P60BI1Y). The stratified model without Coulomb effects (I60BI1Y) diverges from the I60BC1Y curve only at very low luminosity.

Figure 2.3 (b):

Contributing luminosity sources for the stratified $0.60M_{\odot}$ sequence I60BC1Y. The total photon luminosity is indicated by the dashed curve. L_{grav} includes the effects of residual gravitational contraction and conductive cooling. Ater Figure 3 in Iben and Tutukov 1984, *Ap. J.*, **282**, 615.

Figure 2.4(a) we see that at that luminosity, the neutrino luminosity approaches the photon luminosity. From an age of 10^5 to 10^7 years, the neutrino luminosity exceeds the photon luminosity in the W60GC1C sequence. Hence, without this additional energy loss mechanism, the W60GC0C sequence takes a longer time to radiate away its internal energy.

2.5.3 Core Temperature Inversion

The effects of neutrino cooling of the deep interior and nuclear shell burning combine to produce a pronounced core temperature inversion in the AGB evolutionary phase. Typically, the maximum interior temperature occurs below the helium shell source, at roughly the half-mass point. In the $0.60M_{\odot}$ models, however, the temperature profile shows a double-hump because of copious emission of plasmon neutrinos just below the helium shell. As helium burning goes away, the double-humped temperature profile becomes single-humped with the maximum near the position of the "fossil" burning shell. Figure 2.5 shows the run of temperature and total energy generation rate (nuclear burning, subtracting energy losses by neutrino emission) for some representative models from the I60BC1Y sequence. The core does not become isothermal until the models drop well below one solar luminosity.

The behavior of the central temperature as a function of time is illustrated in Figure 2.6 for the $0.60M_{\odot}$ models. In the hot PWD phase, the core is only mildly degenerate, and gravitational contraction leads to a very slow rise in the core temperature as the star drops in total luminosity. When the photon luminosity and the neutrino luminosity become comparable, the core begins to cool. This occurs at an age of about $10^{5.5}$ years for the Iben models, and 10^5 years for the WDEC and modified Paczynski models. The slight difference in age is caused by the dependence of the neutrino emission rates on the core composition: with half oxygen, the Iben models have cooler cores and therefore lower neutrino emission rates. The model without neutrino emission (W60GC0C) takes longer to begin cooling in the center. This model must wait until the core has become sufficiently degenerate so that the effects of conduction alone begin to cool it down.

Figure 2.4 (a)-(c):

Luminosity as a function of age for (a) $0.60M_{\odot}$, (b) $0.78M_{\odot}$, and (c) $0.95M_{\odot}$ pure ^{12}C PWD sequences. The solid lines represent the photon luminosity; the total energy loss by neutrino emission is indicated by the dashed lines.

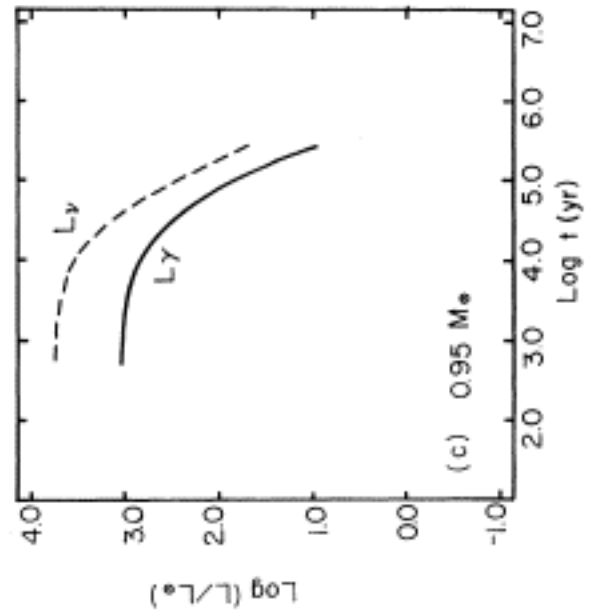
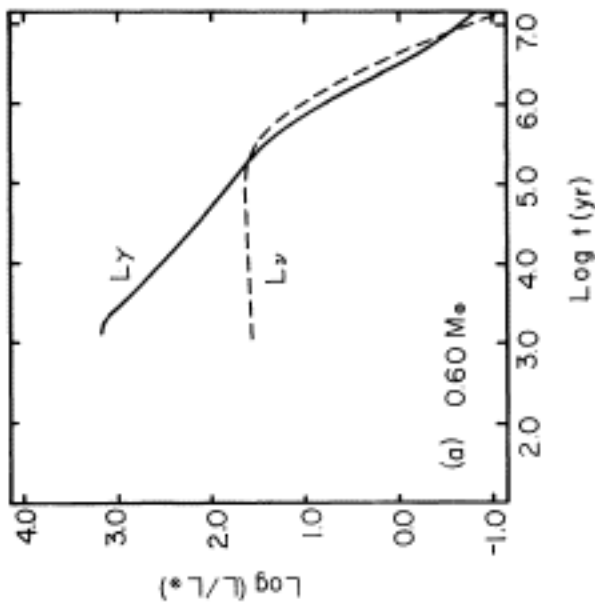
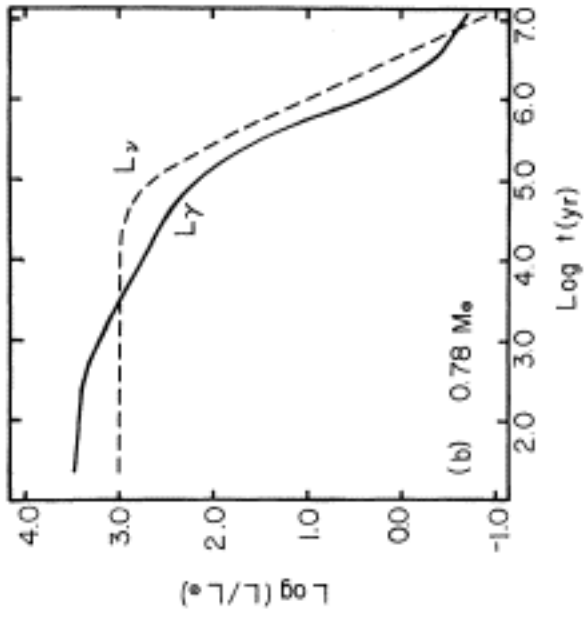


Figure 2.5 (a):

Log of the temperature versus fractional radius for four models in the $0.60M_{\odot}$ stratified sequence (I60BC1Y) with $\log(L/L_{\odot})=3.21, 2.54, 2.01,$ and 0.99 .

Figure 2.5 (b):

The logarithm of the magnitude of the energy generation rate per gram, ϵ , as a function of the fractional radius for (from left to right for curves below $\log|\epsilon|=-2$) $\log(L/L_{\odot})=3.21, 2.54, 2.01,$ and 0.99 in sequence I60BC1Y. Dashed lines indicate that the sign of ϵ is negative (neutrino emission); solid lines indicate positive values of ϵ (nuclear burning).

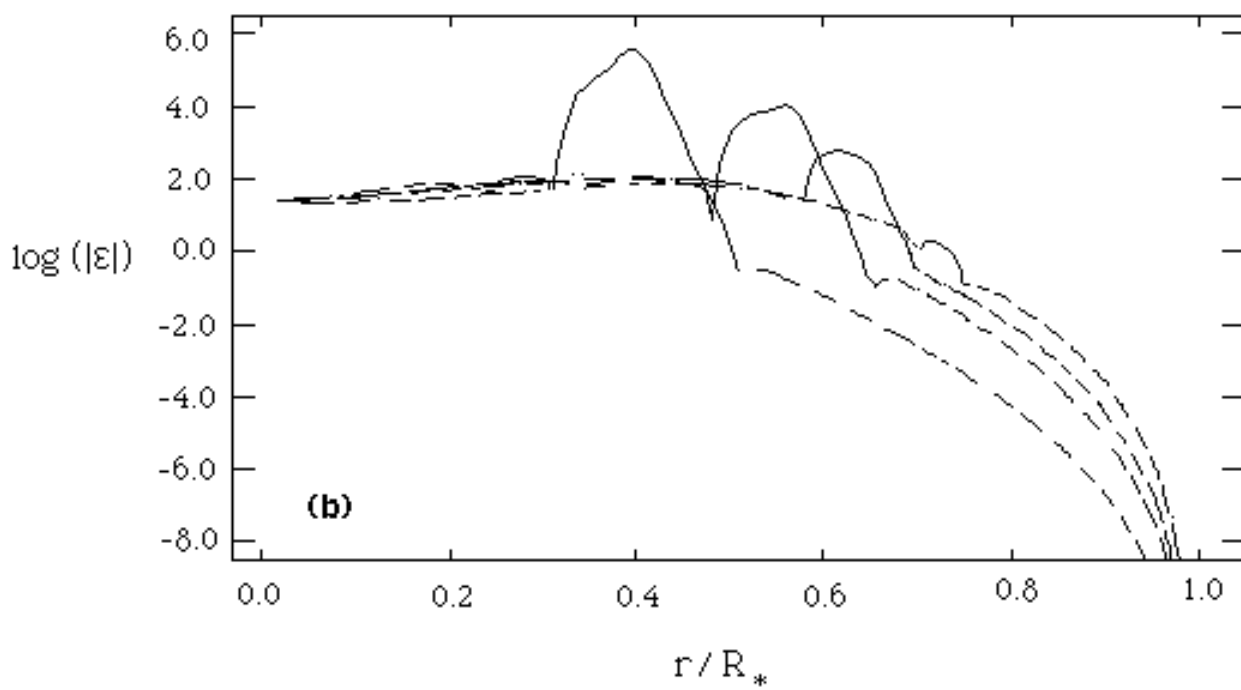
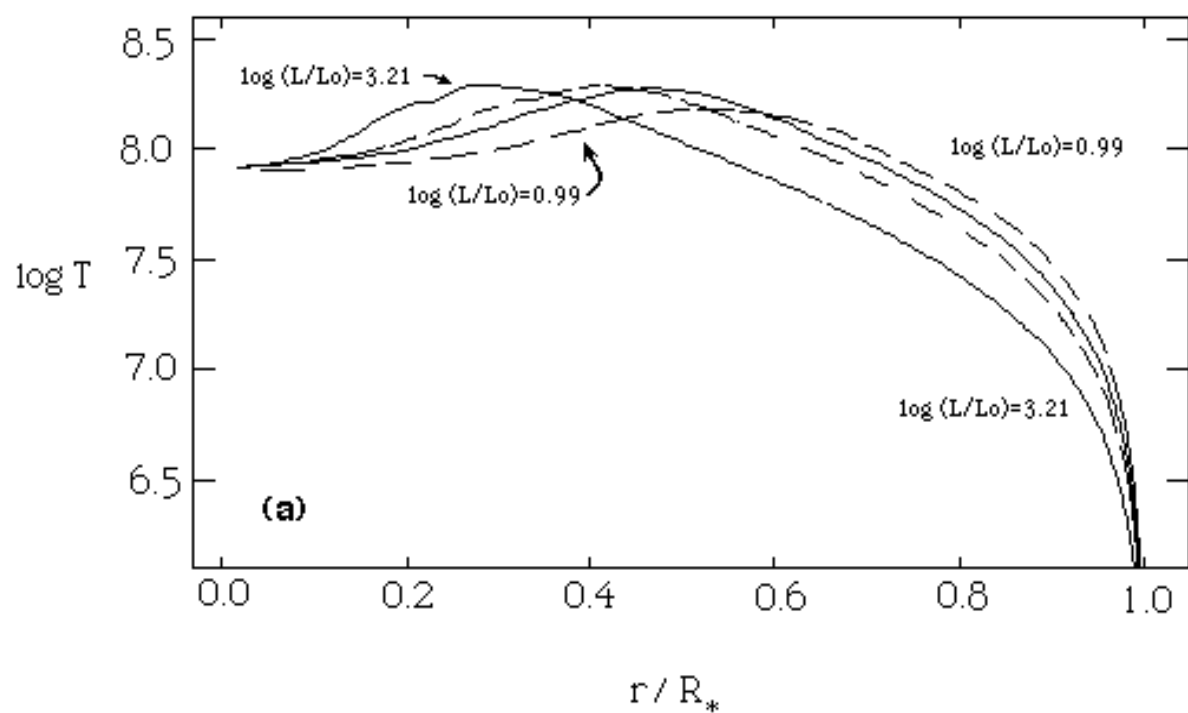


Figure 2.6:

Logarithm of the central temperature as a function of age for several $0.60M_{\odot}$ PWD sequences. From top to bottom we have: the pure ^{12}C sequences with increasing neutrino emission rates: W60GC0C, W60GC2C, and W60GC1C; the modified Paczynski sequence P60BI1Y; and the two stratified sequences I60BC1Y and I60BI1Y.

" You may fly to poetry and music, and quantity and number will face you in your rhythms and your octaves"

-Alfred North Whitehead

CHAPTER 3

LINEAR ADIABATIC NONRADIAL OSCILLATIONS AND SEISMOLOGICAL DIAGNOSTICS

3.1 Introduction

In this chapter, we introduce and develop the tools needed to study the oscillation properties of our stellar models. For more complete treatments of much of this material, see the discussions in Ledoux and Walraven (1958), Unno *et al.* (1979), Cox (1980), Carroll (1981) and Winget (1981).

Our starting point is the set of equations of nonrelativistic fluid dynamics coupled with heat flow in a nonrotating, nonmagnetic self-gravitating system. The first of these are the equation of conservation of mass,

$$\frac{\partial \rho}{\partial t} = - \nabla \cdot (\rho \mathbf{v}) \quad , \quad (3.1)$$

and the equation of motion,

$$\rho \frac{\partial \mathbf{v}}{\partial t} = -\nabla P - \rho \nabla \Phi \quad . \quad (3.2)$$

In equation (3.2) (and below) the pressure tensor has been reduced to the isotropic hydrostatic pressure P . The scalar gravitational potential field, Φ , is obtained from Poisson's equation,

$$\nabla^2\Phi = 4\pi G\rho . \quad (3.3)$$

By neglecting viscosity, we can express the equation of energy conservation in the form

$$\frac{dq}{dt} = \frac{dE}{dt} + P \frac{d(1/\rho)}{dt} \quad (3.4 a)$$

where q is the heat content per unit mass, and E is the specific internal energy. We may write the left-hand side of equation (3.4 a) as

$$T \frac{ds}{dt} = \varepsilon - \frac{1}{\rho} \nabla \cdot \mathbf{F} \quad (3.4 b)$$

(Cox, 1980) where s is the specific entropy, and \mathbf{F} is the energy flux. The quantity ε is the net rate of energy generation per gram (from nuclear sources and neutrino sinks), which, like the equation of state, is assumed to be completely determined as a function of density, temperature, and chemical composition.

The energy flux \mathbf{F} is the sum of the radiative flux and the convective flux. Using the radiative diffusion approximation, we have an expression for the radiative flux,

$$\mathbf{F}_{\text{rad}} = - \frac{4\pi}{3 \kappa \rho} \nabla J \quad (3.5)$$

where J , the mean intensity, is given in the Eddington approximation by

$$J = \frac{ac}{4\pi} T^4 + \frac{1}{4\pi\kappa} T \frac{ds}{dt} \quad (3.6)$$

where κ is the Rosseland mean opacity, and a and c are the usual fundamental physical constants.

In the next section we present the linearized equations corresponding to equations (3.1) - (3.6). We then show how the order of the system of equations is reduced under the adiabatic approximation, and discuss the appropriate boundary conditions. We detail the various procedures we used in solving the adiabatic equations in Section 3.5. In Section 3.6 we review the variational form for the oscillation frequency that leads to the formulation of the adiabatic weight functions. We demonstrate the effects of slow rotation on the resulting frequencies in Section 3.7.

3.2 The Linearized Perturbation Equations

We begin by assuming that there exists a static equilibrium solution to equations (3.1) - (3.6) characterized by $\mathbf{v}=0$ everywhere. We now introduce perturbations to the physical state of the system, such that the perturbed state is also a solution. The perturbed quantities may be written in the form

$$\mathbf{x}(\mathbf{r}, t) = \mathbf{x}_0(\mathbf{r}, t) + \mathbf{x}'(\mathbf{r}, t) \quad (3.7)$$

where $\mathbf{x}_0(\mathbf{r}, t)$ is the equilibrium value, and $\mathbf{x}'(\mathbf{r}, t)$ is the Eulerian perturbation in \mathbf{x} , at position \mathbf{r} and time t . To first order, the Lagrangian perturbation of \mathbf{x} , written as $\delta\mathbf{x}$, is expressed in terms of the Eulerian perturbation as

$$\delta\mathbf{x} = \mathbf{x}'(\mathbf{r}, t) + \delta\mathbf{r} \cdot \nabla\mathbf{x}_0(\mathbf{r}, t) \quad . \quad (3.8)$$

To obtain the equations governing the perturbations to the physical variables, we replace the quantities in equations (3.1) - (3.6) with their perturbed form as in equation (3.7). The equilibrium equations may then be subtracted off, leaving the perturbed fluid equations. If the perturbations themselves are small, then we retain only terms to first order in the perturbation variables. This procedure leads us to the set of linearized perturbation equations (in which we drop the zero subscript for equilibrium quantities):

$$\frac{\delta\rho}{\rho} = -\nabla\cdot\delta\mathbf{r} \quad , \quad (3.9)$$

$$\frac{d^2\delta\mathbf{r}}{dt^2} = -\frac{\nabla P'}{\rho} + \frac{\rho'}{\rho^2}\nabla P - \nabla\Phi' \quad , \quad (3.10)$$

$$\nabla^2\Phi' = -4\pi G\left(1 + \frac{\delta\rho}{\rho} - \frac{1}{\rho}\delta\mathbf{r}\cdot\nabla\rho\right) \quad , \quad (3.11)$$

$$T\frac{d\delta s}{dt} = \delta(\varepsilon - \frac{1}{\rho}\nabla\cdot\mathbf{F}) \quad , \quad (3.12)$$

$$\delta\mathbf{F} = \delta\mathbf{F}_{\text{rad}} \quad , \quad (3.13)$$

$$\mathbf{F}'_{\text{rad}} = -\left[\frac{4\pi}{3\kappa\rho}\nabla J\right]' \quad , \quad (3.14)$$

$$J' = \frac{ac}{\pi}T^3T' + \frac{T}{4\pi\kappa}\frac{d\delta s}{dt} \quad . \quad (3.15)$$

In deriving equation (3.12) we have used the assumption that the equilibrium model is in thermal balance, i.e. $ds_0/dt = 0$ everywhere. Because of their evolutionary nature, the PWD models considered here are not strictly in true thermal balance. In Chapter 5 we demonstrate that neglecting thermal imbalance should not affect the results of our adiabatic calculations.

Note that in equations (3.13) and (3.14) we only consider the perturbation of the radiative flux. We assume that the convective flux is "frozen in" and therefore the perturbations of the convective flux are negligible. Investigations of the adiabatic pulsation properties are insensitive to this assumption. However, for a nonadiabatic

analysis, the consequences of assuming frozen-in convection are potentially important. Since an adequate time-dependent theory of convection does not exist, we are forced to retain this assumption through the remainder of this work. In any case, for those models that were too hot to show any significant convective regions, this assumption is adequate (see also Chapter 6). Equations (3.9)-(3.15) are the equations that we will use to describe linear nonradial oscillations in a nonrotating, nonmagnetic, self-gravitating fluid system.

3.3 The Adiabatic Equations

3.3.1 *The Adiabatic Approximation*

The complexity of the equations of the previous section can be greatly reduced if we consider them under the adiabatic approximation i.e. that no heat is gained or lost from the system either locally or globally. Locally, the adiabatic approximation is a good one for oscillatory motion in regions where the amount of heat lost during a pulsation cycle is much smaller than the amount of heat energy stored there. This condition may be expressed as

$$\Pi_{\text{puls}} \ll \tau_{\text{th}}(m_{\text{r}}) \quad (3.16)$$

where $\tau_{\text{th}}(m_{\text{r}})$ is the thermal timescale defined in equation (2.1) at the mass m_{r} , and Π_{puls} is the pulsation period. In most models considered in this work, the mass at which the adiabatic condition begins to be violated is outward from about $10^{-8} M_{\odot}$ below the surface. Hence, the results of adiabatic calculations should provide an excellent approximation to the oscillation periods because (3.16) is satisfied for all but a negligible fraction of the mass of the star.

The adiabatic condition is equivalent to the statement that $T(d\delta s/dt) = 0$ everywhere in the star. Hence equations (3.12)-(3.15) are superfluous provided that the time derivative of the entropy perturbation is negligible. With this assumption we can use a Maxwell relation for a fluid element to write:

$$\frac{\delta P}{P} = \left(\frac{d \ln P}{d \ln \rho} \right)_{\text{ad}} \frac{\delta \rho}{\rho} = \Gamma_1 \frac{\delta \rho}{\rho} \quad (3.17)$$

Here the adiabatic exponent $\Gamma_1 \equiv (d \ln P / d \ln \rho)_{\text{ad}}$.

3.3.2 The Dziembowski Formulation

In the adiabatic approximation, the equations that remain nontrivial are equations (3.9), the three components of equation (3.10), and (3.11). These, along with the adiabatic condition (3.17) define a system of 6 equations in the unknowns P' , ρ' , Φ' , and the three components of $\delta \mathbf{r}$.

We now assume the spatial and time dependence of the perturbations can be separated in the following way (Cox 1980, Unno *et al.* 1979):

$$\mathbf{x}'(r, \theta, \phi, t) = \mathbf{x}'(r) Y_l^m(\theta, \phi) e^{i\sigma t}, \quad (3.18)$$

where $Y_l^m(\theta, \phi)$, the usual set of spherical harmonics, contain the angular dependence of the perturbation, and $\mathbf{x}'(r)$ is the radial component of the perturbation. The time dependence is in the term $e^{i\sigma t}$, with σ as the angular frequency of oscillation of the mode described by the values of l and m .

With the perturbation variables in this form, the equations of linear, adiabatic oscillation can be written as four first order linear differential equations whose dependent variables include the radial and horizontal displacements. Using the transformation of variables introduced by Dziembowski (1971), the four equations are

$$\frac{dy_1}{d \ln r} = \left(\frac{V}{\Gamma_1} - 3 \right) y_1 + \left[\frac{l(l+1)}{c_1 \omega^2} + \frac{V}{\Gamma_1} \right] y_2 + \frac{V}{\Gamma_1} y_3 \quad (3.19)$$

$$\frac{dy_2}{d \ln r} = (c_1 \omega^2 + A r) y_1 + (1 - U - A r) y_2 + A r y_3 \quad (3.20)$$

$$\frac{dy_3}{d \ln r} = (1-U) y_3 + y_4 \quad (3.21)$$

$$\frac{dy_4}{d \ln r} = -U A r y_1 + \frac{UV}{\Gamma_1} y_2 + \left[l(l+1) - \frac{UV}{\Gamma_1} \right] y_3 - U y_4 \quad (3.22)$$

This system is useful, as it has several computational advantages as discussed in Winget (1981) and Unno *et al.* (1979). Under the Dziembowski transformation, the four variables of the system are the dimensionless quantities:

$$\begin{aligned} y_1 &= \frac{\delta r}{r} \quad ; \quad y_2 = \frac{1}{gr} \left(\frac{P'}{\rho} + \Phi' \right) \quad ; \\ y_3 &= \frac{1}{gr} \Phi' \quad ; \quad y_4 = \frac{1}{g} \frac{d\Phi'}{dr} \quad . \end{aligned} \quad (3.23)$$

The equilibrium quantities are also expressed in a dimensionless form, with:

$$\begin{aligned} c_1 &\equiv \left(\frac{r}{R} \right)^3 \frac{M}{m_r} \quad ; \quad \omega^2 \equiv \sigma^2 \frac{R^3}{GM} \\ U &\equiv \frac{d \ln m_r}{d \ln r} \quad ; \quad v \equiv - \frac{d \ln P}{d \ln r} \\ A_r &\equiv \frac{r}{\rho} \frac{d\rho}{dr} - \frac{r}{\Gamma_1 P} \frac{dP}{dr} \end{aligned} \quad (3.24)$$

where M and R are the mass and equilibrium radius of the model.

3.3.3 Adiabatic Boundary Conditions

In order to solve equations (3.19)-(3.22), we require boundary conditions at the center and surface. These are obtained by using natural physical constraints on the

overall problem. The boundary conditions for the center result from the requirement that all physical variables remain finite. They are derived by expanding the linearized oscillation equations about $r=0$, and keeping only first order terms. This gives:

$$l y_2 - c_1 \omega^2 y_1 = 0 \quad (3.25)$$

and

$$l y_3 - y_4 = 0 \quad (3.26)$$

at the center.

At the surface of the equilibrium model, $P_0=0$; if we assume vanishing pressure in the perturbed state, then $P=0$ as well. Hence P and δP both vanish at the surface. In addition, for regular solutions, the quantity $\delta P/P$ must remain finite at $r=R$ (Cox 1980, §17.6). Under these conditions, the perturbed momentum equation can be manipulated to yield

$$y_1 (c_1 \omega^2 + 4 - U - V) + y_2 \left[V - \frac{l(l+1)}{c_1 \omega^2} \right] - V y_3 - y_4 = 0 \quad (3.27)$$

at the surface. The final boundary condition is that the Eulerian perturbation to the gravitational potential, and the force per unit mass, be continuous across the outer boundary. Thus, at the surface, we must have

$$U y_1 + (l+1) y_3 + y_4 = 0 \quad (3.28)$$

These boundary conditions are appropriate for the modes we analyze; but they fail for very short or very long period modes in white dwarfs (Hansen *et al.* 1985).

We now have four linear, homogeneous, first order differential equations, and four boundary conditions. Since the system is homogeneous, we are left with an arbitrary normalization. For the time being, we choose

$$y_1 = 1 \quad \text{at} \quad r=R . \quad (3.29)$$

Thus we solve the equations (3-19)-(3.22) with boundary conditions (3.25)-(3.28) and normalization (3.29) for the eigenfunctions \mathbf{y} and the eigenvalue σ^2 , the square of the angular oscillation frequency.

3.4 A Local Analysis: Propagation Diagrams

3.4.1 *Dispersion Relation*

Although the full set of adiabatic equations was used in the calculations, in the following analytical discussion we neglect perturbations in the gravitational potential (the Cowling approximation). This is a reasonable assumption for the high order modes which are mainly of interest here, and greatly simplifies the discussion without changing its physical character. We assume the radial part of the eigenfunction is proportional to $e^{ik_r r}$, where k_r is the radial wave number. In this limit, the adiabatic equations lead to a local dispersion relation for the radial wave number k_r (Unno *et al.* 1979):

$$k_r^2 = (\sigma^2 c_s^2)^{-1} (\sigma^2 - S_l^2) (\sigma^2 - N^2) \quad (3.30)$$

where

$$N^2 = -gA \quad (3.31)$$

is the square of the Brunt-Väisälä frequency and

$$S_l^2 = \frac{l(l+1)P\Gamma_1}{r^2 \rho} = l(l+1) \frac{c_s^2}{r^2} \quad (3.32)$$

is the acoustic frequency. Here σ is the eigenfrequency, c_s is the local adiabatic sound speed, P is the total pressure, and l is the colatitudinal angular index of the spherical harmonic; other symbols have their usual meanings. A is related to the

Schwarzschild criterion for convective stability so that N^2 is negative in regions of convective instability.

For a given value of l , the adiabatic oscillation equations allow eigensolutions containing an integral number of nodes in the radial direction. We call these solutions "modes" of degree l and order k , where k is the number of radial nodes. The dispersion relation (3.30) shows under what conditions a given mode is locally propagating. If σ^2 is greater than both S_l^2 and N^2 (p-modes) or σ^2 is less than both of those frequencies (g-modes), then $k_r^2 > 0$ and the mode is oscillatory and propagates locally. Otherwise $k_r^2 < 0$, and the mode is locally evanescent.

Taking the limit of $\sigma^2 \gg S_l^2, N^2$ (the p-mode propagation region), equation (3.30) becomes

$$k_r^2 \approx \sigma^2 c_s^{-2} \quad (3.33)$$

and hence pressure is the principle restoring force for p-modes. In the opposite limit, $\sigma^2 \ll S_l^2, N^2$ where gravity modes propagate, equation (3.30) becomes

$$k_r^2 \approx \sigma^{-2} r^{-2} l(l+1) N^2 \quad (3.34)$$

The propagation of g-modes is therefore determined by the Brunt-Väisälä frequency, with gravity acting as the restoring force.

3.4.2 *The Propagation Diagram*

The global trends in the properties of nonradial oscillations are best illustrated with propagation diagrams. These plots of the squares of the Brunt-Väisälä frequency and the acoustic frequency as functions of position within a stellar model graphically illustrate the regions of a model within which a nonradial mode may propagate. (For a complete discussion, see: Unno *et al.* 1979, §14; Cox 1980, §17.10.)

The nonradial g-modes are locally propagating where $\sigma^2 < S_1^2, N^2$; pressure modes propagate locally where $\sigma^2 > S_1^2, N^2$. In Figure 3.1 we show a typical propagation diagram for a PWD model with a convection zone near the surface. In a centrally condensed model, there may exist a local maximum in N^2 at the point in the star below which most of the mass is contained (Cox 1980, §17.10). In this model, with central condensation (ρ_c/ρ) of 49.7, that point is at $r/R_* \sim 0.4$. We expect, then, that low order (high frequency) g-modes may be effectively trapped below that point.

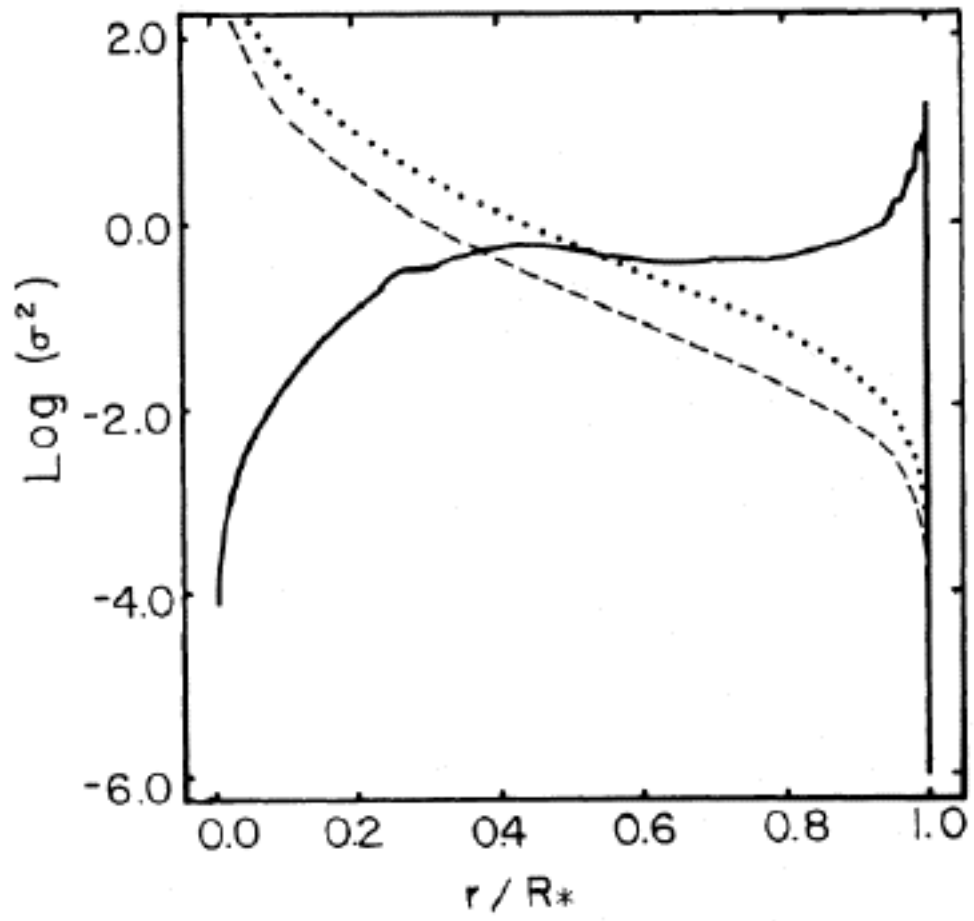
As the PWD evolves, the central condensation decreases, and the degeneracy boundary moves outwards in mass. In a degenerate core, the efficient transport of heat by conduction leads to an isothermal and isentropic core. Hence, the density gradient approaches the adiabatic value, and $A \rightarrow 0$. Hence, as the PWD becomes more degenerate, N^2 will decrease (Osaki and Hansen 1973), and the local maximum will decrease in contrast. Hence, as evolution proceeds, we expect the periods of the nonradial g-modes to generally increase and the region of propagation to gradually shift towards the outer portions of the star.

3.5 Numerical Solution of the Adiabatic Equations

We study the adiabatic nonradial oscillations of the PWD models using computer codes that solve equations (3.19)-(3.22) subject to the boundary conditions (3.25)-(3.29). As Starrfield *et al.* (1983,1984) demonstrated, if the observed pulsations of a few hundred seconds in the DOV stars are indeed nonradial g-modes, then they must be very high overtones, which means many nodes in the displacement eigenfunctions. The pure ^{12}C input models considered here contain between 250 and 300 zones, with the largest zones ($\Delta q < 0.05$) just interior to the primary temperature maximum. Our pulsation codes based on the Newton-Rapheson iteration algorithm (Carroll 1981, Winget 1981) require finer zoning than available in these equilibrium models to resolve all radial nodes. In addition we also seek rates of change of periods; the eigenvalues are to be differenced in time along an evolutionary sequence of equilibrium models. Therefore, we require that the eigenvalues be computed in a very accurate and consistent way from model to model. Unambiguous mode identification

Figure 3.1:

Propagation diagram for $0.95M_{\odot}$ pure ^{12}C PWD model at $\log(L/L_{\odot})=3.10$. The solid line is the square of the Brunt-Väisälä frequency (N^2). The dashed line is the square of the acoustic frequency (S_1^2) for $l=1$; the dotted line, (S_2^2) for $l=2$.



is also necessary to ensure that we are differencing periods representing the same mode in all models. The Newton-Raphson method, which uses only a second-order difference scheme, is not adequate for these tasks.

For the adiabatic investigation, we use a fourth-order Runge-Kutta integrator with error limiters written by H. A. Watts and L. F. Shampine of Sandia Laboratories, NM. The overall method of solving the eigenvalue problem is by "shooting" from the model center to its surface in an iterative fashion until all boundary conditions are satisfied. To resolve closely spaced nodes and to satisfy requirements of the integrator, the equilibrium model quantities are interpolated between zones, by means of cubic splines, in the process of integration. This typically results in 2000 to 3000 effective zones. This procedure produces periods and eigenfunctions that are insensitive to the zoning details of the equilibrium models. The phase diagram scheme (Scuflaire 1974, Osaki 1975; see also Unno *et al.* 1979, §16; or Cox 1980, §17.11) of mode classification has been used to evaluate the order, and hence identify, a given mode. For white dwarfs, which are relatively simple beasts, this scheme is straightforward to apply. We neither miss nor misidentify a mode as it evolves with time.

3.6 Variational Principle and Weight Functions

The equations of motion for adiabatic nonradial oscillations may be derived from a variational principle which expresses the frequency eigenvalue in terms of total integrals of the eigenfunctions weighted by various physical quantities taken from the evolutionary equilibrium stellar model. In the usual formulation it is assumed that both the pressure and density vanish at the stellar surface ("zero" boundary conditions). This assumption, coupled with the self-adjoint nature of the adiabatic system, is sufficient to demonstrate the variational properties (Cox 1980).

As we will show, the variational expression for σ^2 may be cast in the form:

$$\sigma^2 = \frac{\int f[Y(x), x] dx}{\int g[Y(x), x] dx} \quad (3.35)$$

where x is some stellar quantity such as radius, $Y(x)$ is a quadratic function of the eigenfunctions, \mathbf{y} , (as in Dziembowski 1971) and $f(\mathbf{y}, x)$ and $g(\mathbf{y}, x)$ are functionals of the indicated arguments. The denominator is proportional to the kinetic energy of oscillation. The integrand of the numerator serves as a "weight" function in that its relative values through the star inform us, in effect, where the eigenvalue is established. It has been used in an astrophysical context by Epstein (1950), Goossens and Smeyers (1974), and Schwank (1976) among others. The formulation we shall use is based on that of Unno *et al.* (1979, §13). After performing some integrations by parts we may combine equations (13.13) and (13.15) of Unno *et al.* and the definitions of the Dziembowski variables, \mathbf{y} , to find:

$$\sigma^2 = \frac{\int_0^R \{C(\mathbf{y}, r) + N(\mathbf{y}, r) + G(\mathbf{y}, r)\} \rho r^2 dr}{\int_0^R T(\mathbf{y}, r) \rho r^2 dr}, \quad (3.36)$$

where

$$T(\mathbf{y}, r) = r^2 [y_1^{2+l(l+1)} (g/r\sigma^2)^2 y_2^2] \quad (3.37)$$

$$C(\mathbf{y}, r) = g^2 l(l+1) s_l^{-2} (y_2 - y_3)^2 \quad (3.38)$$

$$N(\mathbf{y}, r) = r^2 N^2 y_1^2 \quad (3.39)$$

$$G(\mathbf{y}, r) = -gr U^{-1} [y_4 + l(l+1) y_3]^2. \quad (3.40)$$

Here $T(\mathbf{y}, r)$ is proportional to the kinetic energy density, $C(\mathbf{y}, r)$ contains the square of the acoustic frequency, $N(\mathbf{y}, r)$ varies directly with the Brunt-Väisälä frequency $N^2(r)$, and the perturbative information in $G(\mathbf{y}, r)$ involves only the

gravitational eigenfunctions γ_3 and γ_4 . Thus, C, N, and G may be regarded as weight functions which individually provide diagnostic information on acoustic, gravity wave, and gravitational field contributions to σ^2 . For example, if $N^2(r)$ were to change by a small amount δN^2 without any corresponding change in the other physical characteristics of the static model (which is highly unlikely), then it may easily be shown that the eigenvalue would change by

$$\delta\sigma^2 = [T(R)]^{-1} \int_0^R N(\mathbf{y}, r) \frac{\delta N^2}{N^2} \rho r^2 dr \quad (3.41)$$

(Note that Rayleigh's principle guarantees that induced changes in the eigenfunctions need not be considered because those changes would result in second order corrections to σ^2 .) $N(\mathbf{y}, r)$ is then a kernel for $\delta\sigma^2/\delta N^2$. Such kernels are an essential ingredient in stellar seismic diagnostics and inverse theory and are presently being explored for solar (Deubner and Gough 1984) and terrestrial (Backus and Gilbert 1967) seismology. In this work we shall use these kernels to guide us in our interpretation of the oscillation behavior of hot PWD stars.

Another use of the variational principle is as a numerical check on the accuracy of the computed eigenfunctions. That is, computed eigenfunctions are inserted into equations (3.35) and (3.36) to find the variational value of σ^2 . This is then compared to the eigenvalue computed directly from the analysis that yielded the eigenfunctions in the first place. The agreement between the variational value of σ^2 and the directly computed value may be considered a figure of merit for σ^2 . We find agreement to three to five significant figures in σ^2 computed in these two ways. Some of this small error is most certainly attributable to differences in the surface boundary condition employed by the two techniques. The variational expressions given here require the vanishing of surface pressure and density, whereas we employ somewhat more realistic subsurface boundary conditions for the actual calculations.

3.7 Rotational Splitting of the Eigenfrequency

In nonrotating stars undergoing nonradial pulsation, eigenvalues corresponding to modes with the same degree l and radial order k , but different values of m are degenerate; rotation lifts this m degeneracy. Our separation of the oscillatory perturbations into spherical harmonics implies that we have running waves in the azimuthal (ϕ) direction, with phase velocities inversely proportional to m . The sign of m indicates the direction of propagation; modes with positive values propagate in the $-\phi$ direction. In a rotating star, with $\Omega \ll \sigma$, modes differing in m and therefore in azimuthal phase velocity will be observed at frequencies that differ by approximately the rotation frequency multiplied by the difference in m (Cox 1980 §17 and §19, see also Cox 1984 and references therein).

In particular, for the case of slow ($\Omega \ll \sigma$) uniform rotation of frequency Ω with the rotation and pulsation axes aligned, the pulsation frequency as observed in an inertial frame is given by

$$\sigma_{\text{obs}} = \sigma_0 - m \Omega (1 - C_{\text{rot}}) \quad . \quad (3.42)$$

Here, σ_0 is the pulsation frequency in the rotating frame of the star. C_{rot} is a number that depends on the equilibrium configuration of the star and on the adiabatic displacement eigenfunctions:

$$C_{\text{rot}} = \frac{\int_0^R \rho r^2 dr [2ab + b^2]}{\int_0^R \rho r^2 dr [a^2 + l(l+1) b^2]} \quad (3.43)$$

where a and b are proportional to the radial and horizontal displacements, respectively (Cox, 1980). In particular, we use

$$a = r y_1 \quad ; \quad b = g y_2 / \sigma^2 \quad (3.44)$$

in the calculation of C_{rot} .

To calculate rotational splitting in the presence of differential rotation, we follow the approach of Hansen, Cox and Van Horn (1977). Rotation is assumed to be cylindrically symmetric, with no angular momentum exchange between cylinders of fixed mass. The latter assumption precludes the possibility of momentum transfer by convection, etc. For each model in an evolutionary sequence, we used an angular momentum distribution computed for white dwarf configurations (Ostriker and Bodenheimer 1968) to derive the angular rotation velocity as a function of polar radius, ϖ . We fit a quadratic of the form

$$\Omega(\varpi) = \Omega_{\text{O}} (1 + \Omega_1 \varpi + \Omega_2 \varpi^2) \quad (3.45)$$

to the Ostriker and Bodenheimer distribution, where Ω_{O} is the angular frequency of rotation at the pole, and Ω_1 and Ω_2 are evaluated in a least squares fit to the Ostriker and Bodenheimer rotation law.

With a rotation law of this form, the expression for rotational splitting becomes

$$\sigma_{\text{obs}} = \sigma_{\text{O}} - m \Omega_{\text{O}} (1 - C_{\text{rot}} - C_1) \quad (3.46)$$

where C_{rot} is the uniform rotation coefficient and $C_1 [= C_1(|m|)]$ contains the nonuniform rotation effects. The value of C_1 depends on the adiabatic pulsation properties, the equilibrium structure of the star, and the values of Ω_1 and Ω_2 (see Hansen, Cox and Van Horn 1977, Appendix A); the expression for $C_1(3)$ for the $l=3$ modes was evaluated using the method of Cuypers (1980). Note that C_1 introduces an asymmetry with respect to m into the splitting since it depends on $|m|$ and not m .

CHAPTER 4

ADIABATIC OSCILLATIONS IN HOT DEGENERATES

4.1 Introduction

The most simple and direct comparison that we can make between models and real stars is with the pulsation periods themselves. The periods of most variable stars can be determined to two significant figures with relative ease; these numbers immediately constrain the type of star and the type of mode that is being observed. Once the type of star and mode are known, the properties of appropriate theoretical models then provide important information about the internal structure of the stars. The primary purpose of this chapter is to present the results of the numerical calculations of the adiabatic oscillation properties for the DOV and DBV evolutionary sequences. We concentrate on the high order ($k > 10$) g-modes, as the periods of these modes correspond most closely to those observed in the DOV and DBV stars. For completeness, however, we will also present the periods for some of the low order g-modes.

In the Section 4.2, we present the g-mode pulsation period spectrum for models of planetary nebula nuclei and hot white dwarfs. We also discuss the basic form of the eigenfunctions in that section. From these numerical results we then show how the adiabatic periods depend on model parameters. In Section 4.3, we derive analytic expressions for the characteristic mode spacings and calculate them for the models. Next, we use the adiabatic weight functions to show which parts of the star are most important in setting the period. In the final section, we extend the adiabatic analysis down to temperatures and luminosities appropriate to the DBV stars, exploring the possibility of a direct evolutionary connection between the two classes.

4.2 Period Spectra and Eigenfunctions for DOV Models

The periods for some representative g-modes in the DOV sequences are presented in Tables 4.1-4.4. The first three tables are for the pure carbon sequences with masses of $0.60M_{\odot}$, $0.78M_{\odot}$, and $0.95M_{\odot}$ (W60GC1C, W78GC1C, and W95GC1C). For comparison we present, in Table 4.4, the same modes calculated for the stratified models that include nuclear burning and Coulomb corrections to the equation of state (I60BC1Y). Periods in the range observed in the pulsating PG1159 stars correspond to roughly $k = 25$ (for the $0.60M_{\odot}$ models) to $k = 51$ (for the $0.95M_{\odot}$ models) for $l = 1$ modes. From the local analysis for nonradial modes presented in Section 3.4 (see also Section 4.3 below) the period for a high-order mode scales as the square root of $[l(l+1)]^{-1}$; to obtain periods of ~ 550 seconds for $l=2$, the order of a mode would have to increase by a factor of ~ 1.7 .

At a given luminosity, the periods for the stratified model are uniformly about 10% shorter than in the simple $0.60M_{\odot}$ pure ^{12}C models for the same l and k , even for models in which nuclear burning is an important luminosity source. This result allows us to use the simpler carbon models to study the dependence of the pulsation properties on some of the gross physical characteristics of PWDs with the confidence that any conclusions drawn will also apply to the more realistic models.

The period of a given mode increases with decreasing stellar mass at a given luminosity. The mass dependence of the period, Π , obtained using the periods of the $k=35$, $l=1$ mode from Tables 4.1-4.3, is of the form

$$d(\ln\Pi)/dM = -B \quad , \quad (4.1)$$

where M is the total stellar mass in solar units, and B is a number of order unity. This relation will prove to be useful for the investigation of the effect of steady mass loss on the rate of change of the period (Chapter 5). Not surprisingly, B is a function of luminosity and is ~ 2.0 for $L > 300L_{\odot}$, ~ 1.7 for $L \sim 100L_{\odot}$, and ~ 1.4 for $L < 30L_{\odot}$. The decrease in the value of B with luminosity occurs because the central condensation becomes a very weak function of stellar mass as complete degeneracy is approached.

Table 4.1

Pulsation Periods for Sequence W60GC1C

#	Age [yr]	$\log(L/L_0)$	Π [seconds]				
			$l = 1$				$l = 2$
			$k = 1$	$k = 10$	$k = 25$	$k = 35$	$k = 35$
41	1.91×10^3	3.150	55.310	243.870	559.042	767.028	448.050
47	2.42×10^3	3.081	54.925	244.291	558.766	766.269	447.533
53	2.99×10^3	3.002	54.615	245.038	559.210	766.346	447.526
65	4.27×10^3	2.856	54.166	246.659	560.890	766.765	447.722
73	6.39×10^3	2.705	53.811	248.455	563.545	768.713	448.969
77	1.14×10^4	2.500	53.509	250.958	566.687	773.585	451.755
82	2.19×10^4	2.273	53.467	253.991	570.594	778.182	454.330
86	5.31×10^4	2.000	53.988	258.999	577.268	788.073	460.170
91	1.07×10^5	1.776	55.059	264.246	584.741	799.446	466.837
98	2.51×10^5	1.500	57.913	272.185	596.313	819.282	478.377
102	4.13×10^5	1.304	61.143	278.778	613.048	840.275	490.818
110	7.43×10^5	1.000	66.695	292.889	646.179	886.222	517.714

Table 4.2

Pulsation Periods for Sequence W78GC1C

#	Age [yr]	$\log(L/L_0)$	Π [seconds]			
			$l = 1$			$l = 2$
			$k = 1$	$k = 10$	$k = 35$	$k = 39$
62	1.75×10^3	3.115	38.230	174.456	544.556	...
67	3.00×10^3	3.000	38.038	175.490	546.864	352.171
73	5.93×10^3	2.853	37.719	176.729	546.850	352.864
74	7.06×10^3	2.817	37.625	177.035	547.035	352.975
78	1.21×10^4	2.707	37.276	177.870	547.109	353.301
82	1.78×10^4	2.631	37.007	178.051	546.299	353.114
85	3.25×10^4	2.516	36.657	178.383	544.907	351.940
87	4.33×10^4	2.454	36.602	178.729	544.820	351.634
93	8.62×10^4	2.252	37.450	181.527	550.399	356.316
98	1.50×10^5	1.999	39.621	188.921	568.625	368.067
101	2.13×10^5	1.787	42.489	197.298	590.168	381.516
104	3.18×10^5	1.499	47.080	208.226	624.013	404.119
106	4.24×10^5	1.265	51.353	218.027	655.793	...
108	5.62×10^5	1.015	56.488	230.857	693.908	...

Table 4.3

Pulsation Periods for Sequence W95GC1C

#	Age [yr]	log(L/L _O)	Π [seconds]				
			<i>l</i> = 1			<i>l</i> = 2	
			<i>k</i> = 1	<i>k</i> = 10	<i>k</i> = 35	<i>k</i> = 51	<i>k</i> = 35
63	-5.47x10 ³	3.152	25.389	124.677	385.000	548.062	224.144
67	-2.17x10 ³	3.095	25.076	123.625	381.010	541.944	222.771
73	3.38x10 ³	2.993	24.903	123.346	378.255	538.948	221.151
77	1.68x10 ⁴	2.762	25.704	125.926	383.024	547.942	223.988
82	3.93x10 ⁴	2.454	27.877	131.042	395.562	567.515	231.331
85	5.71x10 ⁴	2.261	29.604	136.056	409.000	586.060	239.208
87	7.14x10 ⁴	2.128	31.179	140.206	420.416	602.266	245.959
92	1.19x10 ⁵	1.776	35.689	151.925	453.385	649.936	265.121
96	1.73x10 ⁵	1.478	40.289	162.206	484.738	695.433	283.592
99	2.28x10 ⁵	1.237	44.118	171.523	512.075	735.630	299.549
102	3.01x10 ⁵	0.981	543.886	...	318.207

Table 4.4

Pulsation Periods for Sequence I60BC1Y

#	Age [yr]	$\log(L/L_{\odot})$	Π [seconds]				
			$l = 1$				$l = 2$
			$k = 1$	$k = 10$	$k = 25$	$k = 35$	$k = 35$
1	-2.13×10^3	3.208	50.313	225.729	522.301	720.414	419.746
2	3.70×10^2	3.117	49.893	226.905	522.652	719.214	418.922
3	2.38×10^3	3.031	49.607	228.336	522.052	718.821	418.722
4	5.38×10^3	2.885	49.280	230.385	523.163	720.157	419.385
6	9.38×10^3	2.693	49.088	232.066	526.517	723.132	...
8	1.34×10^4	2.535	49.103	232.685	528.855	726.934	423.142
9	2.54×10^4	2.231	49.516	234.353	537.833	737.446	429.146
10	4.04×10^4	2.009	50.100	237.818	544.291	745.760	434.115
11	7.65×10^4	1.725	51.264	244.541	555.298	762.580	443.723
12	1.27×10^5	1.499	52.562	251.052	567.598	775.269	450.885
13	2.47×10^5	1.209	54.959	260.393	581.974	797.305	464.022
14	3.97×10^5	0.988	57.444	267.371	594.833	817.135	475.127

In Figure 4.1 we show representative radial ($\delta r / r$) and tangential ($\delta t / r$) displacements for $k=25$, $l=1$ in two $0.60M_{\odot}$ models from W60GC1C. The tangential displacement, in terms of the Dziembowski variable y_2 , is

$$\delta t = g y_2 \sigma^{-2} \quad (4.2)$$

where the normalization for the displacements is given in equation (3.29). This component of the displacement dominates the motion in the outer stellar regions. In the high luminosity models with high central condensation, the maximum amplitude of the total displacement near the center is about 1/30th the displacement at the surface. As the model cools, the relative amplitude of surface displacement increases, and the tangential displacement grows relative to the radial displacement. These effects reflect the approach to neutral stratification ($A \rightarrow 0$; see Section 3.4.2) and resulting decrease in the Brunt-Väisälä frequency in the degenerate cores of the models. This "squeezes" the eigenfunctions out towards the surface.

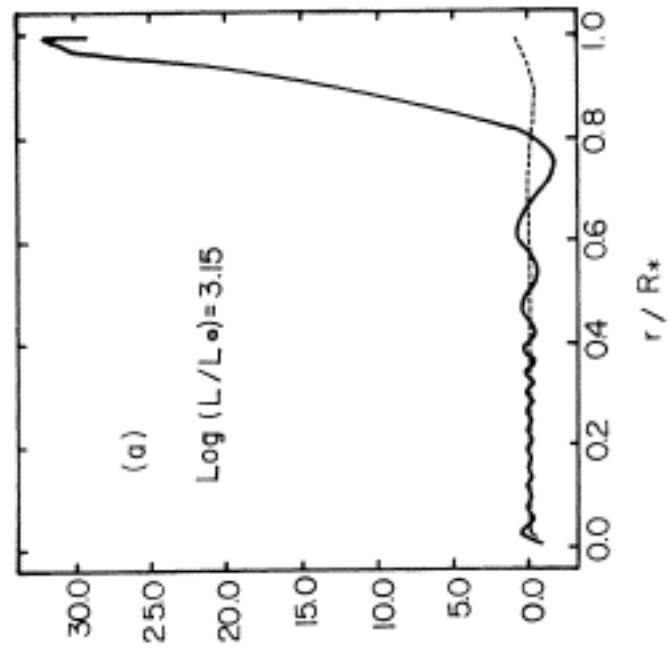
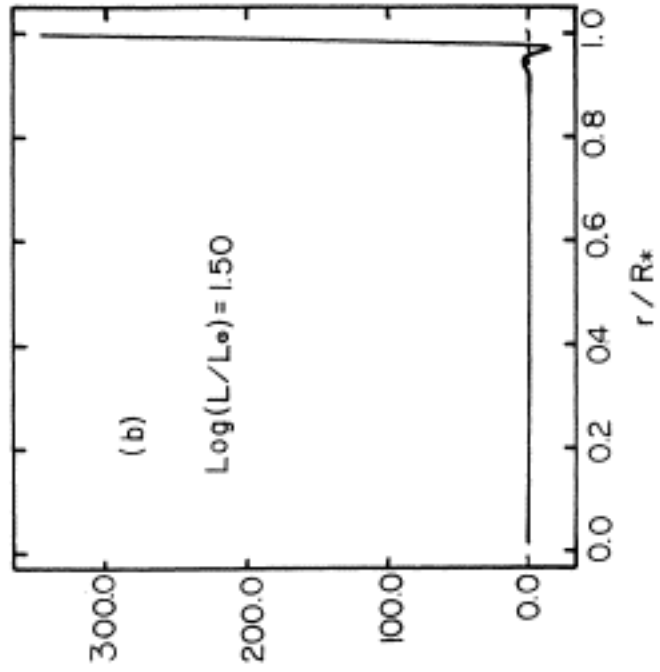
4.3 Characteristic Mode Spacings

As is evident from inspection of Tables 4.1-4.4, the g-mode periods increase linearly with k for a given model; that is, the period spacing between modes with consecutive values of k is approximately a constant for a given value of l . In this section, we derive an analytic expression for the constant period spacing of high-order g-modes of the same degree. Also, we present an expression for the characteristic frequency spacing of the high order p-modes.

In the Cowling approximation in the limit of higher k , the equations of adiabatic oscillations can be manipulated to give a dispersion relation for the radial wavenumber k_r as a function of the oscillation frequency and conditions of the equilibrium model (equation 3.30). Within this description of the oscillations, the acoustic and Brunt-Väisälä frequencies act as the boundaries of two "potential wells" for the eigenfunctions. We may in fact use a modified WKB analysis to estimate the

Figure 4.1 (a) and (b):

Radial (dashed line) and horizontal (solid line) displacement perturbations for the $k=25$, $l=1$ mode, normalized to the radial perturbation of the surface for the following models in the pure ^{12}C PWD sequence W60GC1C: (a) $\log(L/L_0)=3.15$ and (b) $\log(L/L_0)=1.50$.



eigenfrequencies of the system for the high-order modes in analogy with the solutions of the Schroedinger equation for quantum energy states of a given potential (Unno et al. 1979, §15; see also Park 1975, or any introductory quantum mechanics textbook for a general description of the WKB approximation).

4.3.1 *Period Spacing of g-Modes*

For the g-mode propagation region, we take the limit of equation (3.30) for small values of σ^2 with respect to N^2 and S_l^2 :

$$k_r \sim \sigma^{-1} [l(l+1)]^{1/2} N/r \quad (4.3)$$

where k_r is the local radial wavenumber and N is the Brunt-Väisälä frequency at radius r . For the eigenfunctions to satisfy the appropriate boundary conditions, we must have that

$$\int_a^b k_r dr = k \pi \quad (4.4)$$

where k is the number of nodes in the radial direction, and the integral is taken over the range of r in which the mode may propagate. For g-modes, this condition is that $\sigma^2 < N^2, S_l^2$. With this constraint, we integrate both sides of equation (4.3) over the radius r in the region where the above inequality holds, and obtain

$$\Pi \sim k [l(l+1)]^{-1/2} \Pi_0 \quad (4.5)$$

(Toomre 1985) where

$$\Pi_0 \equiv 2\pi^2 [\int_a^b (N/r) dr]^{-1} . \quad (4.6)$$

In practice equation (4.5) does not give particularly accurate estimates of the periods of high-order g-modes. However, the spacing between high-order modes of consecutive k is given to a high level of accuracy by equations (4.5) and (4.6); hence we refer to Π_0 as the "characteristic period spacing" for the g-modes. With this

definition of Π_0 we can estimate the spacing of periods for any value of l by simply dividing Π_0 by $[l(l+1)]^{1/2}$. The asymptotic period spacing determined in this way reproduces the mean period spacing, derived from full adiabatic calculations individual of high-order gravity modes (with $l=1$ and 2) to within about 3%. In Table 4.5 we list the values of Π_0 for several PNN-PWD models.

Since Π_0 can be evaluated using only equilibrium model quantities, it is a convenient parameter with which to compare the expected adiabatic pulsation properties of different models. In pulsating stars with rich power spectra, where presumably larger k modes are being observed, such a period spacing may be obtainable from observational data for direct comparison with the models. In Chapter 7 we show how the observed periods in PG1159-035 may yield an l identification by comparison with theoretical period spacings.

4.3.2 Frequency Spacing of p -Modes

The p -mode oscillation spectrum may also be represented by an asymptotic characteristic spacing, but uniform in frequency instead of period. For p -modes with sufficiently high frequencies, the asymptotic analysis in Section 3.4 gave

$$k_r \sim \sigma c_S^{-1}. \quad (4.7)$$

Integrating both sides of equation (4.3) over the range of r where p -modes are propagating ($\sigma^2 > N^2, S_l^2$) we obtain

$$\sigma \sim k \sigma_0 \quad (4.8)$$

where

$$\sigma_0 = \pi \left[\int_a^b c_S^{-1} dr \right]^{-1}. \quad (4.9)$$

The value of σ_0 , the characteristic frequency spacing, is related to the time needed for a sound wave to travel between successive reflections from the outer boundary. This

Table 4.5

Characteristic Mode Spacings for DOV Models

Sequence	$\log(L/L_0)$	$\Pi_0[s]$ (g-modes)	$\sigma_0[\text{rad s}^{-1}]$ (p-modes)
I60BC1Y	3.208	27.623	7.34×10^{-2}
"	2.535	27.904	1.46×10^{-1}
"	2.009	29.327	2.26×10^{-1}
"	1.499	29.905	2.48×10^{-1}
"	0.988	31.576	2.97×10^{-1}
W60GC1C	3.150	28.556	7.20×10^{-2}
"	3.002	28.561	8.44×10^{-2}
"	2.500	28.950	1.25×10^{-1}
"	2.000	29.602	1.69×10^{-1}
"	1.500	30.825	2.24×10^{-1}
"	1.000	33.533	2.85×10^{-1}
W78GC1C	3.000	20.191	1.55×10^{-1}
"	2.707	20.288	1.93×10^{-1}
"	2.516	20.246	2.32×10^{-1}
"	1.999	21.248	3.66×10^{-1}
"	1.499	23.444	4.48×10^{-1}
"	1.015	26.163	5.10×10^{-1}
W40GC1C	2.255	46.057	6.40×10^{-2}
"	1.996	46.313	7.65×10^{-2}
"	1.504	47.348	9.79×10^{-2}
"	1.256	48.071	1.09×10^{-1}

frequency spacing, observed in the solar 5-minute oscillations, has provided a very important constraint on models of the solar interior (Toomre 1985).

Recent seismological studies of nearby solar-type stars have been able to extract this characteristic frequency spacing from time-resolved studies of line profiles (Noyes *et al.* 1984, Guenther and Demarque 1985, Demarque *et al.* 1985). The high-order p-mode periods ($\Pi < 10$ s) for the hot degenerates present a formidable challenge for current observing techniques. There is no evidence for such variation in PNN-PWD stars. However, we present representative p-mode spacings in Table 4.5 in the hope that future observational techniques may be able to detect such modes if they are present.

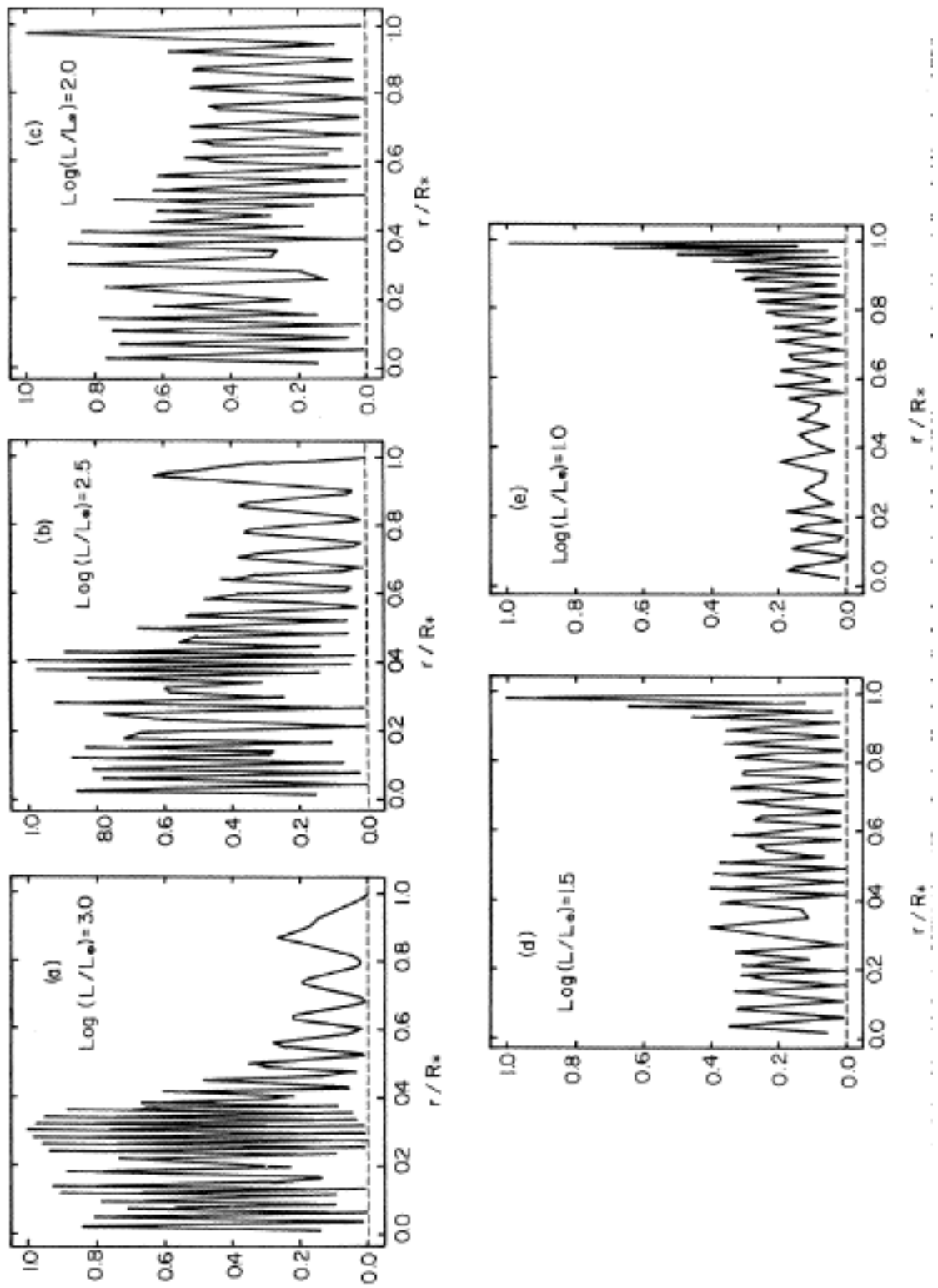
4.4 Weight Functions in the DOV Models

The evolutionary transition from the centrally condensed planetary nebula nucleus to the white dwarf configuration is accompanied by a striking change in the region of period formation, as indicated by the character of the weight function (the integrand of the numerator of equation 3.36). There is a narrow transition range in luminosity where the maximum of the weight function for high order modes moves from well inside the degenerate core ($q \sim 0.5$) out to the outer envelope ($q > 0.98$). This is illustrated in Figure 4.2 for a $k=25$, $l=1$ mode (period of ~ 550 to 650 s) followed through the evolution of the pure ^{12}C $0.60M_{\odot}$ model (W60GC1C).

At high luminosities this mode is uniformly weighted through most of the degenerate interior. Figure 4.2(a) is comparable to Figure 1 of Schwank (1976) for the $k=3$, $l=2$ mode of an $n=3$ polytrope (intermediate central condensation). As the model cools, the weight for the surface increases relative to the interior, as was anticipated by the discussion of Section 3.4.2. Below a transition luminosity ($100L_{\odot}$ for this sequence), the surface weight dominates. The degeneracy boundary of the hot models is at $q \sim 0.85$ (which moves slowly outwards with time) so that at high luminosity phases the adiabatic properties of the pulsations should reflect the conditions in the degenerate core. After the transition from the more global

Figure 4.2 (a)-(e):

Evolution of the weight function (numerator of equation [3.36]) as a function of fractional radius for the $k=25$, $l=1$ mode for the $0.60M_{\odot}$ pure ^{12}C PWD sequence W60GC1C. Luminosities are indicated within each panel. While the weight functions were originally computed using finer zoning (see Section 3.5), the value of the weight function is plotted for the mass zoning of the input model; hence, near $r/R=0.25$, the curve is underresolved.



contributions to envelope dominance of the weight function, the mode becomes increasingly affected by the conditions between the edge of the degenerate core and the surface. We find this behavior of the weights to be relatively insensitive to the value of k and l for g-modes with $k > 10$ and $l = 1, 2$ in a given PWD model.

The oscillatory behavior of the weight functions in Figure 4.2 reflects their dependence on the eigenfunctions. The overwhelming contribution to the weight in equation (3.36) is from the gravity wave term $N(\tau)$, as should be expected for a g-mode. At low luminosities the compressional term $[C(\tau)]$ also contributes to the weight in the envelope. The transition of the maximum in the weight function from core to surface reflects the decrease in central condensation as well as evolutionary changes at fixed mass points (Schwank 1976).

The running integral of the weight function, from stellar center to a given fractional radius, is shown as a function of that fractional radius in Figure 4.3. Such "leaf diagrams" show that, through the high luminosity phases, the period is determined primarily in the degenerate interior within $\alpha < 0.9$, and that the distribution of weight with mass is approximately constant there. At these luminosities, the pulsation properties retain some similarities to those of the red giants (Schwank 1976) of which these models are descendants. Below the transition luminosity ($\sim 100L_{\odot}$) the surface has become important; the integrated weight remains low in the core and increases quickly with radius near the surface. The pulsations have become white-dwarf-like in character. Diagrams such as Figure 4.3 dramatically illustrate the transition from a PNN to a WD configuration, and may be used to define at what point in the H-R diagram a star may be considered a white dwarf.

4.5 Adiabatic Periods in DBV Models

Curiously, as in the DOV stars, periods of the high-order g-modes in DBV models are representative of the periods of pulsation in the DBVs. To represent the observed periods of 500-1000s in the DBVs we consider the g-mode with $k = 25$, but now with $l = 2$. The periods for this mode are given in Table 4.6.

Figure 4.3:

Running integral of the weight functions (see Figure 4.2) to a given fractional radius for the $k=25$, $l=1$ mode in the $0.60M_{\odot}$ pure ^{12}C PWD sequence W60GC1C. From top to bottom, lines are $\log(L/L_{\odot})=3.15, 3.00, 2.50, 2.00, 1.50$, and 1.00 . The dotted lines join points at the indicated mass fraction.

Table 4.6

Periods for the $k = 25$, $l = 2$ Mode in DBV Models

Sequence	Π [seconds]		
	Effective Temperature (10^3K)		
	30	25	20
=====	=====	=====	=====
W40GC1C	778.1	862.9	984.6
W60GC1C	648.5	723.4	841.2
W78GC1C	550.4	621.5	732.5
I60BC1Y	483.7	517.2	571.1
I60B11Y	606.9	670.2	771.7

Periods for this mode range from 484s at $T_e=30,000\text{K}$ to 571s at $T_e=20,000\text{K}$ for the stratified $0.60M_{\odot}$ model that contained Coulomb corrections (I60BC1Y). The periods for the same mode in the $0.60M_{\odot}$ pure ^{12}C model (W60GC1C) were 30-40% longer than in the stratified model. As shown by Osaki and Hansen (1973) the periods of the g-modes are inversely proportional to the square-root of the specific heat. Since the specific heat of the ions is inversely proportional to the mean atomic weight, then the periods of the g-modes are proportional to the square-root of the mean atomic weight in the region of importance to setting the period. Thus the shorter periods in the stratified models reflect the fact that the mean atomic weight in the region of period formation of the stratified models is smaller. The characteristic period spacing of the g-modes (Table 4.7) shows the same dependence on composition as the periods themselves; observable quantities such as periods and period spacings are therefore sensitive probes of the envelope structure and composition of the DBVs.

Inclusion of non-ideal interactions in the interior equation of state for the DBV models results in a smaller radius at a given effective temperature compared with models constructed using an ideal gas equation of state. This effect leads to periods (for a given mode) that are roughly 25% shorter for the I60BC1Y sequence (with Coulomb interactions) than for I60BI1Y (ideal gas) despite otherwise identical structural properties.

Table 4.7

Characteristic Mode Spacings for DBV Models

Sequence	$T_e=30,000\text{K}$		$T_e=25,000\text{K}$		$T_e=20,000\text{K}$	
	$\sigma_0[\text{Hz}]$	$\Pi_0[\text{s}]$	$\sigma_0[\text{Hz}]$	$\Pi_0[\text{s}]$	$\sigma_0[\text{Hz}]$	$\Pi_0[\text{s}]$
W40GC1C	0.208	69.58	0.224	76.81	0.239	87.03
W60GC1C	0.418	57.68	0.432	63.97	0.482	73.88
I60BC1Y	0.440	43.46	0.457	46.76	0.475	51.25
I60BI1Y	0.388	54.57	0.402	60.43	0.419	71.03

CHAPTER 5

EVOLUTION OF THE ADIABATIC PULSATION PROPERTIES

5.1 Introduction

A remarkable property of the pulsating degenerates is the coherence of some of their pulsation periods. Some ZZ Ceti variables, for example, display modes for which upper limits on $|d(\ln\Pi)/dt|$ are of order 10^{-16}s^{-1} (Kepler 1984, Kepler et al. 1981), placing them among the most stable astrophysical clocks in the sky. In some of these, apparent incoherencies actually result from beating between modes with very closely spaced periods, perhaps caused by very slow rotation rates (Robinson, Nather and McGraw 1980, O'Donoghue and Warner 1982, Kepler et al. 1983). Other modes in pulsating degenerates appear very unstable, with photometric behavior that may result from as yet unresolved modes that are very closely spaced in frequency.

The DOV star PG1159-035 shows both kinds of modes. In the detailed study by Winget et al. (1985) only the 516s period appeared stable in both period and amplitude over the entire baseline of observations. This stability, in turn, enabled Winget et al. to measure the rate of change of the 516s period. The relatively large value of $d(\ln\Pi)/dt$, $(-2.3\pm 0.2)\times 10^{-14}\text{s}^{-1}$, results from the rapid evolution of the hot degenerate. Measurement of such a small effect can nevertheless be made with confidence: consider two clocks, both initially keeping perfect time. Clock P speeds up at the same rate as PG1159-035, while Clock A continues to keep perfect time. After 2.25 years, Clock P would be running only 0.15s per day fast. A much more apparent consequence of the speeding up of Clock P is that it would be 60s ahead of the reference clock, Clock A. Similarly, we measure $d\Pi/dt$ in pulsating stars not by looking for period changes themselves, but by measuring accumulated phase shifts (early/delayed maxima) over many pulsation cycles.

In this chapter we will show the rates of period change found for the PNN-PWD models. With the insight gained from the theoretical models, we will show such measurements of rates of period change for stable pulsation modes may be used to deduce the physical properties of the pulsating degenerates. In Section 5.2, we discuss how we calculate the rates of change of the oscillation periods. We present the rates of period change for the PNN and PWD models in Section 5.2, and show how the rate of period change acts as a probe of the cooling and contraction rates within the stellar interior. We demonstrate how $d(\ln\Pi)/dt$ depends on stellar mass, composition, and equation of state. In the following section, we show how energy loss by neutrino emission affects $d(\ln\Pi)/dt$. The observed rate of period change can be affected by the rotational spin-up of a contracting star as it tries to conserve angular momentum; in Section 5.5 we quantitatively demonstrate this effect on $d(\ln\Pi)/dt$. In Section 5.6 we examine the DBV models, and show how $d(\ln\Pi)/dt$ will provide a useful tool for understanding these stars. Finally, we consider other physical effects that may contribute to the observed rates of period change in Section 5.7.

5.2 Calculation of Rates of Period Change

In the pulsation calculations discussed in Chapters 3 and 4, we obtained the adiabatic oscillation periods of the PNN-PWD models. The purpose of this section is to show how we obtain rates of period change using these periods and the evolutionary nature of the models.

When we derived the linearized perturbation equations for nonradial oscillations in Section 3.2, we assumed thermal balance, $dS_O/dt=0$, everywhere. This step is an apparent contradiction of the essential property of the evolutionary models: the structure of these models is not strictly static, but changes in response to the changing thermal conditions within the model. These structural changes result from the slight imbalance among thermal processes such as nuclear burning, contraction, and heat loss by neutrino and photon emission. By setting $dS_O/dt=0$, we are ignoring the evolutionary origin of the model and assuming that it is a static configuration.

The effect of thermal imbalance on the adiabatic oscillation frequencies is of the order of the ratio of the oscillation period to the time scale for structural changes (Cox 1980, §19.4). Structural changes which result from thermal processes occur on the thermal time scale τ_{th} (as defined in equation 2.1) for the whole star. The thermal time scale for PWD models is typically greater than 10^{12-13} seconds, and is more than 10 orders of magnitude longer than the g-mode oscillation periods given in Chapter 4. Hence, departures from thermal balance would affect the adiabatic oscillation periods by only about one part in 10^{10} .

By ignoring the evolutionary term $d s_{\odot} / dt$ in the oscillation equations, we obtain the adiabatic periods quite accurately, although we have lost information as to the time dependence of the periods that is implicitly contained in the evolutionary model. In an effort to retain this information, several authors have attempted to examine the effects of thermal imbalance on the pulsation properties of stellar models, but this remains a thorny problem (for a review, see Cox 1980, §19.4). These procedures have not as yet been applied to "real" evolutionary models. However, from the above discussion, we do not need to worry about thermal imbalance in calculating the adiabatic periods for our models, and so we can take advantage of the evolutionary nature of our models and calculate $d\Pi/dt$. In order to compute $d\Pi/dt$ for a given mode, we calculate the pulsation period of that mode for models in an evolutionary sequence, difference the calculated periods for consecutive evolutionary models [$\Delta \log(\text{age}) < 0.1$] and divide by the age difference of the models.

An observed secular period change results not only from evolutionary changes in the "inertial" adiabatic pulsation period of the star, but from changes in all physical processes that contribute to the observed pulsation period. In order to directly compare with the observed rates of period change, we must include additional effects, such as rotation and mass loss. We will examine the contribution of these effects in Sections 5.5 and 5.7.

5.3 Rates of Period Change for DOV Models

5.3.1 *Pure ^{12}C Models*

In Tables 5.1-5.3 are the rates of change of the periods with time $[d(\ln\Pi)/dt]$ for the pure ^{12}C PWD models. We also show the values of $d(\ln\Pi)/dt$ as functions of luminosity for these sequences in Figure 5.1. We find the adiabatic periods of the high order modes to be increasing (positive $d\Pi/dt$) in all models below $\log(L/L_0)=2.5$. When the luminosity of the model is above the PNN-PWD transition luminosity of $100L_0$ (see Section 4.3), the timescale for period change $[(d\ln\Pi/dt)^{-1}]$ is long compared to e -folding times for surface variables such as luminosity and effective temperature. This is because the period is established throughout the interior of the model, where the cooling and contraction timescales correspond to the thermal timescale of the whole star, $\sim 10^6$ years.

Winget, Hansen and Van Horn (1983, hereafter WHVH) have shown that the expression for $d(\ln\Pi)/dt$ is of the form:

$$d(\ln\Pi)/dt = -a d(\ln T)/dt + b d(\ln R)/dt \quad (5.1)$$

where T is the temperature in the region of maximum weight and R is the stellar radius. Cooling tends to decrease the Brunt-Väisälä frequency, and therefore increase the period of g -modes, as the core becomes more degenerate. Contraction effects lead to decreasing periods with the resulting general increase in sound speed (see Section 3.4). The factors a and b in equation (5.1) are of order unity and are affected by properties such as the temperature dependence of the specific heats, the amount of mass contributing to setting the period, local neutrino energy losses, and other effects such as rotation and nonadiabaticity. We can define a parameter, s , as the ratio of the contraction rate to the cooling rate:

$$s d(\ln T)/dt = d(\ln R)/dt \quad (5.2)$$

Table 5.1

Rates of Period Change for Sequence W60GC1C

#	Age [yr]	$\log(L/L_0)$	$d(\ln\Pi)/dt [10^{-14} \text{ s}^{-1}]$				
			$l = 1$				$l = 2$
			$k = 1$	$k = 10$	$k = 25$	$k = 35$	$k = 35$
41	1.91×10^3	3.150	-48.8	5.50	-11.5	-13.6	-10.4
47	2.42×10^3	3.081	-37.8	13.7	0.47	-2.99	-3.83
53	2.99×10^3	3.002	-27.6	17.6	5.62	0.84	0.32
65	4.27×10^3	2.856	-15.1	14.3	8.08	2.21	2.60
73	6.39×10^3	2.705	-6.69	8.59	5.66	4.39	4.05
77	1.14×10^4	2.500	-1.71	4.97	2.42	3.03	2.86
82	2.19×10^4	2.273	0.48	2.86	1.73	1.50	1.53
86	5.31×10^4	2.000	1.13	1.56	1.01	1.02	1.05
91	1.07×10^5	1.776	1.15	0.94	0.59	0.71	0.71
98	2.51×10^5	1.500	1.08	0.54	0.50	0.51	0.52
102	4.13×10^5	1.304	0.99	0.47	0.53	0.50	0.51
110	7.43×10^5	1.000	0.75	0.45	0.46	0.44	0.44

Table 5.2

Rates of Period Change for Sequence W78GC1C

#	Age [yr]	log(L/L ₀)	d(lnΠ)/dt [10 ⁻¹⁴ s ⁻¹]			
			l = 1			l = 2
			k = 1	k = 10	k = 35	k = 39
62	1.75x10 ³	3.115	-14.9	19.6	9.83	...
67	3.00x10 ³	3.000	-11.1	11.6	4.06	4.15
73	5.93x10 ³	2.853	-7.44	5.16	1.03	0.99
74	7.06x10 ³	2.817	-6.72	4.39	0.86	0.81
78	1.21x10 ⁴	2.707	-4.96	1.26	-0.53	0.03
82	1.78x10 ⁴	2.631	-3.20	0.53	-0.78	-0.51
85	3.25x10 ⁴	2.516	-0.87	0.28	-0.15	-0.49
87	4.33x10 ⁴	2.454	0.17	0.65	0.08	0.10
93	8.62x10 ⁴	2.252	2.32	1.56	1.20	1.34
98	1.50x10 ⁵	1.999	3.14	2.20	1.85	1.77
101	2.13x10 ⁵	1.787	3.35	1.95	1.80	1.78
104	3.18x10 ⁵	1.499	2.82	1.49	1.57	1.57
106	4.24x10 ⁵	1.265	2.40	1.34	1.39	...
108	5.62x10 ⁵	1.015	1.95	1.17	1.15	...

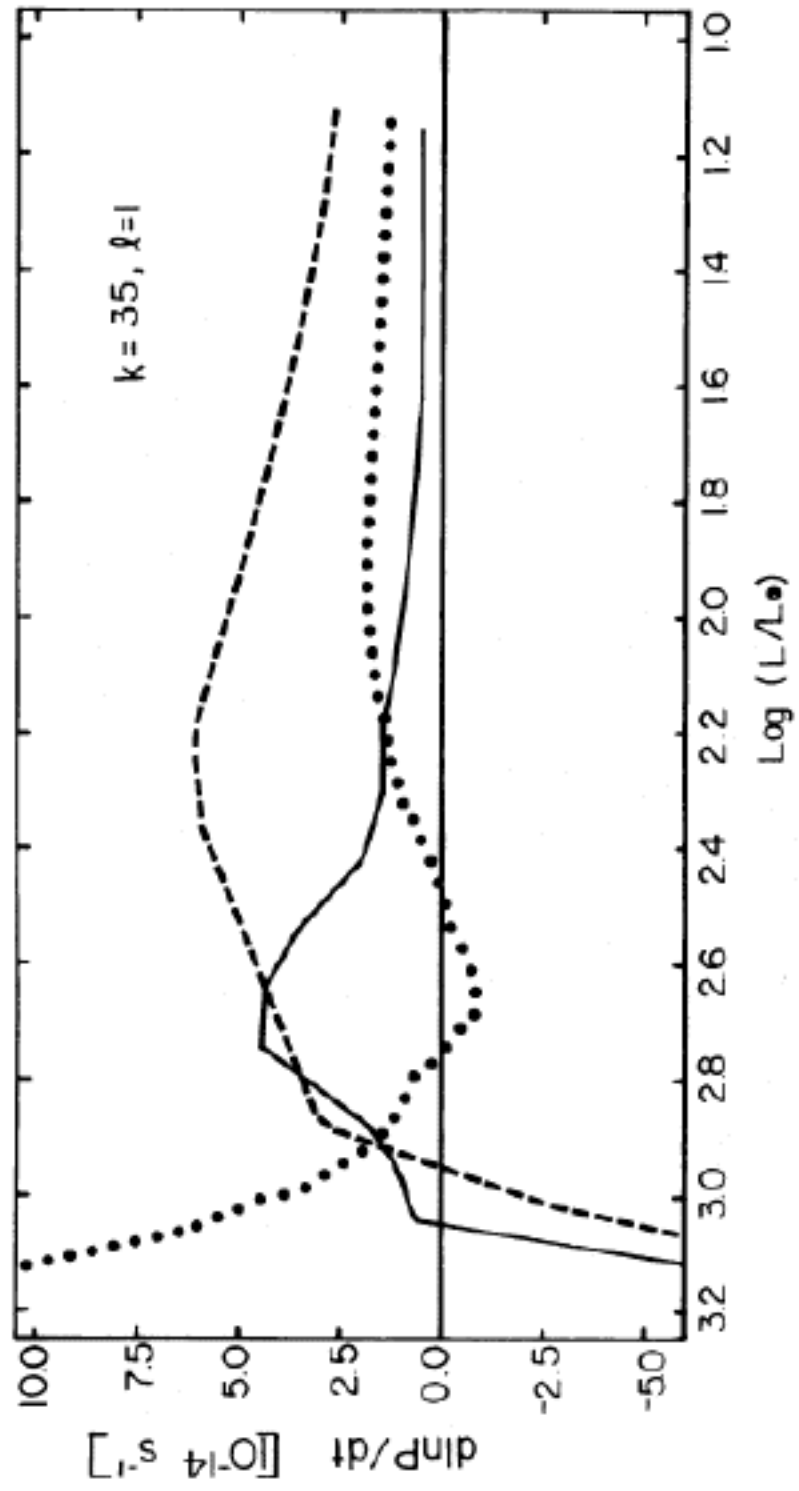
Table 5.3

Rates of Period Change for Sequence W95GC1C

#	Age [yr]	$\log(L/L_0)$	$d(\ln\Pi)/dt [10^{-14} \text{ s}^{-1}]$				
			$l = 1$				$l = 2$
			$k = 1$	$k = 10$	$k = 35$	$k = 51$	$k = 35$
63	-5.47×10^3	3.152	-14.8	-10.6	-12.1	-13.6	-12.3
67	-2.17×10^3	3.095	-9.06	-5.68	-7.90	-8.05	-8.02
73	3.38×10^3	2.993	-0.45	0.61	-1.96	-0.99	-1.97
77	1.68×10^4	2.762	9.18	5.21	3.64	4.36	3.67
82	3.93×10^4	2.454	11.0	6.27	5.40	5.42	5.41
85	5.71×10^4	2.261	11.2	6.67	6.04	5.91	6.08
87	7.14×10^4	2.128	10.8	6.31	5.82	5.79	5.86
92	1.19×10^5	1.776	7.99	4.54	4.44	4.48	4.44
96	1.73×10^5	1.478	6.06	3.49	3.49	3.56	3.50
99	2.28×10^5	1.237	4.77	2.93	2.90	2.95	2.90
102	3.01×10^5	0.981	2.33	...	2.33

Figure 5.1:

The relative rate of period change, $d(\ln\Pi)/dt$, as a function of luminosity for the $k=35$, $l=1$ mode in the $0.60M_{\odot}$ (solid curve), $0.78M_{\odot}$ (dotted curve), and $0.95M_{\odot}$ (dashed curve) pure ^{12}C PWD sequences.



Using this ratio, we rewrite equation (5.1) as:

$$d(\ln\Pi)/dt = (-a+bs) d(\ln T)/dt \quad (5.3)$$

At high luminosities, where contraction dominates ($s>1$), the rate of period decrease is approximated by the rate of radius decrease. When cooling dominates ($s<1$) then the rate of period increase is of the same order as the cooling rate. When the competing effects of cooling and contraction are in approximate balance ($s\sim 1$), then the magnitude of $d(\ln\Pi)/dt$ can be very small or zero, corresponding to a long timescale for period change. The luminosity where this occurs in a given model depends on the combination of factors (all of order unity) in equation (5.3) and is accompanied by a sign change in $d(\ln\Pi)/dt$. We note in passing that observational *limits* to the rate of period change can be as valuable as *measurements* in this regime.

At very high luminosities ($\log(L/L_{\odot})>3.0$) in the $0.95M_{\odot}$ and $0.60M_{\odot}$ models, global contraction effects dominate. Timescales for radius decrease in these models are much shorter than cooling timescales in the zone of large weight. The decreasing periods of these models reflects this condition. Following this phase of rapid contraction, the further radius changes are tempered by the stiffening of the equation of state and these models approach the constant radius phase of evolution. This is reflected in the subsequent increase in period with time. The behavior of $d(\ln\Pi)/dt$ as a function of luminosity is presented in Figure 5.1 for the $k=35$, $l=1$ mode in three sequences W60GC1C, W78GC1C and W95GC1C.

There is a range of luminosities in the $0.78M_{\odot}$ sequence that yields negative values for $d\Pi/dt$. This phase occurs just prior to the broad kink in the evolutionary track for this model (see Figure 2.2). This effect is related to the diffusion of residual thermal energy from the fossil burning shell. The burning shell imposes a steep temperature gradient near the surface, providing radiative support for the overlying mass. As the excess thermal energy diffuses into regions with a very short thermal timescale, the excess support in this zone dissipates. The radius of the regions of the star below the temperature excess then decreases as the new, more shallow temperature gradient becomes established. This transition is an artifact of the

somewhat artificial manner in which the starting model was produced, but is seen in pure $0.78M_{\odot}$ ^{12}C model evolved with WDEC (W78GC1C) and in the further evolution of the stratified $0.78M_{\odot}$ model (P78GI1Y) evolved with the modified Paczynski code. Hence, although it is a detail of the model, the physical effect is real. If the zone of excess thermal energy moves through a region of the star important in setting the oscillation frequency, a negative $d(\ln\Pi)/dt$ could result from the local radius adjustment.

We can make use of the delay between the onset of negative $d(\ln\Pi)/dt$ and the completion of the kink in the evolutionary track to estimate the depth at which the pulsation period is determined. The stellar radius begins to decrease more rapidly at $\log(L/L_{\odot})\sim 2.50$. Negative $d(\ln\Pi)/dt$ appears at $\log(L/L_{\odot})\sim 2.75$. The difference in time between the two models, $\sim 3\times 10^4$ yr, should be comparable to the thermal timescale of the region where the period is determined in the model. Using these values, we find that the delay corresponds to a depth of $0.08M_{\odot}$ below the surface, implying that the period is determined around the position of the degeneracy boundary. This is in qualitative agreement with the weight function for $0.78M_{\odot}$ models at $\log(L/L_{\odot})$ of about 2.6, indicating that our interpretation of the negative $d(\ln\Pi)/dt$ is self-consistent.

The timetable of outward diffusion of thermal energy of the burning shell is sensitive to the treatment of the cessation of nuclear burning in the PWD phase. The transformation from a temperature profile for nuclear burning to one of gravitational contraction is more gradual in the more realistic models than in the simple models presented in this subsection. Hence any of the readjustments in radius such as those that produce negative values of $d(\ln\Pi)/dt$ are less abrupt in more realistic models.

The detailed behavior of $d(\ln\Pi)/dt$ as a function of time is not well determined for the high luminosity ($\log[L/L_{\odot}]>2.7$), rapidly evolving models where the difference between periods in successive models is comparable to our estimates of possible period errors, as in Section 3.6. Hence, error bars of approximately $\pm 1\times 10^{-14}$ should rightly be attached to $d(\ln\Pi)/dt$ above $\log(L/L_{\odot})$ of ~ 2.7 .

Periods are increasing for all models when $\log(L/L_0) \leq 2.5$. Here, $d(\ln\Pi)/dt$ is far more reliable than at higher luminosities; period changes between successive models are much greater than the expected internal errors. The timescales for period change ($\tau = [d(\ln\Pi)/dt]^{-1}$) ranged from 8×10^5 to 20×10^5 years at these lower luminosities, varying inversely with mass at a given luminosity for a given mode.

In Section 3.4.2 the relationship of the time dependence of the oscillation period to the evolutionary changes in the Brunt-Väisälä frequency was discussed with reference to propagation diagrams. This relationship is illustrated in Figure 5.2. The $k=35$, $l=1$ mode for the $0.95M_\odot$ model has $d\Pi/dt = -5 \times 10^{-11}$ s/s in Figure 5.2(a); $d\Pi/dt = +2 \times 10^{-11}$ s/s in Figure 5.2b. The integrated weight function for this mode is indicated with arrows above the N^2 curves in Figure 5.2. The bulk of the eigenvalue is determined before the zone of increasing N^2 in Figure 5.2(b). Contraction is important where N^2 is increasing in the nondegenerate envelope. But in the degenerate core, cooling dominates and N^2 decreases. The overall positive value of $d\Pi/dt$ for the model in Figure 5.2(b) means that the cooling core dominates the contracting envelope in establishing $d\Pi/dt$ as well as Π .

5.3.2 *The Stratified DOV Sequences*

The rates of period change for the compositionally stratified $0.60M_\odot$ sequence I60BC1Y are presented in Table 5.4, and are compared with the pure ^{12}C model in Figure 5.3. Since this model was evolved directly from the AGB, the high luminosity models ($L > 1000L_\odot$) give more physically consistent values for $d(\ln\Pi)/dt$ at these high luminosities than the carbon models. Below $\log(L/L_0) = 2.6$, values of $d(\ln\Pi)/dt$ are systematically larger in the compositionally stratified sequence than in the pure ^{12}C model with neutrinos included; in the luminosity range from $\log(L/L_0) = 2.6$ to $\log(L/L_0) = 1.0$ the period increases about twice as fast. The difference in $d(\ln\Pi)/dt$ reflects the difference in composition of the region of maximum weight: the stratified models are about half carbon and half oxygen in the core. As we will show in Section 5.6.2 and in the Appendix, the conductive cooling rate for degenerate stellar material is proportional to the mean atomic weight. The stratified models have a higher mean atomic weight in the core than the pure ^{12}C models, and therefore cool more quickly.

Figure 5.2 (a),(b):

Expanded propagation diagrams for some $0.95M_{\odot}$ models. In panel (a) we have N^2 for $\log(L/L_{\odot})=3.15$ (solid line), and N^2 for $\log(L/L_{\odot})=3.10$ (short-dashed line). In (b), we have N^2 for $\log(L/L_{\odot})=2.45$ (solid line), and N^2 for $\log(L/L_{\odot})=2.13$ (short-dashed line). The long-dashed line is $S_{l=1}^2$ for $l=1$ in the more luminous model. The value of the integrated weight function is indicated with arrows above the N^2 curves.

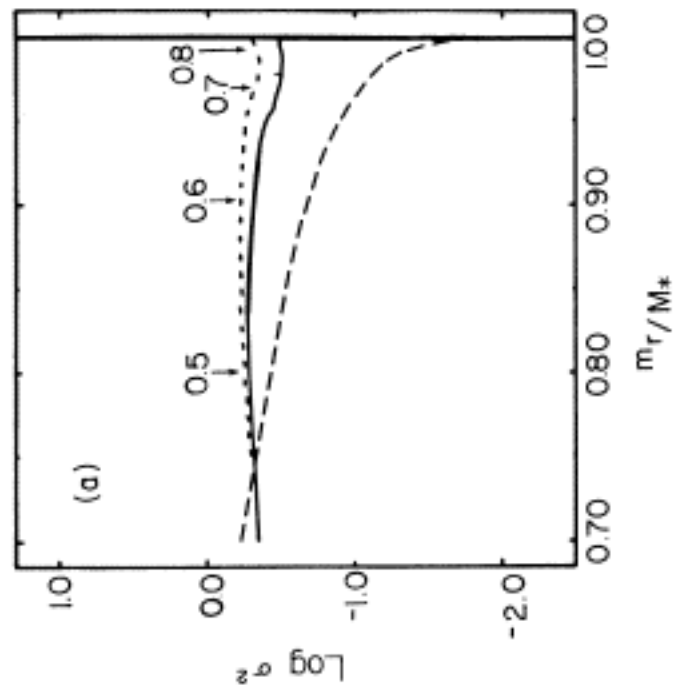
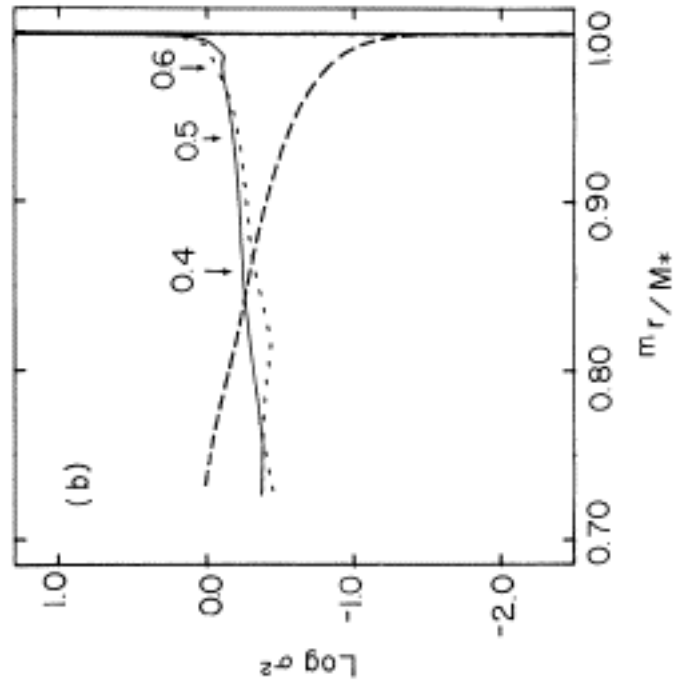


Table 5.4

Rates of Period Change for Sequence I60BC1Y

#	Age [yr]	log(L/L ₀)	d(lnΠ)/dt [10 ⁻¹⁴ s ⁻¹]				
			l = 1				l = 2
			k = 1	k = 10	k = 25	k = 35	k = 35
1	-2.13e+03	3.208	-11.4	4.85	2.22	-2.75	-3.38
2	3.70e+02	3.117	-9.82	8.30	-0.63	-1.47	-1.60
3	2.38e+03	3.031	-8.30	9.75	-0.42	0.18	0.15
4	5.38e+03	2.885	-5.31	7.93	3.87	2.52	2.27
6	9.38e+03	2.693	-1.13	3.22	3.35	3.70	...
8	1.34e+04	2.535	1.02	1.91	3.87	4.19	4.09
9	2.54e+04	2.231	2.36	2.58	3.33	2.96	2.97
10	4.04e+04	2.009	2.27	2.81	2.19	2.19	2.21
11	7.65e+04	1.725	1.78	2.01	1.55	1.45	1.42
12	1.27e+05	1.499	1.40	1.36	1.07	0.91	0.90
13	2.47e+05	1.209	1.04	0.73	0.55	0.61	0.61
14	3.97e+05	0.988	0.84	0.50	0.41	0.47	0.45

Figure 5.3:

Relative rate of period change as a function of luminosity for the $k=35$, $l=1$ g-mode in the $0.60M_{\odot}$ stratified PWD sequence with a helium envelope (I60BC1Y, dashed line) and for the sequence with a pure ^{12}C composition (W60GC1C, solid line).

The rates of period change for the $0.60M_{\odot}$ models described above appear to hold for the general class of PNN-PWD models. The major structural difference between the various stratified sequences with nuclear burning and the simpler homogeneous ^{12}C models is in their envelope structure. For high luminosity models, the period is largely determined in the interior of the star, below any nuclear shell sources. Therefore, at luminosities above the PNN-WD transition luminosity at $100L_{\odot}$, the qualitative features of the pulsation properties of the high-order modes for the three sequences reflect the basic similarities of their degenerate cores, with minor differences attributable to differences in core composition. By the time the models cool below the transition luminosity, where the portions of the star near the surface begin to dominate the weight function, these differences in envelope structure begin to diminish as residual nuclear burning dies away. Hence, the pulsation properties will remain somewhat similar even below the transition luminosity. Therefore we can conclude, with a measure of confidence, that the pulsation properties presented herein are representative of the entire class of theoretical PWD models.

5.4 Neutrino Emission and $d(\ln\Pi)/dt$

At luminosities of interest for the DOV stars, the values of $d(\ln\Pi)/dt$ for the $0.60M_{\odot}$ ^{12}C sequences with reduced neutrino emission (W60GC0C [no neutrino emission] and W60GC2C [neutrino emission cut by a factor of 2]) are much smaller than in the models that include neutrinos. In Figure 5.4, we show the rate of period change as a function of luminosity for the sequences with varying neutrino emission rates, and we tabulate the values of $d(\ln\Pi)/dt$ in Table 5.5. At the luminosity of PG1159-035, $\sim 100L_{\odot}$, $d(\ln\Pi)/dt$ for the $l = 1, k = 25$ mode is $+2.2 \times 10^{-15} \text{s}^{-1}$ for the sequence with no neutrinos. This is a factor of five smaller than in the $0.60M_{\odot}$ ^{12}C model that includes neutrinos. For the sequence with neutrinos cut by a factor of two, $d(\ln\Pi)/dt$ is $+4.7 \times 10^{-15} \text{s}^{-1}$, or roughly a factor of two smaller than in the models that include neutrinos.

The dependence of $d(\ln\Pi)/dt$ on the neutrino rates is a simple consequence of the slower rate of cooling of the core in models where neutrino emission has been

Figure 5.4:

Relative rate of period change as a function of luminosity, for the $k=25$, $l=1$ mode, in $0.60M_{\odot}$ pure ^{12}C PWD sequences differing in the rate of neutrino emission. The short-dashed line is for a sequence with no neutrino emission (W60GC0C), and the dashed line had neutrino emission reduced by a factor of 2 from the rates of Beaudet, Petrosian and Salpeter (1967) (W60GC2C). For comparison, we also show the curve for a sequence that included these standard neutrino emission rates (W60GC1C).

Table 5.5

$d(\ln \Gamma)/dt$ for Different Neutrino Emission Rates ($0.60M_{\odot}$, $l=1$, $k=25$)

	$\varepsilon_{\nu}=\text{BPS}$	$\varepsilon_{\nu}=1/2 \text{ BPS}$	$\varepsilon_{\nu}=0$
	=====	=====	=====
<u>$\log(L/L_{\odot})=2.75$</u>			
Age [yr]	5.76×10^3	6.43×10^3	3.42×10^3
Period [s]	563.1	579.6	692.9
$d(\ln \Gamma)/dt$ [s^{-1}]	6.38×10^{-14}	3.44×10^{-14}	4.05×10^{-13}
<u>$\log(L/L_{\odot})=2.50$</u>			
Age [yr]	1.14×10^4	1.34×10^4	7.90×10^3
Period [s]	566.7	583.4	698.6
$d(\ln \Gamma)/dt$ [s^{-1}]	2.42×10^{-14}	2.17×10^{-14}	3.80×10^{-14}
<u>$\log(L/L_{\odot})=2.00$</u>			
Age [yr]	5.31×10^4	6.54×10^4	6.40×10^4
Period [s]	577.3	590.4	705.7
$d(\ln \Gamma)/dt$ [s^{-1}]	1.01×10^{-14}	4.65×10^{-15}	2.23×10^{-15}
<u>$\log(L/L_{\odot})=1.75$</u>			
Age [yr]	1.20×10^5	1.75×10^5	1.92×10^5
Period [s]	585.8	595.6	707.7
$d(\ln \Gamma)/dt$ [s^{-1}]	5.82×10^{-15}	1.89×10^{-15}	6.63×10^{-16}
<u>$\log(L/L_{\odot})=1.50$</u>			
Age [yr]	2.51×10^5	3.77×10^5	5.16×10^5
Period [s]	596.3	601.1	713.6
$d(\ln \Gamma)/dt$ [s^{-1}]	4.96×10^{-15}	1.59×10^{-15}	4.64×10^{-16}

reduced. At and below luminosities appropriate to PG1159, $d(\ln\Pi)/dt$ is roughly proportional to the rate of neutrino energy losses. However, for models with no neutrino emission, $d(\ln\Pi)/dt$ has a minimum value that depends only on the photon cooling rate. Above $\sim 100L_{\odot}$ $d(\ln\Pi)/dt$ shows the effects of the different prior evolutionary histories of the models.

It is very important to treat the effects of neutrinos self-consistently by evolving with the reduced rates from the base of the AGB for the reasons discussed in Section 3.3.2. The thermal structure of a star on the AGB is very sensitive to the rate of neutrino emission: for example, the AGB sequences with reduced neutrino emission have burning shells that are slightly farther out and narrower in mass than in the standard AGB model at a given luminosity. The evolutionary differences produce qualitatively different temperature profiles in the resulting PNN models. This dependence on prior evolution results in the nonlinear dependence of $d(\ln\Pi)/dt$ on the rate of neutrino emission in the more luminous PNN models ($\log[L/L_{\odot}] > 2.5$). In those models, differences in the residual thermal structure of the core remain significant, and are reflected in the values of $d(\ln\Pi)/dt$. When the models cool to below $\log(L/L_{\odot}) \sim 2.5$, the global cooling effects track the neutrino emission rates more closely, as neutrinos begin to dominate the cooling.

5.5 Effects of Spin-up and Rotational Splitting

As a star contracts and its rotational moment of inertia decreases, it will rotate faster to conserve angular momentum. This rotational spin-up can lead to a change in the rotational splitting of observed nonradial g-modes periods. In this section, we calculate, in the observer's frame, the rate of period change for $0.60M_{\odot}$ models in the presence of slow rotation. Differentiating the equation for rotational splitting in the presence of slow uniform rotation (equation 3.42) with respect to time gives:

$$\frac{d\sigma_{\text{obs}}}{dt} = \frac{d\sigma_0}{dt} - m \frac{d\Omega}{dt} (1-C) + m \Omega \frac{dC}{dt} \quad (5.4)$$

where the symbols are as defined in Chapter 3, and we abbreviate C_{rot} as C . If we assume that the total angular momentum J of the star is conserved and that there is no redistribution of angular momentum within the star, then

$$dJ/dt = d(I\Omega)/dt = 0 \quad , \quad (5.5)$$

where I is the rotational moment of inertia of the star which, like Ω , may change with time. Using this equation and assuming that $\sigma_{\text{obs}} \sim \sigma_0$ we can rewrite equation 5.4 in terms of periods and their time derivatives as

$$\frac{d(\ln\Pi_{\text{obs}})}{dt} = \frac{d(\ln\Pi_0)}{dt} - m \frac{\Pi_0}{\Pi_{\text{rot}}} \left[(1-C) \frac{d(\ln I)}{dt} + \frac{dC}{dt} \right] \quad (5.6)$$

where Π_0 is the pulsation period for the case of uniform rotation.

As the star evolves and cools, it will contract and become less centrally condensed; the rate of decrease in the moment of inertia is proportional to the contraction rate. In the early phases of PWD evolution, when radial contraction is significant, rotational spin up can produce large changes in the observed rate of period change for modes with $m \neq 0$. Prograde modes ($m < 0$) will have reduced values of $d(\ln\Pi_{\text{obs}})/dt$ compared with the nonrotating value, whereas retrograde ($m > 0$) modes will increase $d(\ln\Pi_{\text{obs}})/dt$. Modes with $m=0$ are unaffected by slow rotation. We also note that the effect of rotation on $d(\ln\Pi_{\text{obs}})/dt$ decreases with increasing rotation period.

For rotational splitting in models undergoing differential rotation, we differentiate equation (3.44) and transform frequencies to periods, and find

$$\frac{d(\ln\Pi_{\text{obs}})}{dt} = \frac{d(\ln\Pi_0)}{dt} - m \frac{\Pi_0}{\Pi_{\text{rot}}} \left[\frac{d(C+C_1)}{dt} - (1-C-C_1) \frac{d(\ln\Omega_0)}{dt} \right] \quad (5.7)$$

where, now, Π_{rot} is the rotation period at the poles. To calculate the rate of period change self-consistently for a sequence of models which conserves angular momentum, we desire an expression for $d(\ln\Omega_{\text{O}})/dt$ in terms of the structure of the equilibrium model. For this purpose, we take the limit, as ϖ goes to zero, of the Ostriker and Bodenheimer rotation law in the form as presented in Hansen, Cox and Van Horn (1977) to obtain

$$\Omega_{\text{O}} = 1.1788 J / (MR^2) f \quad (5.8)$$

where

$$f = M^{-1}R^{-2} \int_0^M dm_r / r^2 \quad (5.9)$$

and m_r is the mass within a sphere of radius r . With this expression for Ω_{O} in equation 5.7 we finally obtain

$$\begin{aligned} \frac{d(\ln\Pi_{\text{obs}})}{dt} = \frac{d(\ln\Pi_{\text{O}})}{dt} - m \frac{\Pi_{\text{O}}}{\Pi_{\text{rot}}} \left[\frac{d(C-C_1)}{dt} \right. \\ \left. - (1-C-C_1) \left(\frac{d(\ln f)}{dt} - 2 \frac{d(\ln R)}{dt} \right) \right] \end{aligned} \quad (5.10)$$

as the desired expression for $d(\ln\Pi_{\text{obs}})/dt$ for models with differential rotation.

We have calculated values of $d(\ln\Pi_{\text{obs}})/dt$ for the $0.60M_{\text{O}}$, pure ^{12}C evolutionary sequence W60GC1C. The modes explicitly considered here are the $k=35$ modes. Table 5.6 gives the values of the rotation coefficients (C and C_1) and the various structure quantities used in the calculation of rotational splitting for the $l=2$, $k=35$ mode. The quantities in Table 5.6 were numerically differenced to yield the time derivatives found in equations (5.6) and (5.10). Figure 5.5 illustrates the rates of

Table 5.6
 Rotational Splitting Parameters for
 Pure ^{12}C $0.60M_{\odot}$ PWD Models (Sequence W60GC1C)

Age [10^3y]	$\log(L/L_{\odot})$	Π [s]	R [cm]	I [10^{50}gcm^2]	C	$C_1(1)$	$C_1(2)$	f
2.99	3.002	447.53	9.403	3.1290	0.1640	0.2860	0.2866	53.44
4.27	2.856	447.72	9.366	3.0708	0.1645	0.2750	0.2755	45.27
6.39	2.705	448.97	9.332	3.0127	0.1649	0.2541	0.2546	38.89
11.4	2.500	451.76	9.290	2.9315	0.1652	0.2403	0.2407	32.36
21.9	2.273	454.33	9.250	2.8378	0.1654	0.2254	0.2258	27.23
53.1	2.000	460.17	9.203	2.6955	0.1656	0.1969	0.1972	22.55
107	1.776	466.84	9.168	2.5584	0.1657	0.1794	0.1797	19.76
251	1.500	478.38	9.122	2.3299	0.1658	0.1625	0.1627	17.02
413	1.304	490.82	9.092	2.1780	0.1658	0.1455	0.1456	15.54
743	1.000	517.71	9.054	2.0071	0.1657	0.1293	0.1294	13.86

period change as a function of luminosity for this mode, for a rotation period that was initially 5 times the pulsation period. For the model at $\log(L/L_0)=2.27$, Figure 5.6 shows the dependence of $d(\ln\Pi_{\text{obs}})/dt$ on the rotation rate for various values of m and l .

In consideration of the observed negative value of $d(\ln\Pi)/dt$ for PG1159-035, we have plotted the theoretical value of $d(\ln\Pi_{\text{obs}})/dt$ for negative values of m . Modes with positive values of m would show a larger positive value of $d(\ln\Pi_{\text{obs}})/dt$ than the nonrotating value. It is encouraging to note that full nonadiabatic calculations that implicitly include slow rotation seem to indicate that modes with negative m are slightly more unstable than those with positive m (Carroll and Hansen 1982; Hansen, Cox and Carroll 1978).

Figure 5.5 shows that, as expected, high luminosity models show large negative values of $d(\ln\Pi_{\text{obs}})/dt$, in prograde modes, resulting from the spin-up from contraction. As the model approaches the constant radius phase, the rotational contribution to $d(\ln\Pi_{\text{obs}})/dt$ decreases. At luminosities appropriate to PG1159-035 ($L\sim 100L_0$), rotation periods of a few thousand seconds in modes with pulsation periods of about 500 seconds produce rates of period change that are consistent with observation. For slower rotation rates, the contribution of rotation to $d(\ln\Pi_{\text{obs}})/dt$ for modes with $m \neq 0$ is still significant.

Also indicated in Figures 5.5 and 5.6 is the value of $d(\ln\Pi_{\text{obs}})/dt$ for differential rotation. At luminosities below about $300L_0$, the difference in $d(\ln\Pi_{\text{obs}})/dt$ between the two rotation laws is small. Differential rotation slightly reduces the effect of rotation on $d(\ln\Pi_{\text{obs}})/dt$, compared with uniform rotation, in this luminosity range. This modification of $d(\ln\Pi_{\text{obs}})/dt$ tends to increase with l ; in general, however, the period change due to rotational spin-up is not very sensitive to the form of the rotation law. We note that although these rotational splitting calculations originally assumed slow rotation ($\Pi \ll \Pi_{\text{rot}}$), this condition is not entirely satisfied with the larger values of Π/Π_{rot} considered in Figure 5.6, although the results may be taken as indicative of the effect of rotation.

Figure 5.5:

Relative rates of period change for $k=35$ g-modes in the $0.60M_{\odot}$ model. The dashed line represents $d(\ln\Pi_{\text{obs}})/dt$ in the absence of rotation (or $m=0$ with slow rotation). The solid lines show $d(\ln\Pi_{\text{obs}})/dt$ for the case of uniform rotation with, from top to bottom: $l=2, m=-1$; $l=2, m=-2$; and $l=3, m=-3$. The dotted lines show the evolution of $d(\ln\Pi_{\text{obs}})/dt$ for the differential rotation law described in the text for the same sequence of l and m . The initial value of $\Pi_{\odot}/\Pi_{\text{rot}}$ is 0.20 at $\log(L/L_{\odot})=3.0$; the ratio increases to 0.33 (uniform rotation) and 0.26 (differential rotation) at $\log(L/L_{\odot})=1.0$ as a result of the evolutionary increase in pulsation period and decrease in rotation period.

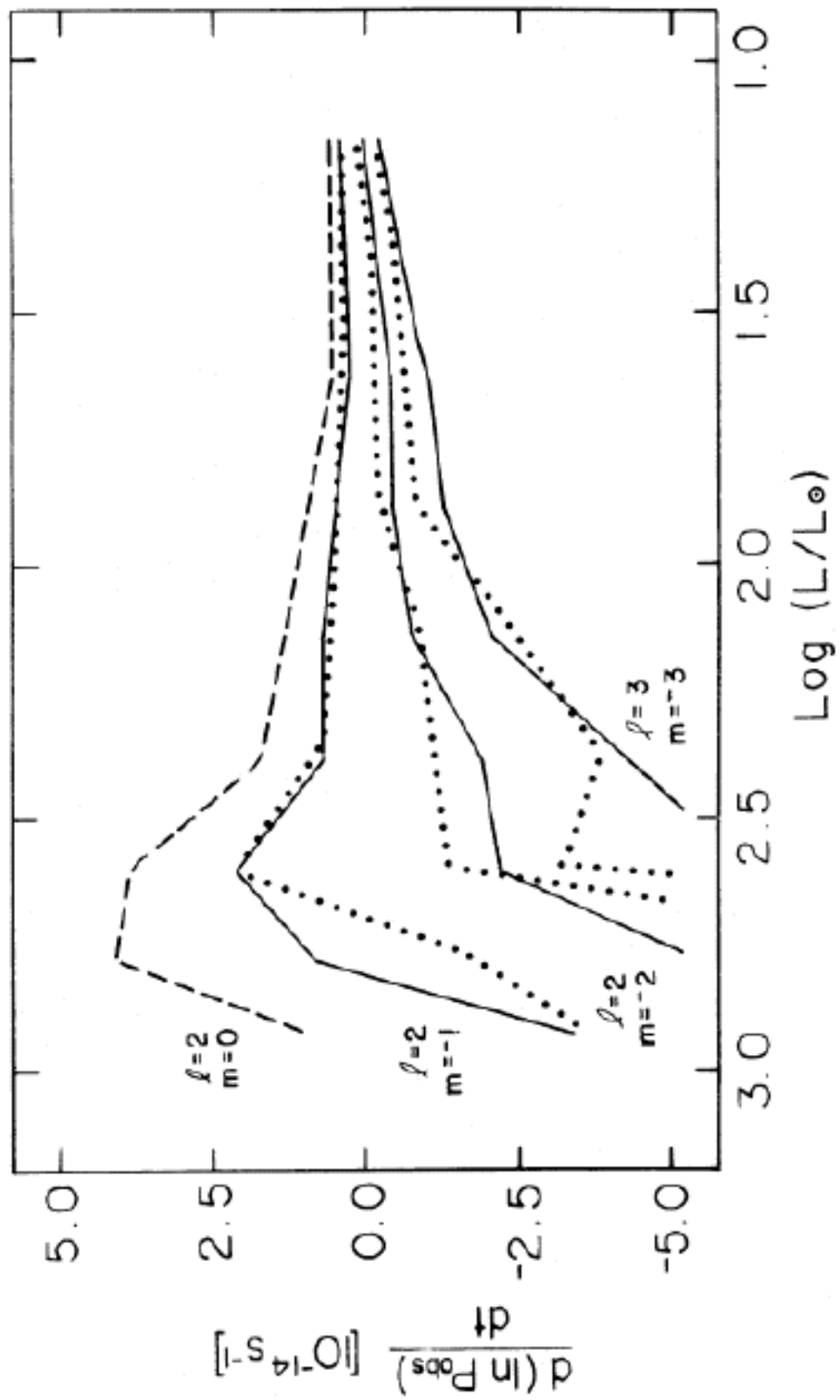
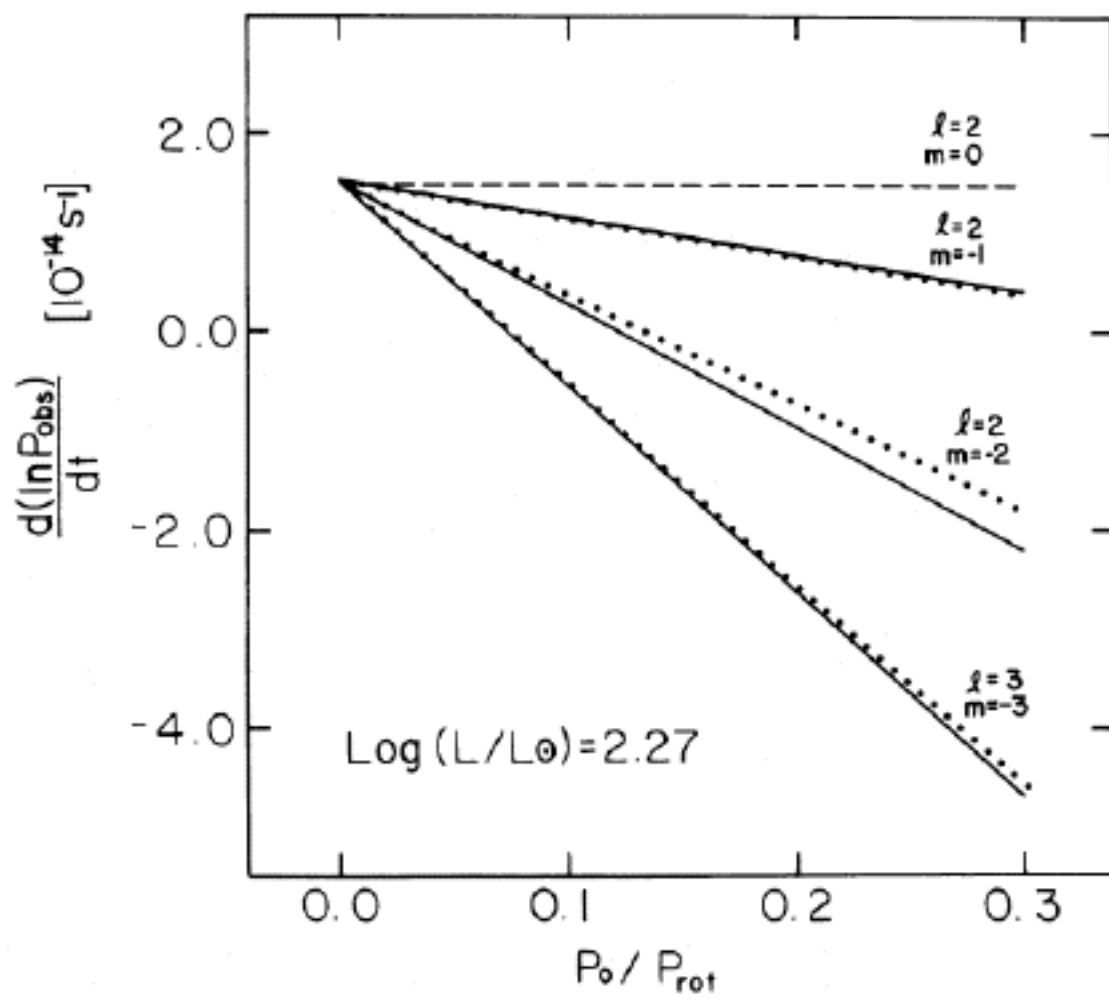


Figure 5.6:

Dependence of $d(\ln\Pi_{\text{obs}})/dt$ on rotation rate for the $\log(L/L_0)=2.26$ pure ^{12}C model in sequence W60GC1C. The horizontal dashed line gives $d(\ln\Pi_{\text{obs}})/dt$ for the case of no rotation (or $m=0$ with slow rotation). Solid lines are for the case of uniform rotation with, from top to bottom: $l=2, m=-1$; $l=2, m=-2$; and $l=3, m=-3$. The dotted lines are for differential rotation.



For PG1159-035, the observed value of $d(\ln\Pi_{\text{obs}})/dt$ for the 516s period implies a rotation period of order 2000 to 4000s for modes with $l=-m=3$. This preliminary estimate corresponds to a rotation velocity of about 35-50km/s, and is consistent with the rotation velocities of DA white dwarfs as reported by Pilachowski and Milkey (1984). We note also that the period ratios in another non-radially pulsating white dwarf, the ZZ Ceti star L19-2, suggest that modes with $l=1$ to 5 are present (O'Donoghue and Warner 1982). Dziembowski (1977,1985) has shown that geometric cancellation effects greatly reduce the luminosity variations for larger values of l . Hence it appears that the values of l and m suggested by this analysis are not unreasonable. In any case, it is clear that the effects of rotation on the observed value of $d(\ln\Pi)/dt$ must be taken into consideration.

The rate of rotational spin-up by contraction is about the same for the models with reduced neutrino emission as for the models that include neutrinos. Since rotation can play an important role in determining the observed rate of period change, observation of $d(\ln\Pi)/dt$ alone is insufficient to uniquely constrain the neutrino rates. However, as measurements of $d\Pi/dt$ for additional modes in PG1159 and other objects become available, the prospects for observationally separating out the rotation effects are good, in which case the constraints will become severe.

5.6 Rates of Period Change for DBV Models

5.6.1 *Numerical Results*

The run of $d(\ln\Pi)/dt$ with respect to effective temperature for DBV models is illustrated in Figure 5.7. For the $0.60M_{\odot}$ model with a helium-rich envelope (I60BC1Y), we find values of $d(\ln\Pi)/dt$ ranging from $2.3 \times 10^{-16} \text{s}^{-1}$ at $T_e=30,000\text{K}$ to about $1.0 \times 10^{-17} \text{s}^{-1}$ at $T_e=20,000\text{K}$. Therefore $d(\ln\Pi)/dt$ is a more sensitive function of T_e than in any other model that we investigated. For example, the pure ^{12}C $0.60M_{\odot}$ sequence showed values of $d(\ln\Pi)/dt$ of $2 \times 10^{-16} \text{s}^{-1}$ at $T_e=30,000\text{K}$

down to $7 \times 10^{-17} \text{s}^{-1}$ at $T_e = 20,000 \text{K}$. This difference in the behavior of $d(\ln \Pi)/dt$ as a function of T_e for two models of the same mass can be understood in terms of the differences between the compositional structure of the pure ^{12}C model and the more realistic compositionally stratified model. These effects will be discussed in more detail in the next subsection.

Examination of the three ^{12}C sequences illustrates the dependence of $d(\ln \Pi)/dt$ on stellar mass. Lower mass models show larger values of $d(\ln \Pi)/dt$ through the range of effective temperature of DBV stars. This reflects the simple fact that, for a given effective temperature, lower mass white dwarfs have a larger radius, therefore higher luminosity, and have a lower total heat capacity; hence the rate of leakage of thermal energy is larger than in more massive white dwarfs.

5.6.2 Comparison With a Simple Cooling Model

The cooling rate for a white dwarf can be estimated analytically using the simple model of Mestel (1952). When neutrinos and nuclear burning are unimportant luminosity sources, the Mestel cooling theory relates the photon luminosity, and therefore the cooling rate, to the temperature of the isothermal core (see the discussion of Van Horn 1971). Assuming a mass-radius relationship for white dwarfs, we can then relate the cooling rate to the effective temperature to obtain:

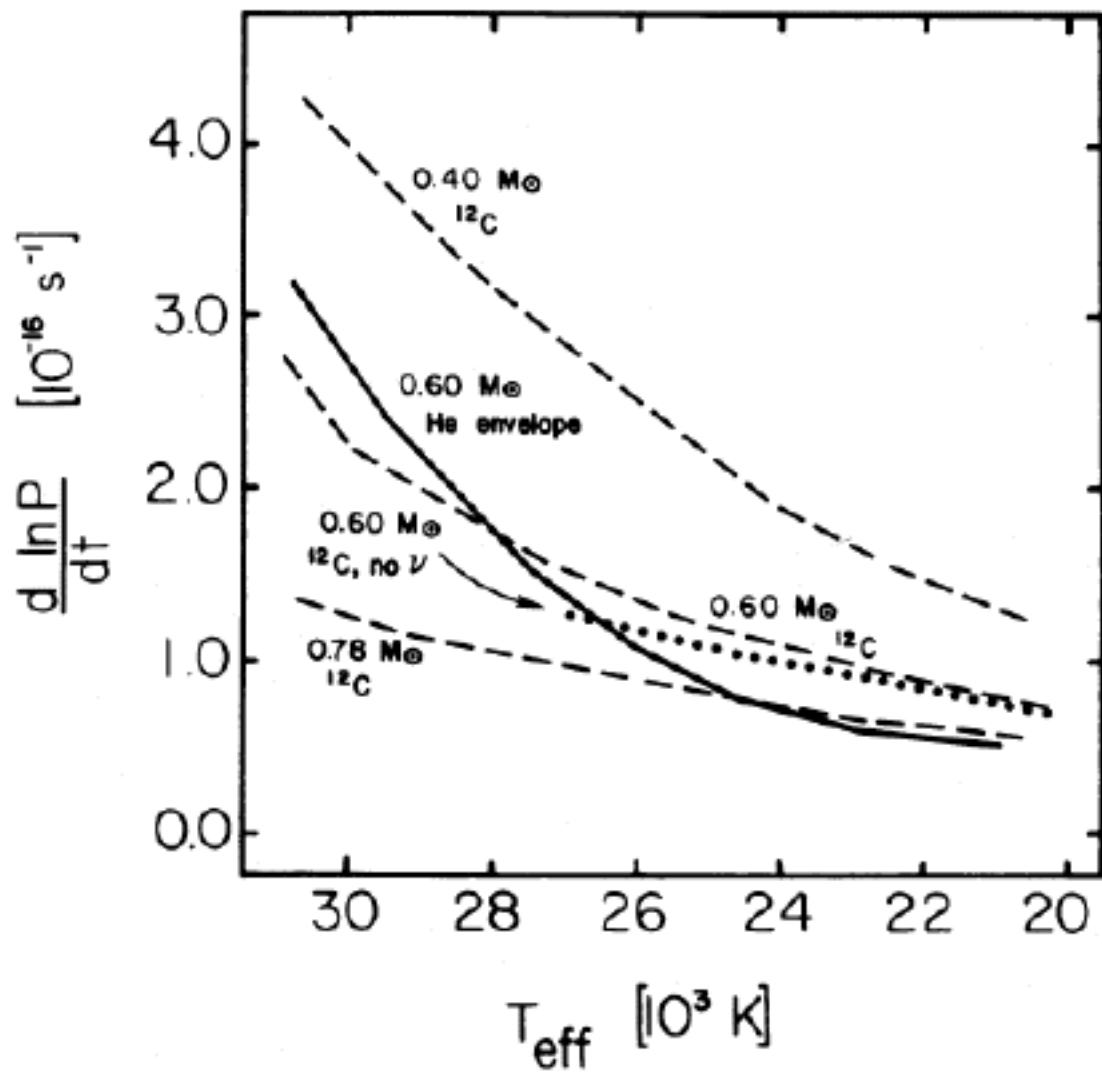
$$\frac{d(\ln T_e)}{dt} = -5 \times 10^{-30} A \left(\frac{\mu}{\mu_e^2} \right)^{0.286} \left(\frac{M}{M_\odot} \right)^{-1.190} T_e^{2.857} \quad (5.11)$$

where μ_e is the mean molecular weight per electron, and A is the atomic mass of the ions. The derivation of equation (5.11) is presented in the Appendix.

For high-order g -modes in slowly rotating ($\Pi_{\text{puls}} \ll \Pi_{\text{rot}}$) stars, the relation of Winget, Hansen and Van Horn (1983) (their equation 3) becomes

Figure 5.7:

Relative rate of period change as a function of effective temperature for the $k=25$, $l=2$ mode in the pure ^{12}C (dashed lines) and stratified carbon and helium (solid line) sequences. The dotted line represents the $0.60M_{\odot}$ sequence without neutrino emission.



$$\frac{d(\ln\Pi)}{dt} = -\frac{1}{2} \frac{d(\ln T)}{dt} + \left(1 - b_{\text{rot}} \frac{\Pi}{\Pi_{\text{rot}}}\right) \frac{d(\ln R)}{dt} \quad (5.12)$$

where T is the temperature in the zone of the star where the adiabatic period is determined. The rotation term, b_{rot} , discussed in the Appendix, is of order unity. For the DBV stars, $d(\ln R)/dt \ll d(\ln T)/dt$. Hence, when a white dwarf cools in the Mestel fashion, $d(\ln\Pi)/dt$ is a measure of the cooling rate of the outer layers of the star, and is uniquely determined by the effective temperature. At low effective temperatures, the values of $d(\ln\Pi)/dt$ in the models do follow the expectations based on the simple Mestel cooling model. The values of $d(\ln\Pi)/dt$ are the same to within a factor of two, and seem to follow a power law of the same slope.

Dependence of the mass-radius relationship for white dwarfs on composition and other factors, plus the complicating effects of non-ideal gas contributions to the equation of state, affect the constant in equation (5.11). Also, we may employ the rate of change of the effective temperature in equation (5.12) in this discussion with appropriate adjustment to the factor of 1/2 that appears there. Since the offset in $d(\ln\Pi)/dt$ between that given by the cool ^{12}C models and that implied by equations (5.11) and (5.12) is roughly constant with mass, we can recalibrate the constants of equations (5.11) and (5.12) empirically. Setting $T=T_e$ and combining yields

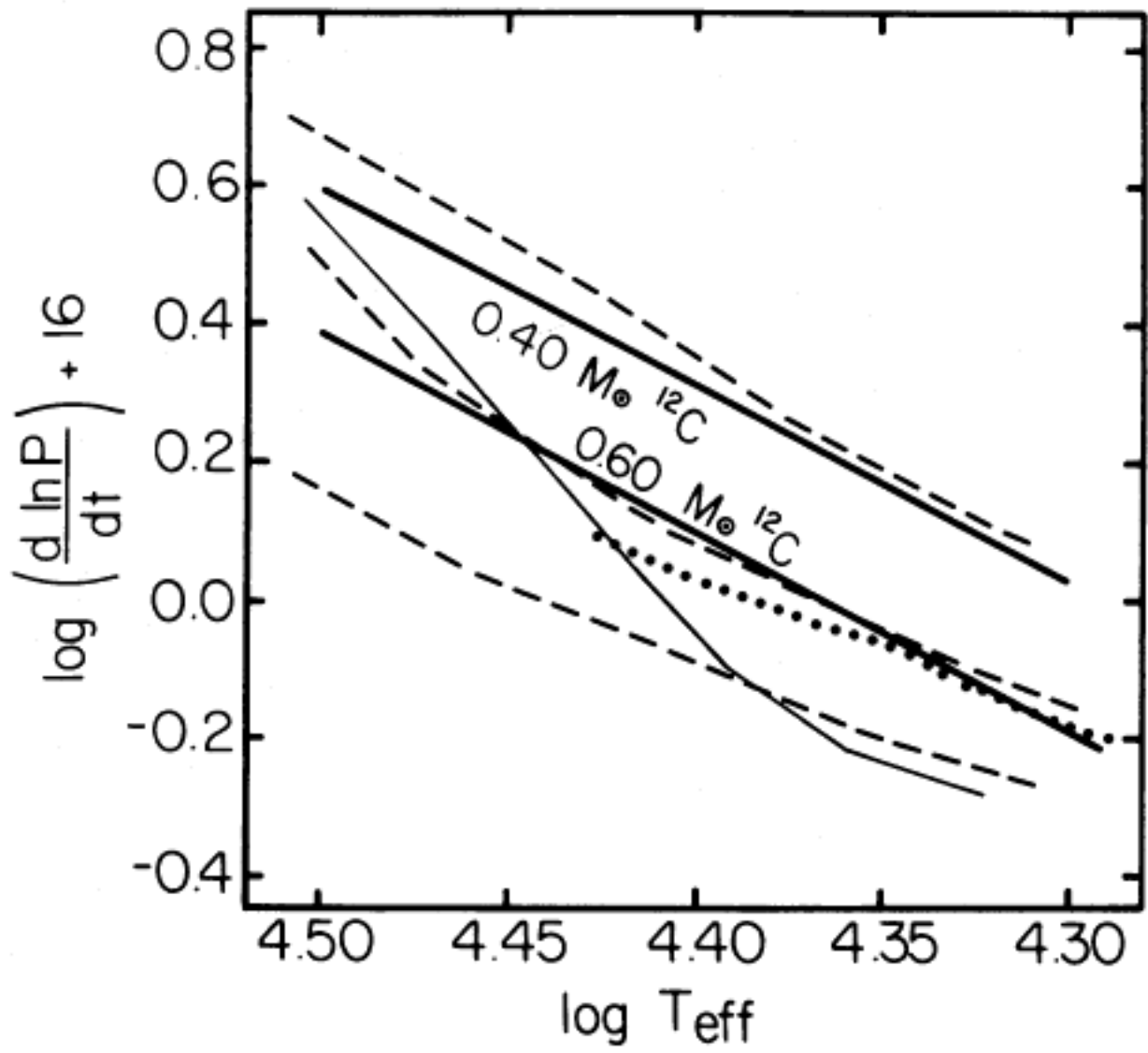
$$\frac{d(\ln\Pi)}{dt} = 2 \times 10^{-30} \text{ A} \left(\frac{\mu}{\mu_e^2}\right)^{0.286} \left(\frac{M}{M_{\text{O}}}\right)^{-1.190} T_e^{2.857} \quad (5.13)$$

which reproduces $d(\ln\Pi)/dt$ quite well for models below $T_e=24,000\text{K}$. In Figure 5.8 we have replotted the numerical results of Figure 5.7 on a logarithmic scale. Also illustrated in Figure 5.8 is the analytically determined value of $d(\ln\Pi)/dt$ (eq. [5.13]) for pure ^{12}C white dwarfs of 0.40 and $0.60M_{\text{O}}$.

We can isolate the effects of neutrino cooling, as measured by the rates of period change, by considering the $0.60M_{\text{O}}$ pure carbon model. At higher effective temperatures,

Figure 5.8:

Same as Figure 5.7, but plotted on logarithmic scales. The straight solid lines are analytic determinations (equation [5.13]) of $d(\ln\Pi)/dt$ for $0.40M_{\odot}$ (top) and $0.60M_{\odot}$ (bottom) pure ^{12}C white dwarfs.



this model cools more rapidly (along a steeper power law) than does the model with no neutrinos, until $L_\nu/L_\gamma \leq 0.2$ ($T_e \sim 25,000\text{K}$). This is apparent in Figure 5.8. Stronger neutrino emission leads to a stronger dependence of $d(\ln\Pi)/dt$ on T_e than in the analytic case until the neutrino luminosity drops well below the photon luminosity.

At high effective temperatures, neutrinos also influence the cooling of the stratified model. Because of the higher core temperature of the stratified model, the energy loss by plasmon and bremsstrahlung neutrino emission was about twice the rate in the pure ^{12}C , $0.60M_\odot$ model. Hence, in the stratified model, neutrinos remain important down to lower T_e . The effects of composition on the cooling rates also contribute to the different behavior of $d(\ln\Pi)/dt$ for the model with a helium-rich envelope. In the model with a helium envelope, most of the thermal energy is released near the outer boundary of the degenerate core. In the temperature range of the DBV stars, this boundary moves outwards into a region containing a substantial mass fraction of helium. Since the period is being formed near this degeneracy boundary, $d(\ln\Pi)/dt$ drops below the value for the pure ^{12}C models. The major reason for this is the factor A in equation (5.13). This is why, at the cool end of the DBV sequence, the helium envelope models show smaller values of $d(\ln\Pi)/dt$ than the pure carbon models.

5.7 Other Effects

The reported value of $d(\ln\Pi)/dt$ for PG1159-035 corresponds to a timescale for period change of about 1 million years. This is in qualitative agreement with the timescales present in $0.60M_\odot$ and $0.78M_\odot$ PWD models at $\log(L/L_\odot) < 2.2$. The high degree of degeneracy in these standard nonrotating post-PNN PWD models precludes any radius changes large enough to produce the negative value of $d\Pi/dt$ observed in PG1159-035. The possibility of placing PG1159-035 at $\log(L/L_\odot) > 3.0$, where contraction in the standard carbon/oxygen models is important, is unattractive; even though the uncertainty in the luminosity of PG1159-035 is large it would then become difficult to match the magnitude of $d\Pi/dt$.

One possibility is that this apparent discrepancy may, in fact, be attributable to our neglect of nonadiabatic effects. Evolution of the star into an instability strip will mean that the growth rate towards instability (see Chapter 6) increases with time. If the adiabatic evolutionary period increase is small ($a \sim b$ in equation 5.3) then the observed value of $d\Pi/dt$ could reflect the nonadiabatic contributions to the pulsation period. The nonadiabatic analysis of evolving PNN models reported in Chapter 6 suggests that this effect is not important when nuclear burning excites the pulsations. Future fully nonadiabatic studies of models of cooler PWD models more appropriate to PG1159 will show if nonadiabatic effects are important for $d\Pi/dt$ in those stars.

Other evolutionary considerations may also contribute to the observed sign of $d\Pi/dt$. For example, a heavier core composition than carbon or oxygen would delay the onset of degeneracy in PNN models, and thus permit significant changes in radius at lower luminosities. It would be very interesting if future refinements of the α -capture cross-sections from ^{12}C and beyond, or the carbon burning rates, lead to a higher mean atomic weight in white dwarf interiors than current models predict.

If the DOV stars are losing mass via a steady stellar wind, the pulsation period will change in response to the changing stellar mass. To first order, the rate of change of the pulsation period due to mass loss is

$$\frac{d(\ln\Pi)}{dt} = \frac{d(\ln\Pi)}{dM} \frac{dM}{dt} . \quad (5.14)$$

For PG1159 models, $d(\ln\Pi)/dM$ ($= -B$ in equation [4.1]) is of order -1.7; hence for the rate of period change via mass loss to exceed the rate of period change due to conservative evolutionary effects, the mass loss rate ($= -dM/dt$) must be greater than or of order $2 \times 10^{-7} M_{\odot}/\text{yr}$. Cerruti-Sola and Perinotto (1985) find mass loss rates in some PNN of 10^{-7} to $10^{-9} M_{\odot}/\text{yr}$. The mass loss rates for PG1159 stars are not known, but they do have some form of stellar wind, based on the presence of

emission features in their spectra (Wesemael *et al.* 1985). Mass loss leads to increasing periods with time, while possible accretion of matter (say from the interstellar medium or in a binary system) will result in decreasing periods with time.

Different progenitors of PWD stars can also be considered. It is interesting to note that models appropriate to hot subdwarfs evolving along the "Extended Horizontal Branch" (e.g., Greenstein and Sargent 1974) in the PG1159 region of the H-R diagram (Wesemael, Winget, Cabot, Van Horn, and Fontaine 1982) were used in WHVH and gave accurate estimates of the observed magnitude and sign of $d\Pi/dt$ for PG1159-035. Another set of models to consider are the "born-again" PNN (Iben *et al.* 1983, Iben 1984), which experience a final helium shell flash at low luminosity that returns them to the AGB to retrace their PNN-PWD evolutionary track. Following the flash, these models experience a phase of radius increase. While this phase is very rapid, leading to a very low expected space density of such objects appropriate to the PG1159 stars, this model may show interesting pulsational behavior.

As we have seen, the observed rate of period change for a hot white dwarf is influenced by various factors such as age, upbringing and environment. Fortunately, we can place limits on the rotation period, mass loss rate, luminosity, and surface temperature from other observations. With these constraints on the models, we should be able to decode the information that the rate of period change provides about the fundamental physics of white dwarf interiors.

"You will find excitement in your working life"

-fortune cookie from *North China* restaurant

CHAPTER 6

G-MODE INSTABILITIES IN PNN MODELS DRIVEN BY NUCLEAR BURNING

6.1 Introduction

One feature that all evolutionary models of PNN have in common is the presence of vigorous nuclear shell burning sources. Models of stars with helium-rich surfaces, such as the stratified models used in this work, are powered by a He-burning shell at high luminosities (see also Iben and Tutukov 1984, Iben 1984, Wood and Faulkner 1986). Early studies, pre-dating the discovery of the DOVs, of the pulsation properties of PNNs reported pulsation driving resulting from the ε -mechanism (see Section 6.3.2 below, and Cox 1985 and references therein) operating in the hydrogen shell burning region (DeGregoria 1977, Sienkiewicz and Dziembowski 1977, Sienkiewicz 1980). Unfortunately, these models are probably inappropriate to the known DOVs for a number of reasons. The most obvious and most important reason is the hydrogen-rich surface layer and the attendant H-burning shell source which destabilizes the models. In addition, at least in the work of DeGregoria (1977), the phase delays in the hydrogen burning networks were ignored in the perturbation of the specific energy generation rate, ε (Cox 1955, Unno *et al.* 1979).

In this chapter we explore the role of the helium shell burning source in the excitation of nonradial g-mode pulsations in PNN and hot PWD models. In the Section 6.2, we briefly describe the linearized nonadiabatic pulsation equations that we solve in order to ascertain the stability of a given mode in a stellar model against self-excited pulsations. We then present the stability coefficient in the form of an

integral to demonstrate the excitation and damping mechanisms that are relevant to PNN models, concentrating on the ε -mechanism. In the final section we report the results of the stability analysis of PNN models, and we discuss the significance of the instabilities.

6.2 Linear Nonadiabatic Oscillations

The linearized perturbation equations for nonradial oscillations are equations 3.9-3.15. For the purpose of investigating the stability of the oscillation mode, we now retain equations 3.12-3.15. In this way, information about the nonadiabatic properties of the solution of the equations is gained, at the expense of having to solve a larger set of equations.

The nonadiabatic equations can be expressed as an extension of the adiabatic Dziembowski equations presented in Chapter 3 (Saio and Cox 1980). They form a system of six first order complex linear differential equations in six complex unknowns. Unlike the adiabatic eigenfunctions, the nonadiabatic eigenfunctions and the eigenvalue are complex quantities. Two additional eigenfunctions are required to complete the set. They are

$$y_5 \equiv \delta s / c_p \quad ; \quad y_6 \equiv (\delta L / L)_{\text{rad}} \quad . \quad (6.1)$$

The eigenfunction y_5 is the Lagrangian perturbation of the specific entropy normalized to c_p , the specific heat at constant pressure. The sixth eigenfunction is the relative Lagrangian perturbation of the radiative luminosity. The details of the derivation of this form of the nonadiabatic equations have been worked out by several others (Saio and Cox 1980, Carroll 1981, Winget 1981) and will not be repeated here. Winget (1981) discusses the limitations of the treatment of perturbations of the convective flux in this scheme; for the models that we analyze in this section such details are not centrally important.

We examine the pulsation properties of our models with a fully nonadiabatic nonradial pulsation code which has been described in detail by Carroll (1981) and Winget (1981). The solution of the equations provides the value of the complex eigenvalue for a given mode in a given model. The eigenvalue may be written (Winget 1981) as

$$\sigma = \sigma_{\text{R}} + i \kappa \quad (6.2)$$

where σ_{R} is the real part of the eigenvalue, and is equal to 2π divided by the pulsation period. In practice, σ_{R} is identical to the eigenfrequency calculated using the adiabatic equations. The imaginary part of the eigenvalue, the stability coefficient κ , has the units of inverse seconds, and is the reciprocal of the e -folding time for the pulsation amplitude. An unstable mode (amplitude grows with time) has a negative value of κ , while a mode that is stable (amplitude decays with time) has a positive value of κ .

6.3 An Integral Expression for the Stability Coefficient

In this section we will derive an integral expression for the stability coefficient κ . We will use this integral to identify the processes responsible for driving and damping nonradial g-modes in PNN models. We will concentrate on the influence of nuclear burning on the stability of g-modes.

6.3.1 *The Work Integral*

We begin by thinking of each mass shell in the model as a separate Carnot engine. The amount of work done by the shell on its surroundings over a complete pulsation cycle, ΔW , is obtained by integrating the equation of conservation of energy (equations [3.4]) over a pulsation cycle:

$$\Delta W = \int T \frac{ds}{dt} dt \quad (6.3)$$

Under the assumption that the equilibrium configuration remains unchanged over a pulsation cycle (see Section 5.2) equation (6.3) is (Unno *et al.* 1979)

$$\Delta W = \int T \frac{ds}{dt} dt = \int \delta T \frac{d \delta s}{dt} dt \quad . \quad (6.4)$$

From equation (3.12)

$$\Delta W = \int \frac{\delta T}{T} \delta \left(\epsilon - \frac{1}{\rho} [\nabla \cdot \mathbf{F}] \right) dt \quad , \quad (6.5)$$

or, expanding the right hand side,

$$\Delta W = \int \frac{\delta T}{T} \delta \epsilon dt - \equiv \frac{\delta T}{T} \delta \left(\frac{1}{\rho} [\nabla \cdot \mathbf{F}] \right) dt \quad . \quad (6.6)$$

Performing the cyclic integrations in equation (6.6), we have

$$\Delta W = \frac{\pi}{\sigma_R} \text{Re} \left\{ \frac{\delta T^*}{T} \delta \epsilon - \frac{\delta T^*}{T} \delta \left(\frac{1}{\rho} [\nabla \cdot \mathbf{F}] \right) \right\} \quad (6.7)$$

If ΔW for a given shell is positive, then energy is added to its surroundings over a pulsation cycle, and the mode is destabilized locally. If the net amount of work done over a cycle is negative, then the shell eats energy and the pulsation is locally damped.

The global stability or instability for a mode is determined by the sum of all these local contributions to damping and driving over the whole stellar model:

$$W = \int_0^M \Delta W dm_r \quad (6.8)$$

If W is positive, then the model is unstable to pulsation; the model is stable if W is negative. The rate of growth or decay of the amplitude of a mode is related to the total energy of the pulsation and the amount of work done by the pulsation over a cycle

(Cox 1980, §9). Specifically, the rate of growth or decay is 1/2 the rate of change of energy in the mode (since the energy of a mode is proportional to the square of the amplitude of the pulsation), or

$$\kappa = \frac{1}{2} \frac{W}{E}, \quad (6.9)$$

where

$$E = \frac{1}{2} \sigma^2 \int_0^M |\delta \mathbf{r}|^2 dm_r \quad (6.10)$$

is the kinetic energy of the system (Cox 1980, §16).

In the numerical calculations of stability, the stability coefficient obtained from the work integral (using the nonadiabatic eigenfunctions) should agree with the imaginary part of the nonadiabatic eigenvalue obtained from the numerical solution of the nonadiabatic equations that yielded the eigenfunctions. In practice, the integrated stability coefficient (equation [6.8]) is usually within a factor of 2 of the eigenvalue stability coefficient. Since the integrated stability coefficient involves numerical integration of quantities that result from the numerical solution of the set of nonadiabatic equations, it is less reliable than the eigenvalue stability coefficient. Therefore, in the discussion of stability in Section 6.4, we will consider only the eigenvalue stability coefficient, although we use the behavior of the work integral to determine the areas of driving and damping.

6.3.2 *The ε -Mechanism*

The term " ε -mechanism" refers to the effects of perturbations of the specific energy generation rate on the excitation and damping of pulsations. These effects are all contained in the first term on the right-hand side of equation (6.7). Since we are interested in the helium-rich DOVs in this analysis we need only concern ourselves with energy losses from neutrino emission and energy production through the helium—burning reaction network. In the case of helium burning we may treat the perturbations of ε in a straightforward manner and do not require consideration of

phase delays; that is, rates of individual reactions comprising the triple-alpha sequence in our models have time scales much shorter than the pulsation periods of interest. Thus the logarithmic derivative of ϵ with respect to temperature at constant density (ν) has its typical equilibrium value of about 40. This is the same conclusion reached by Boury and Ledoux (1965) for radial pulsations in helium core-burning models.

The local contribution of the ϵ -mechanism to the work integral is

$$\Delta W_{\epsilon} = \text{Re}(\epsilon [\left| \frac{\delta T}{T} \right|^2 \nu + \frac{\delta T^*}{T} \frac{\delta \rho}{\rho} \lambda]) \quad (6.11)$$

for a zone, where ν and λ are the usual logarithmic derivatives (Cox 1968, §27). When ΔW_{ϵ} is greater than zero the net effect of the ϵ -mechanism at the zone is to drive the pulsation; a negative value of ΔW_{ϵ} indicates damping.

For regions where energy generation by helium burning is much greater than the energy losses by neutrino emission, ϵ is greater than zero, $\nu \sim 40$, and $\lambda \sim 2$. In such regions, all terms in equation (6.11) are positive, and driving always results. In regions where neutrino energy loss exceeds energy generation by nuclear burning, ϵ is less than zero and the ϵ -mechanism damps oscillations. A sharp filter results because the effect of the ϵ -mechanism is strongly peaked at the position of the narrow burning shell; only modes with significant amplitude in this narrow region are affected. The total stability of a given mode in a given model is a result of the combined effects of driving and damping from the ϵ -mechanism and radiative dissipation processes in all regions of the star.

6.4 Numerical Results: Nuclear Driving in PNNs

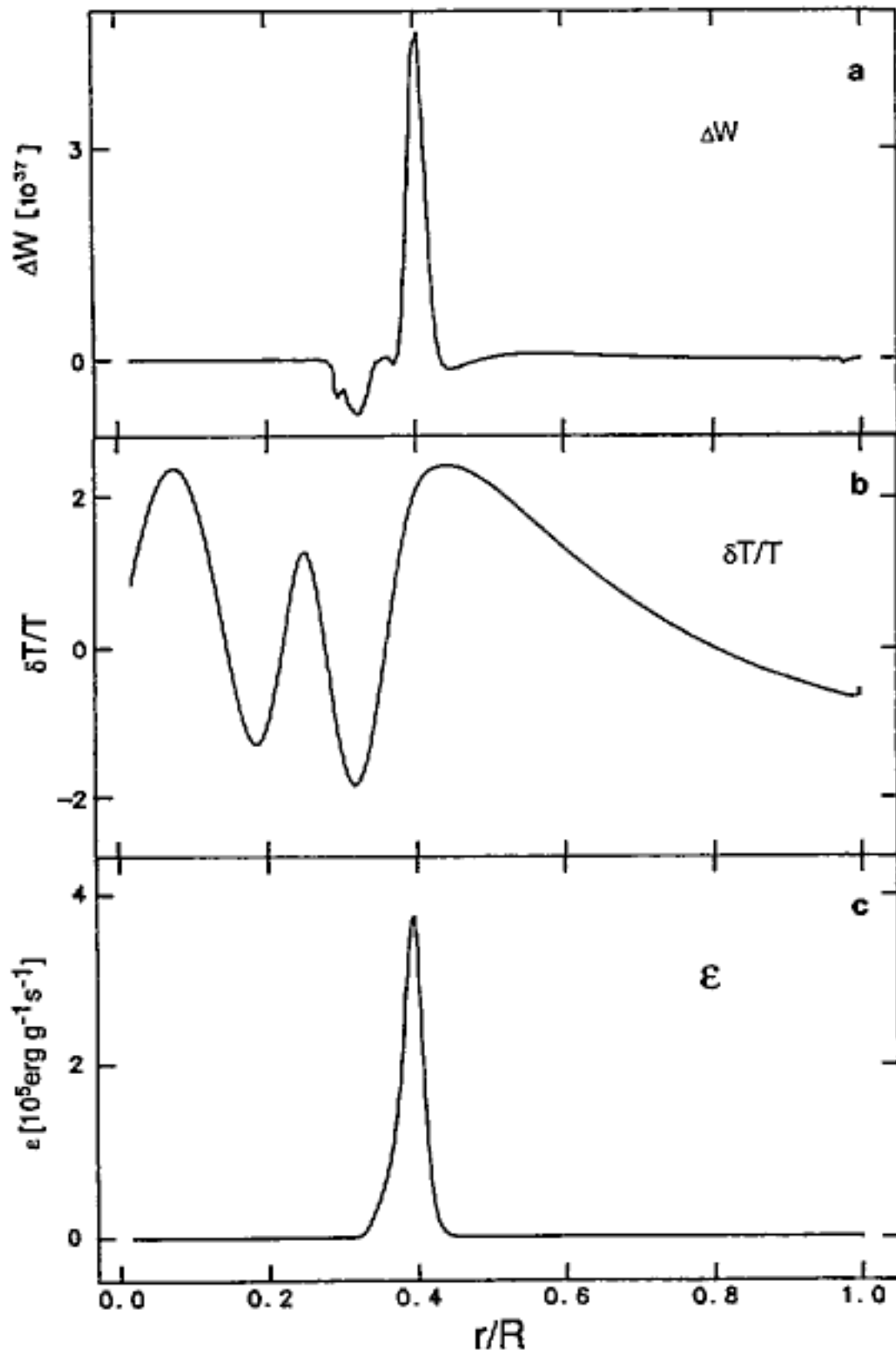
The models used for the nonadiabatic analysis are from the stratified $0.60M_{\odot}$ sequence I60BC1Y. We find nonradial g-mode instabilities, driven by the ϵ -mechanism, in all our models with active helium-burning shells. This is dramatically illustrated for the model at $\log(L/L_{\odot})=3.21$ in Figure 6.1. For this mode, with $l = 1$

Figure 6.1:

(a) Work done as a function of fractional radius for the $l=1$, $k=5$ mode in the $0.60M_{\odot}$ stratified model at $\log(L/L_{\odot})=3.21$ (model 1 in Table 6.1). The large peak is at the position of the helium burning shell (see panel [c]) and results from the ε -mechanism.

(b) The relative Lagrangian temperature perturbation for the mode described in (a).

(c) The specific energy generation rate ε as a function of fractional radius. The sharp peak is the helium burning shell.



and $k=5$, $\delta T/T$ is large at the position of the helium-burning shell, resulting in the large value of ΔW . The second extremum in $\delta T/T$ lies in a region of significant neutrino energy losses below the shell, accounting for some of the damping seen in the top panel of Figure 6.1 at r/R of 0.25.

The PNN models used here (down to $100L_{\odot}$) are too hot to have significant partial ionization zones in the envelope. Thus, without any driving by the κ or γ mechanisms (see Cox 1985 and references therein), radiative damping outside the shell can be significant. Radiative damping leads to a broad low-level damping region just outside the peak of nuclear driving, where $\delta T/T$ is still large above the burning shell.

The global stability or instability for a given mode depends strongly on the position of the final extremum in $\delta T/T$ relative to the burning shell. Figure 6.2 illustrates this remarkable and simple selection mechanism. The behavior of $\delta T/T$ for a given mode is determined by the structure of the g-mode propagation region; the final maximum in $\delta T/T$ occurs near the outer edge of this zone. In the models considered here, modes with lower frequencies have wider g-mode propagation regions, with the outer boundary closer to the surface. When the final extremum in $\delta T/T$ occurs below the burning shell, the mode is usually stabilized by neutrino damping. As k increases (and the frequency decreases), the outermost local maximum in $\delta T/T$ scans across the peak in ϵ , producing instability. As k increases further, the final extremum in $\delta T/T$ moves outside the burning shell and into the envelope, where radiative dissipation stabilizes the mode. Hence nuclear shell burning provides a natural mechanism both for driving the pulsation and selecting which modes are unstable.

Our results for modes with $l = 1$ are summarized in Table 6.1. In Table 6.1, τ_L is the e -folding time for decrease in stellar luminosity, and gives an indication of the evolutionary timescale for the models. Unstable modes have negative values for the stability coefficient; the e -folding times for the pulsation amplitudes are derived from the assumed time dependence of the displacements ($\delta x(t) \propto e^{-t/\tau}$ where $\tau = \kappa^{-1}$ and κ is the stability coefficient defined in Section 6.2). Presumably, a self-excited

Figure 6.2:

The Lagrangian temperature perturbation in a $0.60M_{\odot}$ helium-rich PNN model at $\log(L/L_{\odot})=3.21$ for dipole ($l=1$) modes with $k=2, 4,$ and 6 . The dashed line is the specific energy generation rate.

Table 6.1

Periods and Damping Times for $l = 1$ g-Modes in PNN Models

	(1)	(2)	(3)	(4)	(5)
M^*/M_{\odot}	0.60	0.60	0.60	0.60	0.50
$\log(L/L_{\odot})$	3.208	2.535	2.009	3.215	2.114
T_{eff}	5.254	5.187	5.099	5.176	4.993
τ_L [yr]	1.32×10^4	1.32×10^4	4.05×10^4	5.00×10^3	6.41×10^4
Age [yr]	7.01×10^3	2.25×10^4	4.96×10^4	2.60×10^3	1.61×10^5
$L_{\text{nuc}}/L_{\text{phot}}$	0.756	0.189	0.038	0.605	0.292
Π [s] $k=1$	50.28	49.08	50.08	55.76	68.73
τ [yr]	$+2.03 \times 10^3$	-7.99×10^5	$+1.08 \times 10^6$	$+2.03 \times 10^0$	$+7.10 \times 10^5$
Π [s] $k=2$	67.86	69.88	73.55	72.47	94.11
τ [yr]	-1.21×10^4	-4.60×10^4	-4.07×10^5	$+2.25 \times 10^2$	-2.95×10^4
Π [s] $k=3$	84.29	87.15	91.55	91.66	124.1
τ [yr]	-2.89×10^3	-3.01×10^4	$+9.89 \times 10^4$	$+2.53 \times 10^3$	-2.13×10^4
Π [s] $k=4$	107.1	111.8	117.1	110.7	162.3
τ [yr]	-2.20×10^3	$+4.02 \times 10^4$	$+4.38 \times 10^4$	-2.86×10^3	-1.14×10^5
Π [s] $k=5$	125.6	133.4	140.6	128.5	192.6
τ [yr]	-5.93×10^3	$+1.03 \times 10^4$	$+3.37 \times 10^3$	$+3.33 \times 10^3$	$+3.00 \times 10^4$
Π [s] $k=6$	150.0	154.8	157.7	151.1	213.7
τ [yr]	$+7.40 \times 10^3$	$+1.82 \times 10^3$	$+8.31 \times 10^2$	-3.78×10^3	-3.61×10^4
Π [s] $k=7$	169.5	171.5	178.9	175.8	247.0
τ [yr]	$+1.06 \times 10^4$	$+1.24 \times 10^3$	$+8.00 \times 10^2$	-2.41×10^3	$+4.89 \times 10^5$
Π [s] $k=8$	187.0	193.5	203.8	195.9	283.4
τ [yr]	$+2.11 \times 10^3$	$+8.01 \times 10^2$	$+1.98 \times 10^2$	$+3.45 \times 10^3$	$+4.43 \times 10^4$

mode will reach finite amplitude if it remains unstable over several τ . In the models from I60BC1Y, presented in the first three columns in Table 6.1, this is the case for most of the modes that were unstable. Another interesting result is that even when the helium-burning shell provides only a small fraction of the total luminosity, the ε -mechanism remains potent enough to destabilize some modes, as in the $0.60M_{\odot}$ model at $\sim 100L_{\odot}$.

We find nuclear driving in another set of evolutionary PNN models (P60BI1Y). The instabilities found in these simpler stratified models are very similar to those found in the models discussed above. In addition, we constructed a $0.50M_{\odot}$ PNN sequence (P50BI1Y) that contained an active helium shell source. The pulsation periods for this model, as given in Table 6.1, are about 40% longer than in the $0.60M_{\odot}$ sequences, as one would expect from the discussion in Chapter 4. Clearly, the effects of total stellar mass do not change the basic results of the stability analysis: modes with $k \sim 2$ to 6 are unstable in PNN models.

The inescapable conclusion from these exploratory calculations is that the presence of helium shell burning sources demands that some g-modes are pulsationally unstable. Since the He-shell burning sources are found in essentially all evolutionary calculations of hydrogen-deficient PNNs this result is universally applicable to any stars which may be represented by such models. For modes that are stable against pulsation in our models, the net effect of the ε -mechanism is to reduce the amount of damping in the core, thus possibly allowing any envelope partial ionization driving mechanisms (that we did not find, but see Section 1.3.2) to destabilize the mode. This combined effect of the ε -mechanism and envelope driving mechanisms would destabilize a mode that would be found to be stable when just one or the other effect is considered. Most promising is the possibility of nuclear burning driving providing a filter mechanism which may selectively enhance certain modes destabilized primarily by the κ and/or γ mechanisms. In Chapter 7 we discuss the implications of nuclear burning driven pulsations in PNN on the evolutionary link between these stars and the white dwarfs.

A problem under investigation grows in interaction with its materials, and ... when it is completed it is necessarily rough-hewn. ... If every anomaly in experience, and every ambiguity in concept, were completely ironed out before the work was presented to the public, nothing new would ever appear.

- J.R. Ravetz

CHAPTER 7

PULSATIONS IN HOT DEGENERATES: SUMMARY AND APPLICATIONS

7.1 Summary

Delving into the details of computations of stellar evolution, and exploring adiabatic and nonadiabatic pulsations is in itself a very rewarding and exciting pursuit. But we must always maintain a realistic perspective on the applicability of this work to "real" stars, and to related areas of study. In this final chapter, we step back from the details of the calculations and attempt to place the results of this investigation within the context of our general notions of stellar evolution.

We have investigated the evolution of stars from the PNN phase to the white dwarf phase, and summarize our major conclusions below:

1. The periods seen in the DOV and DBV stars correspond to those of the high radial overtone, low l g-modes in DOV and DBV models. As a star evolves from the PNN phase through the PWD phase, the region of period formation moves from within the degenerate core out into the nondegenerate envelope. In $0.60M_{\odot}$ models, this transition occurred at $100L_{\odot}$. The transition luminosity increases with increasing stellar mass. Thus the observed pulsation periods probe the interiors of the more luminous pulsating degenerates and the envelopes of the cooler pulsators.

2. Cooling effects dominate residual contraction in determining $d\Pi/dt$ for nonrotating post-PNN models appropriate to PG1159-035 and the other DOV stars, as well as the DBVs; therefore the pulsation periods increase with time. The timescales for period change are the thermal timescale of the interior, or about 1 million years for $0.60M_{\odot}$ DOV models. The timescale for period change is sensitive to the rate of neutrino emission in the core, and the prior evolutionary history of the star. Below $100L_{\odot}$, the timescale for period change is insensitive to the radial overtone k or the value of l . Rotation can affect the observed rate of period change for the DOVs; however, because it is proportional to the rate of gravitational contraction, it is not an important effect for the DBVs.

3. In all PNN models with active nuclear burning shells, we find instabilities in the low-order g-modes. These are driven by the ϵ -mechanism acting in the nuclear burning shells. The periods of the unstable modes range from 50s to 214s. In all models, the presence of an active nuclear burning shell demands that some g-modes be unstable.

We now expand on these three areas by applying them to PNN and hot white dwarf stars. In Section 7.2, we apply our results from item 1 to the DOV and DBV stars, and show how the characteristic period spacing may be used to identify the modes of pulsation in these stars. The applications and implications of secular period changes are summarized in Section 7.3. We attempt to link the PNN, their ancestors, and their descendents using the results from the nonadiabatic calculations in Section 7.4. As with all investigations in astrophysics, this study has raised many more questions than it has answered; we complete this chapter in Section 7.5 with a discussion of future investigations.

7.2 Period Spectra as Seismological Indicators

A striking property of the pulsating degenerates is their multiperiodic variation, such as in the DOV star PG1159-035 and in the DBV star GD358. If modes with the same radial overtone k but different l are present, then equation (4.5) and

the models imply that the periods should fall in groups with ratios of about 2.4 : 1.4 : 1 for modes with $l = 1, 2,$ and 3 respectively. If modes with the same value of l but different values of k are present, then the period differences between modes should all be integral multiples of a characteristic period spacing, as we showed in Chapter 4. In searching for those characteristic signatures in real stars, a number of difficulties arise. Rotation, aliasing, and other effects can cause problems in interpreting individual peaks in the power spectrum; suspected relationships between periods of pulsation must be subjected to appropriate statistical tests to ensure that the relationships are not simply coincidental. If one of the above relationships between the observed periods can be demonstrated, then the full power of the theoretical analysis of the adiabatic pulsation properties can be used to make fundamental statements about the stars and their pulsations.

7.2.1 *The DOV Stars*

The period spectrum of PG1159-035 shows compelling evidence for a uniform period spacing. We list the periods of PG1159, taken from Winget *et al.* (1985), in Table 7.1; except for the 424.4 s period, the remaining seven periods are separated by integral multiples of a minimum period interval, $\Delta\Pi$, of 21.0 ± 0.3 s to within the 2σ uncertainties of the periods themselves. With this one number, we can account for the period spectrum of PG1159-035 with a simple empirical model of the mode structure. Seven out of eight of the periods have the same value of l and values of k that differ by the amounts indicated in Table 7.1.

We can use this empirical model of the pulsation spectrum to constrain the theoretical models of the DOV stars if we assume that the periods seen are high-order g-modes. If the modes in PG1159-035 are all dipole ($l=1$) modes, then the observed minimum period interval corresponds to a value of $\Pi_0 (= \Delta\Pi \times [l(l+1)]^{1/2})$ of 29.7s, from the definition of Π_0 in Section 4.3.1. If the modes are $l=2$ modes, then $\Delta\Pi$ corresponds to $\Pi_0=51.4$ s. In Figure 7.1, we plot these two possibilities along with theoretical values of Π_0 for the evolutionary models. If the observed modes are $l=1$ modes, then their period spacing corresponds very closely to the characteristic period spacing in the $0.60M_{\odot}$ models. If the modes are $l = 2$, then Figure 7.1 shows

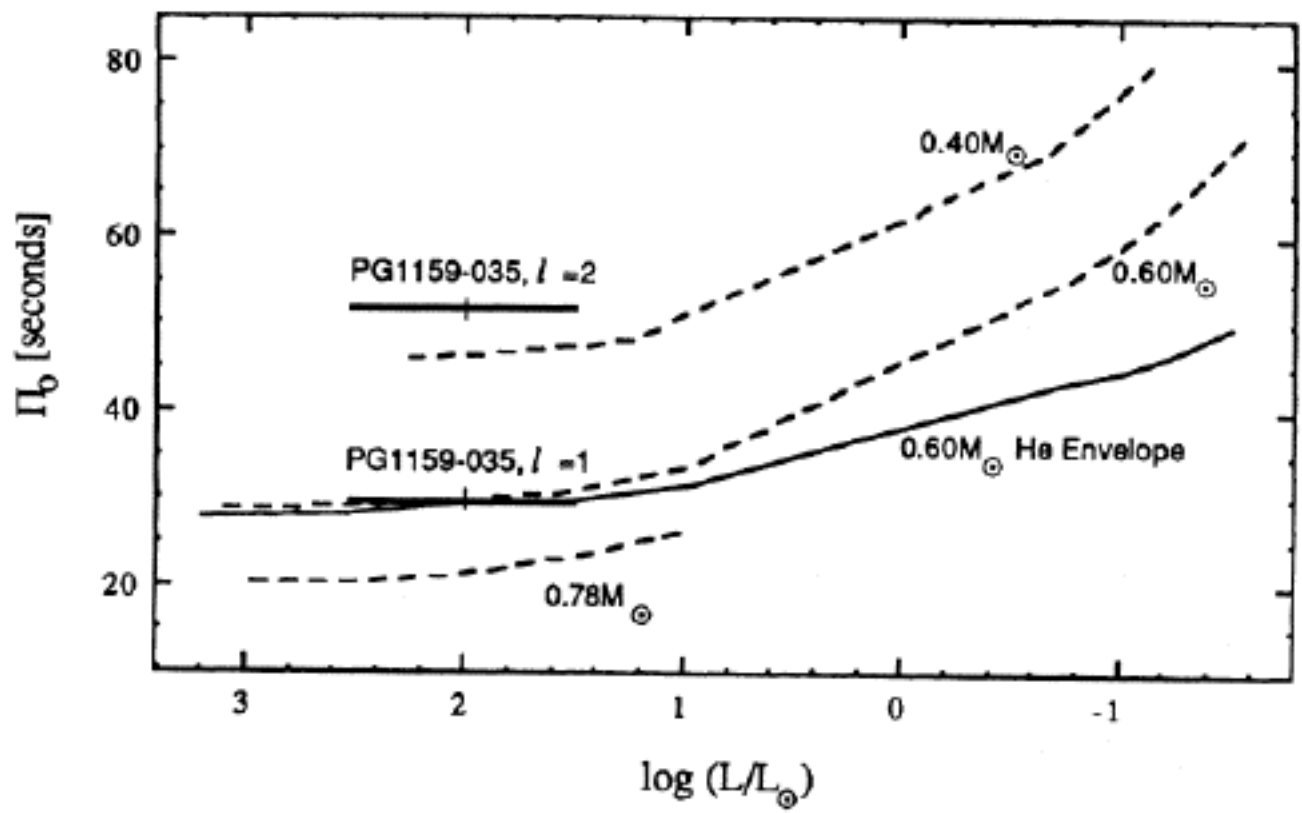
Table 7.1

The Period Spectrum of PG1159-035

Period [s]	k	$\Pi_0 + \Delta\Pi(k - k_0)$ [s] ($\Delta\Pi = 21.0 \pm 0.3$ s)
=====	=====	=====
390.0 ± 0.9	k_0	390.0 ± 0.9
424.4 ± 1.1
451.5 ± 1.2	$k_0 + 3$	453.0 ± 1.2
495.0 ± 1.5	$k_0 + 5$	495.1 ± 1.5
516.0 ± 1.6	$k_0 + 6$	516.1 ± 1.7
538.9 ± 1.7	$k_0 + 7$	537.1 ± 2.0
645.2 ± 2.5	$k_0 + 12$	642.1 ± 3.1
831.7 ± 4.2	$k_0 + 21$	831.2 ± 5.3

Figure 7.1:

Characteristic period spacing as a function of luminosity for PNN-WD models. Dashed lines are for pure ^{12}C models, while the solid line is for the sequence I60BC1Y, a stratified model with a helium-rich envelope. The two data points are for PG1159-035: the upper point is Π_0 , derived from the observed spacing of the periods, if the modes of pulsation in PG1159 are $l=2$ modes; if $l=1$, then the spacing of the periods suggests the lower value of Π_0 . The horizontal error bars associated with these points reflect the uncertainty of the luminosity of PG1159; the vertical error bars show the degree of fit of a single minimum period spacing to the observed periods.



that PG1159-035 would have to have a mass well below $0.40M_{\odot}$, making it very difficult to believe that PG1159-035 is the garden-variety PNN descendent. This is very strong evidence that the mass of PG1159-035 is $0.60M_{\odot}$ and that it is a dipole ($l=1$) pulsator.

Above $10L_{\odot}$, the value of Π_{\odot} is not very sensitive to the composition of the models, and is most sensitive to the total stellar mass. With only a ballpark estimate of the star's mass, if we can determine that a period spectrum contains periods that are separated by integral multiples of a minimum period interval, then comparison with the grid of models results in Section 4.3.1. allows us to uniquely constrain the value of l of the modes present in the power spectrum. Fixing the value of l , we can go back and iteratively use Π_{\odot} to determine the mass of the star more carefully. Given the mass of the star and the value of l , we can estimate the value of k by direct comparison with the period spectra of the models. In models appropriate to PG1159, modes with $k \sim 20$ to ~ 40 appear to have the correct periods. Such mode identifications are extremely valuable for the investigation of the excitation and mode selection mechanisms operating in the DOV stars.

7.2.2 DBV Stars

This method should naturally extend to the pulsating DB white dwarfs. The very rich power spectrum of GD358 (Winget et al. 1983) initially suggested rotational splitting of several $l=2$ modes. However, with additional observations, Hill et al. (1986) find that the uniform frequency splitting is different for some individual runs, and not present at all in others. With further observations, it may be possible to interpret the period spectrum as consisting, for the most part, of a sequence of periods separated by integral multiples of a minimum period interval. In the luminosity range containing the DBV instability strip ($-0.9 \leq \log(L/L_{\odot}) \leq 1.6$), for $0.60M_{\odot}$ the theoretical value of Π_{\odot} is sensitive to the composition of the outer layers. If the pulsation modes observed in the DBVs correspond to several large values of k with the same l then an identification of Π_{\odot} could provide a new handle on the envelope composition of the DB white dwarfs.

The additional dependence of Π_0 on composition makes the use of period spacings as a mode identifier more complicated in the DBVs than in the DOVs. However, the mass and temperature of a given DBV can be constrained if $(d\ln\Pi)/dt$ is known for the model. In Section 7.3.2 below, we show how an observed rate of period change can be a temperature probe for the DBVs or, given the effective temperature from spectroscopic determinations, $d(\ln\Pi)/dt$ is sensitive to the mass and composition. The use of period spacings and measured rates of period change in concert with the more conventional diagnostics of gravity and effective temperature should make mode identification possible for the rich DBV pulsators as well.

7.3 Rates of Period Change

Because of the sensitivity of $d(\ln\Pi)/dt$ to such quantities as stellar mass, structure, composition, and evolutionary phase, its measurement will be a valuable probe of the properties of DOV and DBV stars. We note that in contrast to the DOV stars, the DBV models evolve at almost constant radius. Thus the radius term in equation (5.12) is unimportant relative to the cooling term, and the rate of period change is insensitive to the rotation rate, removing one additional dimension of uncertainty for these stars.

7.3.1 *DOV Stars*

We have shown that the measured value of $d\Pi/dt$ for PG1159-035 agree with the theoretical value for nonrotating models in magnitude, but not in sign. Rotation effects require a value of l of 2 or 3 for the 516 s mode to reverse the sign of $d\Pi/dt$. This is in contradiction to the value of l of 1 from the period spacing. In addition, if rotation effects are important enough to result in the negative value of $d\Pi/dt$, then the resulting frequency splitting would overwhelm the uniform period spacing for consecutive values of k . Hence the sign of $d\Pi/dt$ and the apparent uniform period spacing require two incompatible interpretations. The solution to this problem would benefit greatly from the measurement of $d\Pi/dt$ for another mode in PG1159-035. If $d\Pi/dt$ were different in sign or magnitude, this would be compatible

with a rotational explanation since modes with different m are likely to be present. If $d\Pi/dt$ is the same for all measurable modes, implying that the analysis in Section 7.2 is correct, then alternative explanations for the sign of $d\Pi/dt$ will be required. For example, as discussed in Chapter 5, a heavier core composition of the PG1159 stars could account for the decreasing periods. Such models would imply that carbon and oxygen burning took place in a prior evolutionary stage.

Measurement of the rates of period change for other DOVs are now essential to establish their evolutionary status. If negative values of $d\Pi/dt$ turn out to be another of their class properties, and they are not attributable to rotation, then these stars do not fit into the standard picture of post PNN evolution as presented here. If we can sort out the effects of rotation, then the rate of period change is telling us something significant and fundamental about the physics of the pulsating PG1159 stars.

7.3.2 *DBV Stars*

Within the framework of the preliminary theoretical results of Chapter 5, the measurement of $d(\ln\Pi)/dt$ in DBV stars will help greatly in sorting out the remaining uncertainties in the evolutionary models. Observationally, the mass distribution of the white dwarfs is quite narrow, and is centered on $0.6M_{\odot}$ (Weidemann and Koester 1983); the mass distribution of the DB stars is almost the same (Oke *et al.* 1984). Hence, if we know (or assume) a mass of $0.6M_{\odot}$ for the DBV stars, $d(\ln\Pi)/dt$ can be used as an independent temperature estimator. If the composition of the model is roughly correct, then an uncertainty in the measured value of $d(\ln\Pi)/dt$ of 10% translates to a temperature uncertainty of about 3.5%, or about 900K at 24,000K.

Alternatively, with the spectroscopically determined value of T_{eff} , the observed $d(\ln\Pi)/dt$ will be an indicator of the mass of the star, and of the chemical composition at the degeneracy boundary. For example, consider a DBV at a temperature of 24,000K. Based on the results for the stratified model, we expect that the value of $d(\ln\Pi)/dt$ should be $7.2 \times 10^{-17} \text{s}^{-1}$. If the observed period change was measured to be significantly larger than this value ($>10^{-16} \text{s}^{-1}$), then that would strongly suggest a mass smaller than $0.6M_{\odot}$. Conversely, a smaller rate of period

change ($<5 \times 10^{-17} \text{s}^{-1}$) would indicate a mass significantly greater than $0.6M_{\odot}$. Whatever analysis is undertaken, we see that knowledge of $d(\ln\Pi)/dt$ will provide a new tool in probing the nature of DB white dwarfs.

We can estimate the time required to observe secular changes of this magnitude using the concept of the (O-C) diagram (cf. Solheim, *et al.* 1984, Winget *et al.* 1985). A curve in the (O-C) diagram represents the difference, in seconds, between a time of maximum computed from an ephemeris and the observed time of maximum as a function of the number of cycles that have elapsed. This curve can be represented as an expansion about derivatives of the period,

$$(O-C) = \Delta t_{\odot} + \Delta\Pi E + 1/2\Pi E^2 (d\Pi/dt) + \dots \quad (7.1)$$

where Π is the pulsation period, E is the number of cycles through which the star pulsates in a baseline time of t , and $\Delta\Pi$ is the change in period over the baseline. The first term in equation (7.1) represents a correction to the time of maximum (or time of zero according to arbitrary normalization). The second term represents a correction to the best period, Π . If we assume we have the best fit for t_{\odot} and Π , then the first two terms in equation (7.1) are zero. If we further assume that the first and second derivatives of the period with respect to time are small (as we have found for the theoretical models), then we can neglect the higher order terms and we have

$$(O-C) = 1/2 \Pi E^2 (d\Pi/dt) \quad (7.2)$$

or, since $E=t/\Pi$,

$$t = \{2[d(\ln\Pi)/dt]^{-1}[O-C]\}^{1/2} \quad (7.3)$$

Here (O-C) represents the accumulated delay associated with the period change. To detect a change, clearly the accumulated (O-C) must be larger than the error of measurement. Thus, assuming a typical timing accuracy of 1 second, we can tabulate the time base required to detect a rate of period change, implied by the stratified $0.60M_{\odot}$ model, as a function of effective temperature:

$$\begin{aligned}\tau_{30000\text{K}} &= 2.6 \text{ yr} \\ \tau_{25000\text{K}} &= 4.5 \text{ yr} \\ \tau_{20000\text{K}} &= 6.3 \text{ yr.}\end{aligned}$$

We can now evaluate the prospects for detecting a rate of period change in the two DBV stars currently being monitored. GD358 has been under observation since its discovery in May, 1982. Although no data were obtained on the object in 1983, high quality data are available from 1984 to the present. If it is possible to bridge back to the 1982 data, we anticipate that a detection of $d\Pi/dt$ for GD358 will be made within the next 1-3 observing seasons, depending on its effective temperature. The second star, PG1351+489, has been monitored since May 1984 (Winget, Nather, and Hill 1986). The light curve of this star is consistent with only two periods, dominated by a single, large amplitude peak at 489s. For this reason, individual timings are intrinsically more accurate than for GD358 where at least 28 modes are simultaneously present. The decreased timing errors for the large amplitude peak in PG1351+489 may compensate for the shorter available time baseline on the object. Hence, PG1351+489 may become the first DBV star for which a secular period change will be observed.

7.4 Pulsations in PNN

The instabilities in hydrogen-deficient PNNs described in Chapter 6 provide us with a possible tool with which we can link the AGB parents of PNN and their PWD descendants within a single evolutionary scheme. The obvious interpretation that the observed DOV pulsations are related to the instabilities that result from nuclear burning has one outstanding problem: the periods that we find unstable are roughly a factor of 3 or 4 shorter than the periods in the known DOVs, and are many times shorter than those in the central star of K1-16. The significance of this difference is unclear. Perhaps the difference can be accommodated by the uncertainties inherent in the specific details of the structure and composition of the evolutionary models, or in the details of the pulsation analysis.

If the results presented in Chapter 6 are insensitive to these details, then the consequences are more interesting. In this case there are two alternatives. First, objects pulsating with these periods exist and have not been found because of observational selectional effects such as the difficulties of observing photometric variations of an object embedded in nebulosity, or simply their low space-density. The second alternative is that the basic characteristics of the evolutionary models in this region are incorrect and the He-shell burning sources are extinguished in a prior evolutionary stage. This exacerbates the already difficult situation in modeling these objects and has serious implications for our understanding of a significant part of post-main sequence evolution. It is entirely plausible that, in the process of PN formation, enough mass is lost from the surface that the remaining helium-rich layer is too thin to support a helium burning shell. Alternatively, the helium buffer between the burning shells in the AGB progenitor may be smaller than is currently thought, with the consequences, again, that the helium-rich layer in the resulting PNN is too thin to support helium burning. Such conclusions would have a major impact, as well, on our studies of the presumed descendents of these stars: the DBV stars.

7.5 Now What?

Now that a preliminary theoretical framework exists for interpreting observations of the hot pulsating degenerates, we are in a position to identify deficiencies in our theoretical understanding, and pinpoint promising areas for further research. There are many problems, both theoretical and observational, that suggest themselves for further study. The resolution of even a few of these will go a long way towards gaining a more complete understanding of the metamorphosis of PNN into white dwarfs.

First of all, we need rates of period change for additional modes in PG1159-035, and for other DOV stars. A determination of the rotation period of PG1159-035 that is independent of the pulsation observations will determine if the effect of rotation is an important factor in $d\Pi/dt$. With these measurements and

reduced uncertainties in the luminosities and effective temperatures of the DOV stars, we will be able to firmly establish the evolutionary status of this class of stars, based on the framework presented here. This will, in turn, provide a new and quantitative calibration of the rates of energy loss by photon and neutrino emission as well as other more exotic species of weakly interacting particles such as axions (Dicus *et al.* 1978, 1980), under conditions found within the cores of evolved stars.

We have shown how $d\Pi/dt$ is sensitive to the mass, effective temperature, and envelope composition in the DBV stars. Ongoing observations of the DBVs should provide us with $d\Pi/dt$ for two of them in the near future for direct comparison with the theoretical models presented in this work.

An extended observational survey of hot, hydrogen-deficient compact objects for periodic photometric variations is therefore in order. PNN that have enough helium remaining to allow shell burning and the resulting instabilities would evolve into DB white dwarfs, and possibly DAs (see below). The results of such a photometric study will be of value in tracing the production of different species of white dwarfs, and may provide a direct link to the DBVs from the PNN stage. This model would also provide new quantitative information about the episode of PN formation.

A class of models that we did not consider explicitly in this work must also be discussed. Currently, the limits to the amount of hydrogen at the surface of the DOV stars is not very stringent. It is possible to have a significant fraction of surface hydrogen ($\text{He}/\text{H} \geq 1$) in the hot DOVs that would be undetectable with current techniques. Hydrogen present at this level could support a weak hydrogen-burning shell between the helium-burning shell and the surface that could drive pulsations. Longer periods than those that are destabilized by helium burning alone would be destabilized; the region where hydrogen burning can drive pulsations would lay in the nondegenerate envelope, where the amplitude of $\delta T/T$ is significant for higher overtone modes (see Chapter 6). The nebula that is associated with such a PNN would be expected to show significant amounts of hydrogen and helium. Cooler former PNNs with no visible nebula remaining may be hot enough to be disguised as DOs

even if they have some surface hydrogen (see below). New evolutionary models, and stellar atmosphere calculations, will be able to address these issues. These should be backed up by an extensive series of numerical investigations of the pulsation properties of such objects, because although it seems unlikely at present, it is possible that these models may not only be relevant to the observed DOV, but may be the only relevant models.

As these preliminary results indicate, PNNs with active helium burning shells should show periods that are shorter than those seen in the DOV stars; models with active hydrogen shells may have unstable periods that are the same or longer. If a hydrogen-deficient PNN or PWD has a small mass fraction of hydrogen in the surface layers, then as it evolves the hydrogen will diffuse outwards; eventually, perhaps, it will turn into a DA white dwarf with a thin, pure hydrogen envelope. For example, a DOV with a surface mass fraction of 10% hydrogen in the outer $10^{-5}M_{\odot}$ would evolve into a DA white dwarf with an almost pure hydrogen envelope of $10^{-6}M_{\odot}$. Hence, given the present uncertainty in the surface abundance of PG1159-035, descendants of the DOV stars could be DA as well as DB white dwarfs. More accurate determinations of the surface hydrogen, helium, carbon, and oxygen abundances of PNN and DOV stars are essential to sorting out the true evolutionary links between these stars and the cooler white dwarfs. Such abundances determinations are also important for investigating the pulsation driving mechanisms in the DOVs.

New observational equipment and techniques are constantly being developed and applied to challenging problems in astrophysics. For example, the global network of high-speed photometers proposed by R.E. Nather and collaborators at the University of Texas will provide extended coverage for all types of pulsating stars. This extended coverage will reduce the difficulties of interpreting photometric observations by removing the diurnal gaps from time-series data. With this system, the complex power spectra of hot degenerates like GD358 and PG1159-035 will be unambiguously resolved. The preliminary theoretical investigation reported in this dissertation should serve as a guide for exploiting the seismological evidence that the pulsating degenerates will continue to provide. Future refinements will be made to the input physics and computational techniques, such as more sophisticated

multi—component plasma equations of state, opacity data, and self-consistent techniques for calculating the evolution of models from the AGB through the planetary nebula formation phase. While we have learned many things about the transition from PNN to WD in this investigation, much work is needed before we will satisfactorily understand these rapid and exciting stages of advanced stellar evolution. The purpose of this work has been to provide an initial step on what will be a long and productive journey towards a better understanding of the final stages of stellar evolution, and most importantly, the physics which governs them.

APPENDIX

A.1 The Cooling Rate of a White Dwarf Photosphere

In the Mestel (1952) theory of white dwarf cooling, the luminosity of the star is derived from leakage of thermal energy of the ions in the interior. Assuming that the heat capacity of the nondegenerate ion gas is much larger than that of the electrons, and that the core is nearly isothermal, it can be shown that

$$L = - \frac{3}{2} \frac{kM}{AH} \frac{\partial T_C}{\partial t} \quad (\text{A.1})$$

(Van Horn 1971, equation [5]). In equation (A.1) A is the mean atomic weight, M is the total stellar mass, k is Boltzmann's constant, and H is the atomic mass unit. By representing the opacity in the nondegenerate envelope with Kramer's law ($\kappa = \kappa_0 \rho T^{-3.5}$), we can integrate the equations of envelope structure analytically to obtain a relationship between the core temperature and photon luminosity (Van Horn 1971, equation [7]). We can combine that relationship with equation (A.1) to produce an equation relating the cooling rate of the core to the core temperature,

$$\frac{d(\ln T_C)}{dt} = -6.2 \times 10^{-36} A \left(\frac{\mu}{\mu_e^2} \right) T_C^{2.5}, \quad (\text{A.2})$$

where μ is the mean molecular weight per particle, and μ_e is the mean molecular weight per electron.

Assuming a mass-radius relationship for white dwarfs of the form

$$R = 7 \times 10^8 (M/M_\odot)^{-1/3} \quad (\text{A.3})$$

and noting that $L = 4\pi R^2 \sigma T^4$, we can use equation (7) of Van Horn (1971) to relate the core temperature to the effective temperature:

$$T_C = 240 \text{ A} \left(\frac{\mu}{\mu_e^2} \right)^{2/7} \left(\frac{M}{M_O} \right)^{-10/21} T_e^{8/7} . \quad (\text{A.4})$$

Combining equations (A.1) and (A.4), we obtain an expression for the core cooling rate as a function of effective temperature:

$$\frac{d(\ln T_C)}{dt} = -5.8 \times 10^{-30} \text{ A} \left(\frac{\mu}{\mu_e^2} \right)^{2/7} \left(\frac{M}{M_O} \right)^{-25/21} T_e^{20/7} \quad (\text{A.5})$$

Finally, by differentiating equation (A.4) and substituting for $d(\ln T_C)/dt$ in equation (A.5) we have the desired equation for the cooling of the stellar photosphere as a function of effective temperature (equation [5.11]):

$$\frac{d(\ln T_e)}{dt} = -5 \times 10^{-30} \text{ A} \left(\frac{\mu}{\mu_e^2} \right)^{0.286} \left(\frac{M}{M_O} \right)^{-1.190} T_e^{2.857} \quad (\text{A.6})$$

A.2 Upper Limit to Rotation Effects on $d(\ln \Pi_{\text{obs}})/dt$

For a slowly rotating star which conserves angular momentum, equation (5.6) gives the rate of period change for the case of uniform rotation. For white dwarfs, the rotation coefficient C_{rot} is approximately $(I[l+1])^{-1}$ (Brickhill 1975). Since the moment of inertia for a uniform sphere is proportional to R^2 , we have as an upper limit to the rate of change for I in a white dwarf:

$$d(\ln I)/dt \leq 2 d(\ln R)/dt. \quad (\text{A.7})$$

With the above relations, equation (5.6) becomes

$$\frac{d(\ln \Pi_{\text{obs}})}{dt} \approx \frac{d(\ln \Pi_O)}{dt} - m \frac{\Pi_O}{\Pi_{\text{rot}}} \left[\left(2 - \frac{2}{l(l+1)} \right) \frac{d(\ln R)}{dt} \right]. \quad (\text{A.8})$$

The term in equation (A.8) that arises from the rotation of the model is proportional to $d(\ln R)/dt$, and can be identified as the term b_{rot} in equation (5.12).

The value of m may be any integer between $-l$ and $+l$, or zero. Hence,

$$|b_{rot}| \leq 2 \left(\frac{l^2 + l - 1}{l + 1} \right) \quad (\text{A.9})$$

represents an upper limit to the magnitude of the rotation term b_{rot} in equation (5.12).

REFERENCES

- Backus, G. E., and Gilbert, J. F. 1967, *Geophys. J. R. A. S.*, **13**, 247.
- Barry, D. C., Holberg, J. B., Forrester, W. T., McGraw, J. T., and Wegner, G. 1986, in preparation.
- Beaudet, G., Petrosian, V., and Salpeter, E. E. 1967, *Ap. J.*, **150**, 979.
- Bond H. E., Grauer, A. D., Green, R. F., and Liebert, J. 1984, *Ap. J.*, **279**, 751.
- Boury, A., and Ledoux, P. 1965, *Annales d'Astrophysique*, **28**, 353.
- Carroll, B. 1981, Ph. D. thesis, University of Colorado.
- Carroll, B., and Hansen, C. 1982, *Ap. J.*, **263**, 352.
- Cerruti-Sola, M., and Perinotto, M. 1985, *Ap. J.*, in press.
- Cox, J. P. 1955, *Ap. J.*, **122**, 286.
- Cox, J. P. 1968, *Principles of Stellar Structure* (New York: Gordon & Breach).
- Cox, J. P. 1980, *Theory of Stellar Pulsation* (Princeton: Princeton University Press).
- Cox, J. P. 1984, *P. A. S. P.*, **96**, 577.
- Cox, J. P. 1985, in *IAU Colloquium 82, Cepheids: Observation and Theory*, ed. B. F. Madore (Cambridge: Cambridge University Press), p. 126.
- Cuypers, J. 1980, *Astr. Ap.*, **89**, 207.
- DeGregoria, A. J. 1977, *Ap. J.*, **217**, 175.
- Demarque, P., Guenther, D., and van Alena, W. 1986, *Ap. J.*, **300**, 000.
- Deubner, F., and Gough, D. 1984, *Ann. Rev. Astr. Ap.*, **22**, 593.
- Dicus, D. A. 1972, *Phys. Rev. D*, **6**, 941.
- Dicus, D. A., Kolb, E. W., Teplitz, V. L., and Wagoner, R. V. 1978, *Phys. Rev. D*, **18**, 1829.
- Dicus, D. A., Kolb, E. W., Teplitz, V. L., and Wagoner, R. V. 1980, *Phys. Rev. D*, **22**, 839.

- Drilling, J., and Schöenberner, D. 1985, preprint.
- Dziembowski, W. 1971, *Acta Astr.*, **21**, 289.
- Dziembowski, W. 1977, *Acta Astr.*, **27**, 203.
- Dziembowski, W. 1985, preprint.
- Festa, G. G., and Ruderman, M. A. 1969, *Phys. Rev.*, **180**, 1227.
- Feynman, R., and Gell-Mann, M. 1958, *Phys. Rev.*, **109**, 193.
- Fontaine, G., Graboske, H. C., and Van Horn, H. M. 1977, *Ap. J. Suppl.*, **35**, 293.
- Fontaine, G., and Michaud, G. 1979, *Ap. J.*, **231**, 826.
- Fontaine, G., and Van Horn, H. M. 1976, *Ap. J. Suppl.*, 1976, **31**, 467.
- Fowler, W., Caughlan, G., and Zimmerman, B. 1975, *Ann. Rev. Astr. Ap.*, **13**, 69.
- Goossens, M., and Smeyers, P. 1974, *Ap. Space Sci.*, **26**, 137.
- Grauer, A. D., and Bond, H. E. 1984, *Ap. J.*, **277**, 211.
- Greenstein, J. L., and Sargent, A. I. 1974, *Ap. J. Suppl.*, **28**, 157.
- Guenther, D. B., and Demarque, P. 1986, *Ap. J.*, **301**, 000.
- Hansen, C., Cox, J., and Carroll, B. 1978, *Ap. J.*, **226**, 210.
- Hansen, C., Cox, J., and Van Horn, H. 1977, *Ap. J.*, **217**, 151.
- Hansen, C. J., Winget, D. E., and Kawaler, S. D. 1985, *Ap. J.*, **297**, 544.
- Harris, M., Fowler, W., Caughlan, G., and Zimmerman, B. 1975, *Ann. Rev. Astr. Ap.*, **21**, 165.
- Hill, J. A., Winget, D. E., and Hansen, C. J. 1986, in preparation.
- Iben, I. Jr. 1975, *Ap. J.*, **196**, 525.
- Iben, I. Jr. 1976, *Ap. J.*, **208**, 165.
- Iben, I. Jr. 1982, *Ap. J.*, **260**, 821.
- Iben, I. Jr. 1984, *Ap. J.*, **277**, 333.
- Iben, I. Jr., and McDonald, J. 1985, *Ap. J.*, **296**, 540.

- Iben, I. Jr., and Renzini, A. 1983, *Ann. Rev. Astr. Ap.*, **21**, 271.
- Iben, I. Jr., and Tutukov, A. V. 1984, *Ap. J.*, **282**, 615.
- Jacoby, G. H., and Ford, H. A. 1983, *Ap. J.*, **266**, 298.
- Kaler, J. 1985, *Ann. Rev. Astr. Ap.*, **23**, 89.
- Kaler, J., and Feibelman, W. 1985, *Ap. J.*, **297**, 724.
- Kawaler, S. D. 1982, Masters thesis, University of Texas at Austin.
- Kawaler, S. D., Hansen, C. J., and Winget, D. E. 1985a, *Ap. J.*, **295**, 547.
- Kawaler, S. D., Winget, D. E., and Hansen, C. J. 1985b, *Ap. J.*, **298**, 752.
- Kawaler, S. D., Winget, D. E., Iben, I. Jr., and Hansen, C. J. 1986, *Ap. J.*, **302**, 000.
- Kepler, S. O. 1984, Ph. D. thesis, University of Texas at Austin.
- Kepler, S. O., Robinson, E. L., and Nather, R. E. 1983, *Ap. J.*, **271**, 744.
- Kippenhahn, R., Weigert, A., and Hoffmeister, E. 1967, in *Methods of Computational Physics*, eds. B. Alder, S. Fernbach, and M. Rotenberg (New York: McGraw Hill).
- Knapp, G. R., Phillips, T. G., Leighton, R. B., Lo, K. Y., Wannier, P. G., Wooten, H. A., and Huggins, P.J. 1982, *Ap. J.*, **252**, 616.
- Koester, D., Weidemann, V., and Vauclair, G. 1983, *Astr. Ap.*, **123**, L11.
- Koester, D., Vauclair, G., Dolez, N., Oke, J. B., Greenstein, J. L., and Weidemann, V. 1986, *Astr. Ap.*, in press.
- Kovetz, A., and Harpaz, A. 1981, *Astr. Ap.*, **95**, 66.
- Lamb, D. Q. 1974, Ph. D. thesis, University of Rochester.
- Lamb, D. Q., and Van Horn, H. M., 1975, *Ap. J.*, **200**, 306.
- Landolt, A. U. 1968, *Ap. J.*, **153**, 151.
- Lasker, B., and Hesser, J. 1971, *Ap. J. (Letters)*, **163**, L89.
- Ledoux, P., and Walraven, T. 1958, *Handbook of Phys.*, **51**, 353.
- Liebert, J., Wesemael, F., Hansen, C., Fontaine, G., Shipman, H., Sion, E., Winget, D., and Green, R. 1986, preprint.

- McGraw, J. T. 1977, Ph. D. thesis, University of Texas at Austin.
- McGraw, J. T., Starrfield, S. G., Liebert, J., and Green, R. F. 1979, in *I. A. U. Colloquium 53, White Dwarfs and Variable Degenerate Stars*, eds. H. M. Van Horn and V. Weidemann (Rochester: University of Rochester), p.377.
- Mestel, L. 1952, *M.N.R.A.S.*, **112**, 583.
- Munkata, H., Kohyama, Y., and Itoh, N. 1985, *Ap. J.*, **296**, 197.
- Nather, R. E. 1972, Ph. D. thesis, University of Cape Town.
- Noyes, R., Baliunas, S., Belserene, E., Duncan, D., Horne, J., and Widrow, L. 1984, *Ap. J. (Letters)*, **285**, L23.
- O'Donoghue, D., and Warner, B. 1982, *M.N.R.A.S.*, **200**, 563.
- Oke, J. B., Weidemann, V., and Koester, D. 1984, *Ap. J.*, **281**, 276.
- Osaki, Y., and Hansen, C. J. 1973, *Ap. J.*, **185**, 277.
- Osaki, Y. 1975, *Pub. Astr. Soc. Japan*, **27**, 237.
- Ostriker, J. P., and Bodenheimer, P. 1968, *Ap. J.*, **151**, 1089.
- Paczynski, B. 1969, *Acta Astr.*, **19**, 1.
- Paczynski, B. 1970, *Acta Astr.*, **20**, 47.
- Paczynski, B. 1971, *Acta Astr.*, **21**, 417.
- Paczynski, B. 1974, *Ap. J.*, **192**, 483.
- Park, D. 1974, *Introduction to the Quantum Theory, 2nd Edition* (New York: McGraw Hill).
- Pilachowski, C. A., and Milkey, R. W. 1984, *P. A. S. P.*, **96**, 821.
- Robinson, E. L., Nather, R. E., and McGraw, J. 1980, *Ap. J.*, **210**, 211.
- Saio, H., and Cox, J. P. 1980, *Ap. J.*, **236**, 549.
- Salam, A. 1968, *Nobel Symposium No. 8*, eds. N. Svarthorn (Stokholm: Almquist and Wiksell), p. 367.
- Salpeter, E. E., and Van Horn, H. M. 1969, *Ap. J.*, **155**, 183.
- Schöenberner, D. 1979, *Astr. Ap.*, **79**, 108.

- Schönenberger, D. 1981, *Astr. Ap.*, **103**, 119.
- Schönenberger, D. 1983, *Ap. J.*, **272**, 708.
- Schwank, D. C. 1976, *Ap. Space Sci.*, **43**, 459.
- Scuflaire, R. 1974, *Astr. Ap.*, **36**, 107.
- Sienkiewicz, R. 1980, *Astr. Ap.*, **85**, 295.
- Sienkiewicz, R., and Dziembowski, V. 1977, in *IAU Colloquium 42, The Interaction of Variable Stars with Their Environment*, eds. R. Kippenhahn, J. Rahe, and V. Strohmeier (Bamberg), p. 327.
- Sion, E. M., Greenstein J. L., Landstreet, J. D., Liebert, J., Shipman H. L., Wegner G. A. 1983, *Ap. J.*, **269**, 253.
- Sion, E. M., Liebert, J., Starrfield, S. G. 1985, *Ap. J.*, **292**, 471.
- Solheim, J. E., Robinson, E. L., Nather, R. E., and Kepler, S.O. 1984, *Astr. Ap.*, **135**, 1.
- Starrfield, S. G., Cox, A. N., Hodson, S. W., and Pesnell, W. D. 1983, *Ap. J. (Letters)*, **268**, L27.
- Starrfield, S. G., Cox, A. N., Kidman, R. B., and Pesnell, W. D. 1984, *Ap. J.*, **281**, 800.
- Starrfield, S. G., Cox, A. N., Kidman, R. B., and Pesnell, W. D. 1985, *Ap. J. (Letters)*, **293**, L23.
- Toomre, J. 1985, in *Solar Seismology from Space*, eds. R. Ulrich, J. Harvey, E. Rhodes, Jr., and J. Toomre (Pasadena: N.A.S.A.), p. 7.
- Tuchman, Y., Sack, N., and Barkat, Z. 1979, *Ap. J.*, **234**, 217.
- Unno, W., Osaki, Y., Ando, H., and Shibahashi, H. 1979, *Nonradial Oscillations of Stars* (Tokyo: University of Tokyo Press).
- Van Horn, H. M. 1971, in *I.A.U. Symposium #42: White Dwarfs*, ed. W. J. Luyten (Dordrecht: Reidel), p. 97.
- Wegner, G., Barry, D. C., Holberg, J. B., and Forrester, W. T. 1982, *Bull. A.A.S.*, **14**, 914.
- Weidemann, V., and Koester, D. 1983, *Astr. Ap.*, **121**, 77.
- Weidemann, V., and Koester, D. 1984, *Astr. Ap.*, **132**, 195.

- Weinberg, S. 1967, *Phys. Rev. Lett.*, **19**, 1264.
- Wesemael, F., Green, R., and Liebert, J. 1985, *Bull. A.A.S.*, **14**, 915.
- Wesemael, F., Green, R., and Liebert, J. 1985, *Ap. J. Suppl.*, **58**, 379.
- Wesemael, F., Winget, D. E., Cabot, W., Van Horn, H. M., and Fontaine, G. 1982, *Ap. J. (Letters)*, **254**, 221.
- Willson, L. A. 1979, in *I.A.U. Colloquium #46, Changing Trends in Variable Star Research*, eds. F. Bateson, J. Smak, and I. Urch (Hamilton: University of Waikato), p. 199.
- Winget, D. E. 1981, Ph. D. thesis, University of Rochester.
- Winget, D. E., Hansen, C. J., and Van Horn, H. M. 1983, *Nature*, **303**, 781. (WHVH)
- Winget, D. E., Kepler, S. O., Robinson, E. L., Nather, R. E., and O'Donoghue, D. 1985, *Ap. J.*, **292**, 606.
- Winget, D. E., Lamb, D. Q., and Van Horn, H. M. 1993, in preparation.
- Winget, D. E., Nather, R. E., and Hill, J. A. 1986, in preparation.
- Winget, D. E., Robinson, E. L., Nather, R. E., and Balachandran, S. 1984, *Ap. J. (Letters)*, **279**, L15.
- Winget, D. E., Robinson, E. L., Nather, R. E., and Fontaine, G. 1982, *Ap. J. (Letters)*, **262**, L11.
- Winget, D. E., Van Horn, H. M., Tassoul, M., Hansen C., and Fontaine, G. 1983, *Ap. J. (Letters)*, **268**, L33.
- Wood, P.R. and Faulkner, D. J. 1986, preprint.
- Wyler, R., and Ames, G. 1955, *The Golden Book of Astronomy - A Child's Introduction to the Wonders of Space* (New York: Simon and Schuster).

VITA

Steven Daniel Kawaler was born on 9 April, 1958 in Valley Stream, New York, as the third (and last) son of Justin and Evelyn (Schnall) Kawaler. His oldest brother Foster's early enthusiasm for astronomy resulted in the accumulation of early space-age paraphernalia in the Kawaler house; their subsequent hand-me-down status (as Foster turned to the more usual pursuits of the mid-teen years), ensured that they would make their way down to Steven. After learning how to read using *The Golden Book of Astronomy* (1955) young Steven decided to try to make a career in astronomy. In 1972 and 1974 he attended Camp Uraniborg, a summer camp in astronomy. The camp was presided over by the indefatigable Joe Patterson, who remains a friend and inspiration. Following graduation from Valley Stream Central High School in 1976, he attended Cornell University. At Cornell, he was exposed to astronomical research as a research assistant with Drs. Joseph Veverka and Frank Drake. He was also employed as a teaching assistant in the Department of Astronomy. In May, 1980 he received his B.A. in physics from Cornell, with concentrations in physics, astronomy, and mathematics. He began graduate study in the Department of Astronomy at the University of Texas at Austin in September 1980, after spending the summer of 1980 in Washington, DC as a summer intern in the Astronomy-Relativity Branch of N.A.S.A. Headquarters. At Texas, his interest in stellar evolution was sparked by a course taught by J. Craig Wheeler. Following Dr. Wheeler's suggestion, he completed a research project studying the late stages in low-mass stellar evolution, and was awarded an M. A. in Astronomy in December, 1982 for his efforts. After his marriage to Leslie Beth Hertz in May of 1983, he began his study of hot white dwarfs.

Permanent Address: 64 Lynwood Drive
Valley Stream, NY 11580

This thesis was typed by Steven Daniel Kawaler.